

# **Biomechanics of Vascular Wall: the Role of Structural Organization of Elastin and Collagen**

THÈSE N° 4712 (2010)

PRÉSENTÉE LE 19 MAI 2010

À LA FACULTÉ SCIENCES DE LA VIE

LABORATOIRE D'HÉMODYNAMIQUE ET DE TECHNOLOGIE CARDIOVASCULAIRE (SV/STI)  
PROGRAMME DOCTORAL EN BIOTECHNOLOGIE ET GÉNIE BIOLOGIQUE

ÉCOLE POLYTECHNIQUE FÉDÉRALE DE LAUSANNE

POUR L'OBTENTION DU GRADE DE DOCTEUR ÈS SCIENCES

PAR

**Rana SAITTA-REZAKHANIHA**

acceptée sur proposition du jury:

Prof. V. Hatzimanikatis, président du jury

Prof. N. Stergiopoulos, directeur de thèse

Prof. S. Greenwald, rapporteur

Prof. D. Pioletti, rapporteur

Prof. A. Rachev, rapporteur



ÉCOLE POLYTECHNIQUE  
FÉDÉRALE DE LAUSANNE

Suisse  
2010



*A mon mari, Sandro*

*A mes parents, Farzaneh & Bahman*

تقدیم بہ ہمسرم، ساندر و

پدر و مادرم، بہمن و فرزانه





# Abstract

This thesis contributes to the field of biomechanics of vascular wall. The focus is particularly on the microstructure of vascular elastin and collagen constituents and their contribution to the macroscopic mechanical behavior of the wall. The analysis is done in the framework of continuum mechanics. The work characterizes structural features of elastin and collagen fibers using microscopy techniques and introduces these features to constituent-based constitutive models. The models are applied to the experimental data, derived from inflation-extension tests, to predict the gross mechanical behavior of the tissue. The developed constitutive models could be further used to study in detail the mechanics of vascular tissue in health and disease. The thesis is presented in form of an introduction, four chapters (corresponding to four papers) and a conclusion.

The introduction provides the motivation for this thesis as well as the background on vascular wall structure and mechanics. A brief description of the imaging techniques used is presented. Also, structural constitutive modeling of vascular wall is briefly discussed with particular attention to the modeling of elastin and collagen constituents.

The first paper focuses on anisotropic properties of elastin in veins. We show that earlier constituent-based strain energy functions (SEFs), where elastin is modeled as an isotropic material, fail in describing accurately the tissue response to inflation-extension loading. We hypothesize that these shortcomings are partly due to unaccounted anisotropic properties of elastin. We extend the previously developed biomechanical model in our laboratory (Zulliger et al., 2004, *J. Biomech.*, 37(7): 989-1000 (2004)) to account for elastin anisotropy and present an anisotropic strain energy function for elastin with one family of fibers in the longitudinal direction. The model is validated using experimental data from inflation-extension tests on rabbit facial veins. The tissue is tested under a fully relaxed smooth muscle state, for longitudinal stretch ratios ranging from 100% to 130% of the *in vivo* length. The model with the anisotropic elastin fits well the data for a wide range of longitudinal stretch ratios. The main finding of this paper is that the anisotropic description of elastin is required for a full 3-D characterization of the biomechanics of the venous wall.

The second paper addresses the role of elastin in anisotropic properties of arteries with particular attention to the structural organization of elastin. A constituent-based model including an anisotropic elastin, with one family of fibers in the circumferential direction, is presented. Micro-structural imaging, based on electron microscopy techniques, is used to support this anisotropy. Inflation-extension tests, on intact and elastase-treated arteries, provide a data set to validate the model and to study the effect of elastin removal. We show that the SEF, with an anisotropic elastin part, characterizes more accurately the mechanical properties of the arterial wall as compared to models with simply an isotropic elastin. Transmission electron microscopy (TEM) and serial block-face scanning electron microscopy (SBF-SEM) show interlamellar elastin fibers in the circumferential direction and therefore support the nature of the assumed anisotropy. The model predicts an earlier engagement of collagen in elastase-treated arteries compared to the intact arteries and thus suggests a clear functional interaction between the elastin and collagen component that is often neglected in constituent-based SEFs.

The third paper presents a structural constitutive model of the vascular wall which integrates both waviness and orientational dispersion of collagen fibers. We extend the model of Zulliger et al., which already accounts for collagen waviness, to include orientational distribution of collagen. We study the effect of parameters related to the orientational

distribution on macro-mechanical behavior of the tissue during inflation-extension tests. The model is further applied to the experimental data from rabbit facial veins. The model accurately fits the experimental data of veins, but it does not improve the quality of the fit compared to the one without dispersion. We show that the orientational dispersion of collagen fibers can be compensated by a less abrupt and shifted to higher strain collagen engagement pattern. This should be taken into consideration when the model is used to fit experimental data and model parameters are used to study structural modifications of collagen fiber network in physiology and disease.

In the fourth paper, we measure and quantify the waviness and orientational distributions of collagen in rabbit carotids. Quantification of collagen orientation distributions at the zero stress state of arteries is needed to develop realistic and precise biomechanical models. Using the fluorescence collagen marker CNA38-OG488 and confocal laser scanning microscopy, we visualize collagen fibers in adventitia of rabbit common carotids *ex vivo*. To get the properties related to the zero stress state, the arteries are cut open along their longitudinal axes. We use semi-automatic and automatic techniques to measure parameters related to the waviness and fiber orientation. We show that the straightness parameter (i.e. the ratio between the distances of endpoints of a fiber to the fiber length) is distributed with a beta distribution. The shape of the probability density distribution does not depend on the mean angle orientation of fibers. In addition, our measurements reveal four axially symmetric families of fibers with mean orientations of  $0^\circ$ ,  $90^\circ$ ,  $43^\circ$  and  $-43^\circ$  and circular standard deviations of  $40^\circ$ ,  $47^\circ$ ,  $37^\circ$  and  $37^\circ$ , with respect to the axial direction, respectively. To the best of our knowledge, this is the first study focusing on structural properties of collagen in the zero stress state and quantifying fiber waviness. The results of this study can be used to develop more precise structural models of the adventitia including waviness and orientational dispersion of fibers.

The conclusion section summarizes the main results of the thesis, presents the improvements made over previous studies, and proposes future perspectives of this work.

**Keywords:**

structural modeling, strain energy function, constitutive modeling, vascular wall, arteries, veins, anisotropy, vascular structure, elastin, collagen, waviness, orientation

# Résumé

Ce travail, qui s'inscrit dans le cadre de la mécanique des milieux continus, traite essentiellement de la contribution de l'élastine et du collagène et de leur microstructure sur la mécanique de la paroi vasculaire. Les caractéristiques de ces éléments structurels sont déterminées par des techniques de microscopie et fournissent l'information nécessaire à l'élaboration de modèles constitutifs. Afin de décrire le comportement global du tissu vasculaire, ces modèles sont comparés à des données expérimentales issues d'essais de gonflement-traction. Cette thèse est rédigée sous la forme d'une introduction suivie de quatre chapitres (articles) et d'une conclusion.

L'introduction énumère les motivations de cette thèse, détaille la structure de la paroi vasculaire et de son comportement mécanique. Une brève description des techniques d'imagerie utilisées est également présentée. Enfin, l'accent est mis sur la modélisation des parois vasculaires et plus particulièrement de ses constituants principaux, l'élastine et le collagène.

Le premier article traite des propriétés anisotropiques de l'élastine des veines. En effet, la plupart des énergies de déformation élastique (SEF), qui sont pourtant dérivées d'information structurelle mais supposent l'élastine isotrope, ne décrivent que partiellement la réponse des tissus soumis aux essais de gonflement-traction. Le modèle précédemment développé dans notre laboratoire (Zulliger et al., 2004, *J. Biomech.*, 37(7): 989-1000 (2004)) est étendu afin d'inclure l'anisotropie de l'élastine sous forme d'une famille de fibre orientée dans la direction longitudinale. Le modèle est confronté à des données expérimentales issues d'essais de gonflement-traction sur des veines de lapin. La réponse passive du tissu, c'est-à-dire, lorsque les cellules musculaires lisses sont entièrement relâchées, est étudiée pour des elongations allant de 100% à 130% de la longueur physiologique. Le modèle anisotrope décrit avec succès les données et ceci pour la plage d'elongation considérée. Il en ressort que la description anisotrope de l'élastine est nécessaire pour une description tridimensionnelle de la paroi veineuse.

Le second article détaille le rôle de l'élastine et plus précisément l'importance de son organisation structurelle dans les propriétés anisotropiques des artères. Un modèle structurel anisotrope, comprenant une seule famille de fibres d'élastine orientée dans la direction circonférentielle de l'artère, est introduit. Cette configuration circonférentielle et interlaminaire de l'élastine est illustrée par des images prises par la microscopie électronique (MET et SBF-SEM). La contribution mécanique de l'élastine est étudiée par des essais de gonflement-traction menés sur des artères traitées ou non à l'élastase. Ces données sont également confrontées au modèle anisotrope qui permet une étude détaillée sur l'effet de la suppression de l'élastine. En effet, le modèle prédit un recrutement précoce des fibres de collagène dans les artères traitées à l'élastase. Il démontre clairement une interaction fonctionnelle entre l'élastine et le collagène, un aspect souvent négligé dans les énergies de déformation élastique structurelle.

Le troisième article introduit un modèle constitutif structurel de la paroi vasculaire qui comprend à la fois l'ondulation et la dispersion de l'orientation des fibres de collagène. Le modèle de Zulliger et al., qui tenait déjà compte de l'ondulation des fibres, est étendu en ajoutant une distribution de l'orientation des fibres de collagène. La sensibilité des paramètres de distribution sur la réponse mécanique du tissu, soumis à des essais de gonflement-traction, est étudiée. Ce modèle est ensuite confronté aux données expérimentales issues des

essais sur des veines de lapin. Le modèle décrit précisément les données expérimentales, mais n'améliore pas sensiblement la qualité de la description comparé au modèle sans dispersion des fibres. Une amélioration notable est observée lorsque la dispersion des fibres est remplacée par un modèle de recrutement de fibres moins abrupte et retardé vers des déformations plus importantes. Cette observation devrait être considérée lors de l'ajustement du modèle sur les données expérimentales. Plus particulièrement lorsque les paramètres du modèle sont utilisés pour étudier les modifications structurelles du réseau de fibre de collagène, lors de cas pathologique ou non.

Le quatrième article traite de la quantification de l'ondulation et de la distribution d'orientation du collagène dans l'adventice. Cette information est essentielle dans l'élaboration de modèles constitutifs structurels de la paroi vasculaire. Plus particulièrement, la quantification des distributions dans des tissus non contraints est nécessaire pour le développement de modèles réalistes. L'utilisation du microscope confocal et du marqueur de collagène fluorescent CNA38-OG488 permet de visualiser le collagène de l'adventice des artères de lapin. Afin d'obtenir des tissus non contraints, les artères ont été incisées le long de leur axe longitudinal. Des techniques semi-automatiques et automatiques ont été utilisées pour la mesure des paramètres liés à l'ondulation et à la distribution des orientations des fibres de collagène. Le paramètre de *straightness* (le rapport entre la distance qui sépare les extrémités d'une fibre avec la longueur de l'arc) a une distribution beta. La forme de la densité de probabilité ne dépend pas de l'orientation moyenne des fibres. Les mesures révèlent quatre familles de fibres axialement symétriques ayant des orientations moyennes (par rapport à l'axe longitudinal) de  $0^\circ$ ,  $90^\circ$ ,  $43^\circ$  et  $-43^\circ$  et une déviation standard circulaire de  $40^\circ$ ,  $47^\circ$ ,  $37^\circ$  et  $37^\circ$  respectivement. A notre connaissance, ceci est la première étude qui se concentre sur les propriétés structurelles du collagène du tissu non contraint et qui quantifie la distribution des fibres. Ces résultats permettent de développer des modèles structurels de l'adventice qui tiennent compte de la dispersion des orientations des fibres et de leur ondulation.

Enfin, la conclusion reprend les résultats principaux de la thèse, souligne les améliorations faites par rapport aux études précédentes et propose des perspectives de travaux futurs dans le domaine de la mécanique de la paroi vasculaire.

### **Mots-clé**

Modélisation structurelle, modélisation constitutive, artères, veines, paroi vasculaire, anisotropie, élastine, collagène, structure vasculaire, recrutement de collagène, ondulation, orientation

# Acknowledgements

I have been looking forward to writing this acknowledgement. Getting through my thesis, I became more and more conscious of all those people who supported me both scientifically and personally during my studies.

I would like to thank Prof. Nikos Stergiopoulos for giving me the opportunity to be a part of his laboratory. He provided me with the scientific advice and the enthusiasm without which this work could not be possible. Moreover, I would like to thank him for his encouragement and support to establish collaborations and for his friendship and understanding.

I would also like to thank the members of the jury for their time and expertise: Prof. Stephen Greenwald, Prof. Alexander Rachev, Prof. Dominique Pioletti and Prof. Vassily Hatzimanikatis.

My thanks also go to the people from Bioimaging and Optics (BIOP) and Bioelectron Microscopy (Bio-EM) core facilities at EPFL, specially Alessandra Griffa, J.C. Sarria (Floyd), Thierry Laroche, Dr. Graham Knott, Stephanie Rosset and Christel Genoud for their help on microscopy; Special thanks to Jelle T.C. Schrauwen and to Profs C.V.C Bouten & F.N. van de Vosse from technical university of Eindhoven, for it was a great pleasure to collaborate with them; thanks to Daniel Sage from biomedical imaging group for his ideas and expertise, to Prof. Demougeot from University of Besancon for our fruitful collaboration; Also, to Prof. Alain Curnier from institute of mechanical engineering at EPFL for the help and discussions on continuum mechanics and to Arne Vogel for the translation of the abstract to French.

And I owe certainly a great thank to the former and current LHTC people who made the lab a pleasant and challenging place to be; To Edouard for our daily endless conversations, to Rafaela for her joyful laughs and energy, to Dimitris for his sense of humor and his help on any mathematical question, to Philippe for his enthusiasm in science and engineering, to Tyler for his funny stories, to Tamina for our conversations on oriental medicine, to Michel for his good humor and technical help, to Sylvain for his scientific advice, to Martin for the discussions on modeling, also to Virginie, Fred, Bryn, Adan, Veronica, Aurelie, Orestis, Stephan, Aristotelis and Alkis.

Big thanks also to my friends in Lausanne and around the world. Without your friendship and support, my phd studies could not be so cheerful: to Rana, for our endless breakfast conversations and her sense of reality, to Mana for her unique personality and true friendship over years, to Sahar for her warm welcome upon my arrival in Switzerland and years of friendship that followed, to Basira for the joy of life and sound judgments, to Charlotte for her Belgian spirit and deep understanding, and to my old day friends: Farnaz, Elnaz, Shirin, Yalda, Samin, Zari, Paria, Mehran, Pary, Sareh, Ali and Ehsan who were always available for me.

Special thanks also to my Aunt Parvaneh, my cousin Mani and *ma francaise préférée* Camille for all the love and family spirit they have offered me. Also to Dominique & Jean-Pierre, Gianni, Luigi & Monica, Vanessa, Valentina, Antonino and Guilia for accepting me with open arms and making me feel like home in Switzerland; and of course, to Lilia for being the cutest little girl ever.

I would like to thank my parents for their endless love and support. The day my dad advised me to consider EPFL for graduate studies, I could not imagine that, 5 years later, I would

look back to this great experience with this personal satisfaction. Dad, without you and your trust in me, this thesis would have never been started. Mom, you gave me all the love and passion of learning I would need to reach here. Big thanks to my sister, Golnar, for the joy she brings constantly to me and all people around her.

Finally, and most importantly, I would like to thank my husband Sandro who has been a great source of support during this thesis. Sandro, thanks for listening, for your encouraging words, for your scientific enthusiasm, for all those weekends you spent proofreading my manuscripts and for all the passion and love you constantly bring to me.

# Contents

<b>Abstract</b>		<b>i</b>
<b>Résumé</b>		<b>iii</b>
<b>Acknowledgements</b>		<b>v</b>
<b>Introduction</b>		<b>3</b>
	Motivation	3
	Background	4
	Scope and overview	11
<b>Chapter 1</b>	A structural model of the venous wall considering elastin anisotropy	<b>19</b>
<b>Chapter 2</b>	Role of elastin anisotropy in structural strain energy functions of arterial tissue	<b>47</b>
<b>Chapter 3</b>	A structural constitutive model for vascular wall considering angular dispersion and waviness of collagen fibers	<b>69</b>
<b>Chapter 4</b>	Experimental investigation of collagen waviness and orientation in the adventitia	<b>87</b>
<b>Summary, conclusions and perspectives</b>		<b>111</b>
<b>Curriculum vitae</b>		<b>115</b>





# Introduction

---



# Motivation

## Clinical Motivation

Cardiovascular disease (CVD) is the number one cause of death worldwide. Only in Europe, CVD causes over 4.3 million deaths every year which is nearly half (48%) of all deaths. The mortality rate, on its own, would be a sufficient reason to investigate the cardiovascular system and its failures, but in addition to it, comes costs of healthcare, productivity losses and informal care of patients. Overall, CVD is estimated to cost the EU economy €192 billion a year [39].

## Cardiovascular Biomechanics

Biomechanics deals with the response of tissue to mechanical loads. Many clinical issues in cardiovascular physiology and pathology demand a detailed understanding of biomechanics. Some basic science issues and applied problems in cardiovascular solid mechanics are listed briefly in Figure 1. An example of these applications is the treatment of coronary artery disease. This disease results, in part, from the built-up of an atherosclerotic plaque within the inner layer of the arterial wall. Several clinical treatments such as balloon angioplasty rely on the mechanical modification or removal of these plaques. Therefore, a detailed understanding of the biomechanical properties of the diseased as well as the non-diseased portion of the arterial wall is needed to design improved interventional devices (e.g. balloon catheter used in angioplasty, atherectomy device for removing plaques, or intravascular stents for implantation) and the associated clinical protocols (eg. duration of inflation, size of the balloon or stent).

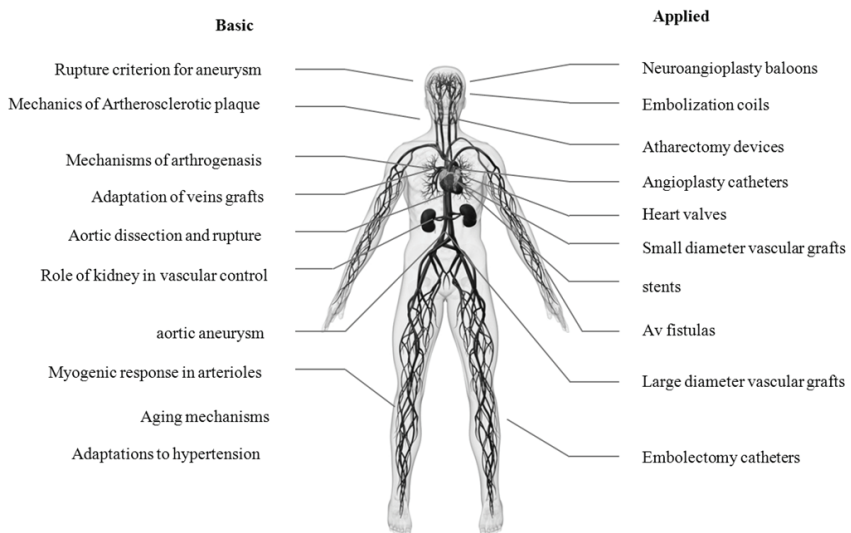


**Fig. 1 Some basic and applied clinical problems in solid biomechanics**

The mechanical behavior of vascular wall results from material properties, structural organization and interconnections of its constituents. A change in any of these factors affects the wall mechanics. Models of vascular wall based on composition and structural arrangement of the tissue try to give a detailed understanding of the function, structure and mechanics of vascular wall in health and disease. For instance, in case of aging, arteries become stiffer due to alterations in their morphology and the composition of their major structural constituents elastin and collagen. The elastic lamellae undergo fragmentation and thinning resulting in a transfer of mechanical load to collagen, a much stiffer protein than elastin. In addition, the remaining elastin becomes stiffer due to calcification and formation of cross-links (see Greenwald [18] for a detailed review on aging of conduit arteries).

In summary, a detailed knowledge of vascular mechanics based on structural organization of its wall components is required for understanding the physiology and pathophysiology of blood vessels. This provides the motivation for the further study of vascular biomechanics based on the wall structure.

## Background

Mechanical properties of a blood vessel results from its content, material properties, organization and interlinks of its constituents.

### Vascular Wall Structure

The wall of blood vessels consists of three layers i.e. the intima, the media and the adventitia (Figure 2). Regardless of the organization of layers, vascular wall is mainly composed of four building blocks: endothelial cells (ECs), elastin, collagen and smooth muscle cells (SMCs) [4].

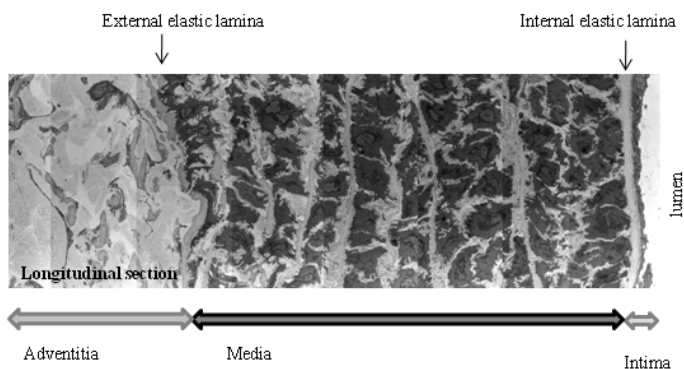


**Fig. 2** A longitudinal section of a rabbit common carotid artery showing three layers of the vascular wall i.e. the intima, the media and the adventitia. The intima and the media are separated by the internal elastic lamina while the media and the adventitia are separated by the external elastic lamina.

The intima is typically consisting of a monolayer of endothelial cells and an underlying fine basement membrane composed predominantly of type IV collagen [27]. Endothelial cells are usually flat and elongated in the direction of blood flow, often about 0.2 to 0.5  $\mu\text{m}$  thick, 10 to 15  $\mu\text{m}$  wide, and 25 to 50  $\mu\text{m}$  long [25]. The healthy intima contributes little structurally to the mechanical properties of blood vessels.

The media contains smooth muscle cells that are embedded in an extracellular matrix of elastin and collagen as well as a ground substance matrix containing proteoglycans. These constituents are organized in a complex 3D structure. Vascular smooth muscle cells are spindle-shaped, typically 100  $\mu\text{m}$  long and about 5  $\mu\text{m}$  in diameter. The smooth muscle cells are embedded in an extracellular matrix. An illustration of medial organization in the aorta is shown in Figure 3. In elastic arteries, medial smooth muscle is organized into 5 to 15  $\mu\text{m}$  thick concentric layers separated by thin fenestrated sheets of elastin as seen in Figure 4. Smooth muscle cells are surrounded by interlamellar collagen (primarily of Type I, III and IV) and elastin fibers. Elastin fibers run from laminae to the smooth muscle cells. Collagen fibers are wavy and run between elastic lamellae and smooth muscle cell layers. In muscular arteries, on the other hand, the smooth muscle appears as a single thick layer bounded by a thick internal and less marked external elastic lamina. Exceptions are the cerebral arteries which do not have an external lamina. Collagen fibers in the media are formed in wavy bundles [9] and the orientation of fibers is dispersed [34].

Finally, the adventitia, i.e. the outermost layer of the wall, consists primarily of a dense network of type I collagen fibers with admixed elastin, nerves, fibroblasts and the vasa vasorum. Collagen acting as a protective sheath, the adventitia is thought to limit acute over distension in blood vessel. Similarly to the collagen in the media, the adventitial collagen is wavy and its main orientation is distributed statistically. However, it has a higher angular dispersion [14] and forms thicker bundles compared to the collagen in the media. Wavy adventitial collagen bundles in common carotid arteries are shown in Figure 5.

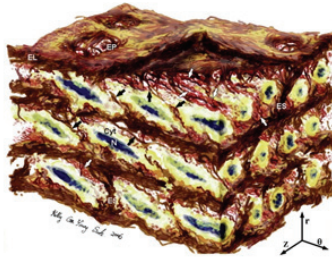


**Fig. 3** An illustration of the medial organization of rat aorta, using scanning electron microscopy. Elastin features include elastic lamellae (EL), dense network of interlamellar elastin fibers (IEF shown with black arrows), elastin struts (ES), and elastin pores (EP). Smooth muscle cell (SMC) oriented circumferentially with radial tilt. Collagen fibers are adjacent to lamellar surfaces, arranged in layers of parallel bundles [34].

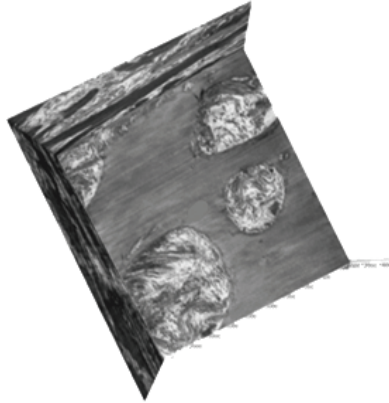


**Fig.4 Fenestrations in an elastin lamella of rabbit common carotid based on 3D serial block-face microscopy technique**

The basic structure of the veins is similar to that of the arteries. Compared to the arteries, the relative wall thickness is generally lower, and the media contains lower elastic tissue and the adventitia is relatively thicker [4].

The organization and direction of vascular smooth muscle cells, collagen and elastin fibers depend on various factors such as location along the vascular tree, species and local adaptations. For instance, in rat abdominal aorta SMCs lay in the circumferential direction [34], however in the abdominal vena cava and its main tributaries, and in mesenteric veins they are prominently longitudinal [15].

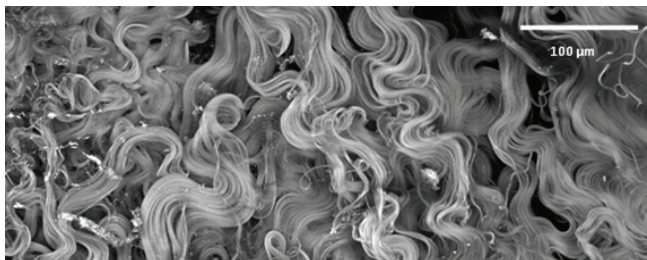


**Fig. 5 Collagen bundles on the adventitia of common carotid of rabbits. Collagen fibers are wavy and running in different directions.**

## Mechanical Properties of Blood Vessels

Vascular tissue has an inhomogeneous structure, undergoes nonlinear large deformations and shows anisotropic and viscoelastic behavior with strain rate insensitivity. Also, it is assumed to be incompressible as experimentally investigated by the work of Chuong and Fung [8].

Biological soft tissues are geometrically and mechanically nonlinear. Each structural component exhibits nonlinear behavior, and the nonlinearity is enhanced by the structure. Arteries are non-linearly elastic, becoming stiffer as they are distended, typically by a factor of 100 between mean pressures of 60 and 180 mmHg. In 1957 Roach and Burton proposed a qualitative model of arterial elasticity in which it was supposed that at low pressures (and therefore low degrees of circumferential stretch) tension is born by elastin while the much stiffer collagen fibers remain folded [37]. As pressure and stretch increases, the gradual unfolding collagen fibers take on an increasing fraction of the tension and the vessel becomes progressively stiffer, thus preventing over-distension at high pressures.

Collagen and elastin are intrinsically anisotropic [24]. In addition to their intrinsic properties, the fibers are also oriented in different directions to optimize the tissue functionality.

In the absence of smooth muscle tone, blood vessels exhibit hysteresis under cyclic loading, stress relaxation under constant extension, and creep under constant loads. Thus, vascular behavior is viscoelastic, although the viscoelasticity is relatively insensitive to changes in strain rate [10]. However, blood vessels also exhibit a nearly repeatable response to cyclic loading once they have been *preconditioned*. In physiological conditions, such repeated loading happens due to the periodic pumping of the heart. Therefore, Fung [15] proposed that vascular behavior may be regarded as *pseudoelastic* in many problems involving cyclic loading. This means that we can treat the material as an elastic material in loading and another elastic material in unloading. As Fung emphasizes, this is not an intrinsic property of the material, but a convenient description of the stress-strain relationship.

## Residual Stresses

Residual stress is the stress that exists in a body in the absence of externally applied loads. The excised intact, unloaded arterial ring opens up in response to a radial cut. The opening of the ring implies that the inner wall of the intact unloaded ring is in compression and the outer wall is in tension. Residual stresses can vary along the vascular tree on different locations and are different for inner and outer layers of arteries [19]. These residual stresses are quantified by the opening angle of the arteries.

## Mechanics of Vascular Wall Constituents

It is important to determine material properties of wall constituents to formulate structural-based stress-strain relations. This, however, is difficult in practice, given the complexity of the tissue structure and interactions.

One possible approach is to isolate the constituent of interest by removing selectively the unwanted constituents prior to testing. This is not as easy as it may sound. For instance, to isolate elastin, two basic ways have been used i.e using collagenase to digest collagen or exploiting the thermal stability of elastin. Among others, Lillie et al. [32] chose the latter based on prior studies that suggested the collagenase may affect the structure of elastin. They autoclaved samples of porcine aorta, to denature the collagen and kill the smooth muscle. Collagen denatures at many different temperatures, depending on the time of thermal

exposure and the mechanical load state during heating [7]. However, it is not clear that elastin does not denature, at least partially, under extreme conditions imposed in an autoclave [25]. As for the collagen, one could use enzymatic digestion of elastin [21, 28]. Again, however, it is not clear how well the isolated collagen reflects the properties of the native material. Following this method, Figure 6 shows the tension-extension curve of a fresh human iliac artery, taken from Roach and Burton [37]. When the artery is digested with trypsin to selectively remove elastin from the tissue, the tissue becomes less extensible. The slope of the curve is very similar to that of the non-treated, fresh tissue in the region of high tension. On the other hand, the selective removal of collagen with formic acid, results in a more extensible mechanical behavior with the slope of the curve, similar to that of the intact tissue in the small tension.

Other possible approach is to simply perform tests on tissues that are composed primarily of the constituent of interest. Figure 7 shows stress-strain relations for the canine nuchal ligament, sole tendon, and intestinal smooth muscle, which are rich in collage, elastin, and smooth muscle (cell), respectively, taken from a study by Hasegawa and Azuma (1974) [24]. The elastin-rich nuchal ligament has much less strength and much more extensibility than the collagen-rich sole tendon. The intestinal smooth muscle is much softer than the other two tissues, and its stress-strain curve has a wide hysteresis loop, which indicates that the tissue is viscoelastic. The elastic moduli calculated from these relations are approximately 0.4, 350, and 0.03 MPa in the nuchal ligament, sole tendon, and intestinal smooth muscle, respectively.

Therefore, the vascular wall behaves as a composite material made up of components having diverse properties. It is also important to consider which element is brought into action at what strain and what the structural organization of these components is.

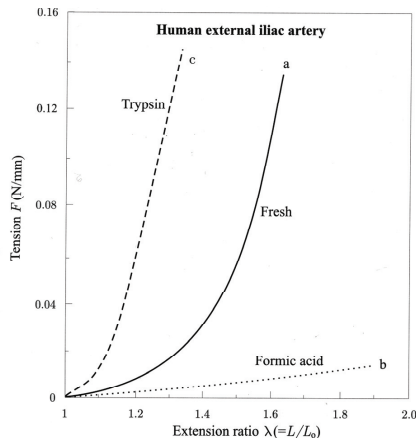


**Fig. 6 Tension extension ratio curves of fresh, formic acid-treated, and trypsin-treated arterial wall (Roach and Burton (1957))**



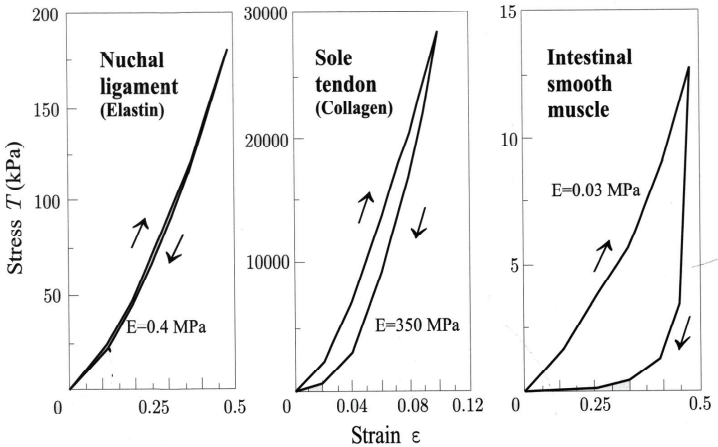


**Fig. 7 Tensile properties of elastin-rich canine nuchal ligament, collagen-rich sole tendon, and intestinal smooth muscle (Hasegawa and Azuma (1974))**

## Structural Modeling of Vascular Wall

Vascular tissue shows highly nonlinear and anisotropic characteristics and goes through large deformations. These properties make the use of strain energy formulation a suitable method to describe three dimensional mechanics of soft tissue. Many strain energy functions (SEF) have been developed for the description of soft tissue and in particular arteries. Early SEFs were purely phenomenological, i.e. they described the tissue behavior by some fairly arbitrarily chosen mathematical functions and coefficients. The best known phenomenological SEF for the description of soft biological tissue is the SEF by Chuong and Fung [16]. Recently, much effort has been put to develop strain energy functions that integrate information on composition and structural arrangements of tissue to avoid ambiguities in material characterization. In this way, they offer an insight into the function, structure and mechanics of the principal wall components, i.e. elastin, collagen and vascular smooth muscle cells (VSMCs). Structural constitutive models have been developed for a variety of tissues and tissue components including blood vessels [23, 42, 45], skin [33], pericardium [40], heart valves [13], tendons and ligaments [26].

### Elastin in Structure-Based Models of Vascular Wall

Elastin has been mainly considered as an isotropic material in structural models of vascular tissue. For instance, Holzapfel et al.[22] proposed a fiber reinforced continuum model for passive response of vascular wall with one isotropic and one anisotropic term. The anisotropic term was associated with the collagen fibers and the neo-Hookean isotropic term with other wall constituents. Zulliger et al. [44], similarly, divided the SEF into isotropic and anisotropic terms and explicitly associated the isotropic one to elastin. In these models, collagen is the only constituent which contributes to the anisotropic properties of the vascular tissue and elastin is considered as an isotropic material.

However, electron microscopy of arterial wall shows that vascular elastin is present in a complex 3D structure in three different features i.e. elastin sheets (lamellae), interlamellar elastin fibers and elastin struts. Also, there is evidence that the tissue behaves anisotropically at low strains, i.e. the elastin dominant region. The low strain modulus of porcine vascular tissue obtained from aorta, carotid, iliac and vena cava is reported to be different in the transverse and longitudinal directions [41]. Gundiah et al. [20] suggested material orthotropy for arterial elastin but concluded that a neo-Hookean isotropic model is suitable to describe the mechanics of arterial elastin. The results were based on uniaxial tests on isolated elastin from the swine thoracic aorta. Further histological and mechanical investigations are needed to clarify the role of elastin in anisotropic behavior of the tissue.

### **Collagen in Structure-based Models of Vascular Wall**

In blood vessels, collagen fibers are arranged in coiled and wavy bundles in their unloaded state [9, 12] and are dispersed around a mean orientation [6, 14]. In media, collagen fibers are strongly co-aligned [14]. However, within the adventitia layer, they show a large angular dispersion [14]. These properties result in highly nonlinear and anisotropic behavior of the vascular wall. The wavy nature of collagen fibers causes a gradual engagement of collagen. The directional organization of the fibers affects the anisotropic mechanical response of the tissue. A complete structural constitutive model for vascular collagen should incorporate both waviness and orientational distribution of fibers.

Many works on collagen modeling in soft tissue have followed an earlier work by Lanir for structural modeling of fibrous tissue [30, 31]. In this framework, the total SEF is assumed to be a result of the collective contribution of the individual fibers linked with tensor transformations from the fiber coordinates to the global tissue coordinates. Following this framework, some studies have incorporated waviness [44, 46] or orientational distribution of collagen fibers [2, 13, 40]. Other studies have followed a different approach and involved the use of invariants [17, 44, 46]. Yet, currently, there is no SEF for the vascular wall, which includes both waviness and angular distribution of collagen fibers and which has been verified using standard inflation-extension tests.

To include waviness and angular distribution of collagen fibers in constituent models, quantitative measurements of these parameters in the stress-free state as well as the loaded state are required.

### **Smooth Muscle in Structure-based Models of Vascular wall**

In this thesis, we focus on modeling of passive vascular wall, i.e. when smooth muscles are totally relaxed. In this state, following some earlier studies [10, 16], we assume that the effect of passive smooth muscle cells, on mechanical properties of the tissue, is negligible and that the passive response results solely from the mechanical properties of the intramural elastin and collagen.

Certainly, smooth muscle cells affect vascular behavior in their active state. Relatively, few studies have modeled active properties of vascular wall. Rachev and Hayashi [36] studied the effects of VSM on strain and stress distribution in the arterial wall using a SEF for passive stress to which an active stress with variable tone in the circumferential direction was added. Rachev and Hayashi [36] used their approach to modeling of the variations in opening angles with change in VSM tone. Following this study, Zulliger et al. [46] suggested a pseudo SEF describing the biomechanical properties of large conduit arteries under the influence of vascular smooth muscle tone. The model is composed of three parts associated with elastin, collagen and smooth muscle. The pseudo SEF models not only arterial mechanics at

maximum contraction, but also the myogenics contraction of the VSM in response to local increase in the stretch.

## Imaging Techniques

Visualization and quantitative characterization of structure and ultra-structure of the vascular wall is needed to develop structural models of vascular tissue. The mechanical properties of a material depend not only on its composition, but also on its structure and ultra-structure. Histological study of the contents is relatively easy, but a quantitative study of the structure is very difficult.

Different imaging techniques have been used to study the structure and ultra-structure of vascular tissue such as light and polarized light microscopy (LM and PLM) [6, 38], conventional laser confocal microscopy (LCM), two-photon microscopy [43], electron microscopy (EM), x-ray diffraction [1] and magnetic resonance imaging (MRI) [35]. Particularly, electron microscopy techniques have elucidated in detail the ultra-structure of vascular tissue [9, 34]. In addition, immunohistochemistry techniques have enabled scientists to visualize specifically the constituent of interest in the vascular wall. Here, we would briefly go through two main recent imaging methods used in this thesis to get the structural information of the tissue. The first method is the serial block-face scanning electron microscopy (SBF-SEM). This method was used in this study, to get ultra-structural information on the organization of arterial wall and more particularly elastin structure. The second method, involves confocal microscopy using CNA35, a new collagen specific fluorescent marker, which was used in this study, to visualize adventitial collagen.

In this study, the SBF-SEM has been used in chapter 2. The SBF-SEM technique was recently developed by Denk and Colleagues, to produce nano-structural information in three dimensions [5, 11]. The equipment consists of a scanning electron microscope (SEM) with an in-chamber ultra-microtome which repeatedly removes uniform sections from the specimen surface. Therefore, subsequent surfaces are exposed for block-face imaging by the SEM. The tissue block position is fixed and the image registration is inherent and image distortion (as in TEM) is absent, greatly simplifying volume reconstruction. O'Connell et al. [34] used this novel technique to obtain 3D volumetric information of aortic medial microstructure and described in detail the 3D organization of each wall element in rat abdominal aorta. The tissue fixation procedure is the same as the one used in TEM which enables conservation of geometry. The device offers great potentials to study ultra-structure of the blood vessels in health and disease.

In chapter 4, we have used the CNA35 collagen specific marker developed by Krahn et al. [29]. This probe is a new collagen fluorescence marker for tissues and live cell cultures which enables high resolution 3D imaging of collagen fibers in wet fresh tissues [3]. The CNA35 probe is specific for collagen and can reveal small collagen fibers as well as more mature structures in living tissues without altering collagen structure. Therefore, the probe could be used to visualize collagen fibers of blood vessels under various mechanical loadings which could be very useful to acquire the structural arrangement of collagen for modeling purposes.

## Scope and Overview

The overall aim of this thesis is to contribute to the field of structural constitutive modeling to describe passive behavior of vascular wall. We particularly focus on the role of elastin and collagen constituents to identify structural strain energy function of vascular tissue. Specific

aims of this thesis are a) to determine whether elastin should be considered as an anisotropic material, in definition of structural SEFs of vascular wall in veins, b) to answer the same question as above in arteries and to understand the underlying micro structural evidence, also to investigate the potential mechanical interactions between elastin and collagen, c) to develop a SEF for vascular wall which takes into account both waviness and orientational dispersion of collagen fibers and to parametrically study the gross mechanical response of the tissue under inflation-extension tests and d) to measure quantitatively the parameters related to waviness and orientational dispersion of adventitial collagen in the stress-free state of arteries.

## **1<sup>st</sup> Paper**

The 1st paper studies the necessity of including an anisotropic term to define structural strain energy functions of the tissue in veins. Venous wall is tested under a wide range of longitudinal stretches using the standard inflation-extension test. The experimental data provides a complete description of passive mechanical response of venous wall and is used to validate the suggested SEF. The structural SEF of Zulliger et al. [44] is extended to include an anisotropic term for elastin. The original and extended models are fitted to the experimental data to determine capabilities of these models to predict gross mechanical behavior of the tissue for a wide range of deformations.

## **2<sup>nd</sup> Paper**

In the 2<sup>nd</sup> paper, we investigate the role of elastin in anisotropic properties of arteries with particular attention to the structural organization of elastin and its interlinks with collagen. A structure-based model with an anisotropic elastin is presented. Micro-structural imaging based on electron microscopy techniques is used to investigate the anisotropic structure of elastin. Inflation–extension tests, on intact and elastase-treated arteries, provide a data set to validate the model and to study the effect of elastin removal in arteries.

## **3<sup>rd</sup> Paper**

The 3<sup>rd</sup> paper presents a structural constitutive model of the vascular wall which integrates information on both waviness and orientational distribution of collagen fibers. We extend the model by Zulliger et al. [44], which already accounts for the waviness, to include orientational distribution of collagen. We study the effect of parameters related to the orientational distribution on macro-mechanical behavior of tissue during inflation-extension tests. The model is further applied on experimental data from rabbit facial veins to study the necessity and suitability of adding orientational distribution.

## **4<sup>th</sup> Paper**

In the 4<sup>th</sup> paper, we measure and quantify the waviness and orientational distributions of collagen in the adventitia as needed to be integrated in structural models. We mark the collagen by the fluorescence collagen marker CNA38-OG488 to visualize collagen fibers in adventitia of arteries. To get the properties related to the zero stress state, the arteries are cut open along their longitudinal axes. We use semi-automatic and automatic techniques to measure parameters related to waviness and fiber orientation.

## Suggested Readings

The reader is referred to the following textbooks for an introduction to the basic principles of continuum mechanics and vascular wall constitutive modeling.

Biomechanics: Mechanical Properties of Living Tissue, Fung, Y. C., 1993, Springer-Verlag, New York.

Cardiovascular Solid Mechanics: Cells, Tissues, and Organs, Humphrey, J. D., 2002, Springer-Verlag, New York.

Biomechanics of soft tissue in cardiovascular systems, ed. by Holzapfel and Ogden, 2003, Springer, Wien

## References

1. **Bigi A, Ripamonti A, and Roveri N.** X-ray investigation of the orientation of collagen fibres in aortic media layer under distending pressure. *Int J Biol Macromol* 3: 287-291, 1981.
2. **Billiar KL, and Sacks MS.** Biaxial mechanical properties of the native and glutaraldehyde-treated aortic valve cusp: Part II--A structural constitutive model. *J Biomech Eng* 122: 327-335, 2000.
3. **Boerboom RA, Krahn KN, Megens RT, van Zandvoort MA, Merckx M, and Bouten CV.** High resolution imaging of collagen organisation and synthesis using a versatile collagen specific probe. *J Struct Biol* 2007.
4. **Boron WF, and Boulpaep EL.** *Medical Physiology: a cellular and molecular approach*. Philadelphia, Pennsylvania: Elsevier Saunders, 2005.
5. **Briggman KL, and Denk W.** Towards neural circuit reconstruction with volume electron microscopy techniques. *Curr Opin Neurobiol* 16: 562-570, 2006.
6. **Canham PB, Finlay HM, Dixon JG, Boughner DR, and Chen A.** Measurements from light and polarised light microscopy of human coronary arteries fixed at distending pressure. *Cardiovasc Res* 23: 973-982, 1989.
7. **Chen SS, and Humphrey JD.** Heat-induced changes in the mechanics of a collagenous tissue: pseudoelastic behavior at 37 degrees C. *J Biomech* 31: 211-216, 1998.
8. **Chuong CJ, and Fung YC.** Compressibility and constitutive equation of arterial wall in radial compression experiments. *J Biomech* 17: 35-40, 1984.
9. **Clark JM, and Glagov S.** Transmural Organization Of The Arterial Media - The Lamellar Unit Revisited. *Arteriosclerosis* 5: 19-34, 1985.
10. **Cox RH.** Passive mechanics and connective tissue composition of canine arteries. *Am J Physiol* 234: H533-541, 1978.
11. **Denk W, and Horstmann H.** Serial block-face scanning electron microscopy to reconstruct three-dimensional tissue nanostructure. *PLoS Biol* 2: e329, 2004.
12. **Dingemans KP, Teeling P, Lagendijk JH, and Becker AE.** Extracellular matrix of the human aortic media: an ultrastructural histochemical and immunohistochemical study of the adult aortic media. *Anat Rec* 258: 1-14, 2000.
13. **Driessen NJB, Bouten CVC, and Baaijens FPT.** A structural constitutive model for collagenous cardiovascular tissues incorporating the angular fiber distribution. *J Biomech Eng* 127: 494-503, 2005.
14. **Finlay HM, McCyflough L, and Canham PB.** Three-dimensional collagen organization of human brain arteries at different transmural pressures. *J Vasc Res* 32: 301-312, 1995.

15. **Fung YC.** *Biomechanics: Mechanical Properties of living tissues.* Springer-Verlag, 1981.
16. **Fung YC.** *Biomechanics: motion, flow, stress and growth.* New York: Springer-Verlag New York Inc. , 1990.
17. **Gasser TC, Ogden RW, and Holzapfel GA.** Hyperelastic modelling of arterial layers with distributed collagen fibre orientations. *Journal Of The Royal Society Interface* 3: 15-35, 2006.
18. **Greenwald SE.** Ageing of the conduit arteries. *The Journal of Pathology* 211: 157-172, 2007.
19. **Greenwald SE, Moore JE, Jr., Rachev A, Kane TP, and Meister JJ.** Experimental investigation of the distribution of residual strains in the artery wall. *J Biomech Eng* 119: 438-444, 1997.
20. **Gundiah N, B Ratcliffe M, and A Pruitt L.** Determination of strain energy function for arterial elastin: Experiments using histology and mechanical tests. *J Biomech* 40: 586-594, 2007.
21. **Hayashi K, Takamizawa K, Nakamura T, Kato T, and Tsushima N.** Effects of Elastase on the Stiffness and Elastic Properties of Arterial-Walls in Cholesterol-Fed Rabbits. *Atherosclerosis* 66: 259-267, 1987.
22. **Holzapfel GA, Gasser TC, and Ogden RW.** A new constitutive framework for arterial wall mechanics and a comparative study of material models. *Journal of Elasticity* 61: 1-48, 2000.
23. **Holzapfel GA, Gasser TC, and Stadler M.** A structural model for the viscoelastic behavior of arterial walls: Continuum formulation and finite element analysis. *European Journal of Mechanics, A/Solids* 21: 441-463, 2002.
24. **Holzapfel GA, and Ogden RW.** *Biomechanics of soft tissue in cardiovascular systems.* Udine: Springer Wien New York, 2003.
25. **Humphrey JD.** *Cardiovascular solid mechanics: cells, tissues, and organs.* New York Berlin Heidelberg: Springer-Verlag, 2002.
26. **Hurschler C, Loitz-Ramage B, and Vanderby R, Jr.** A structurally based stress-stretch relationship for tendon and ligament. *J Biomech Eng* 119: 392-399, 1997.
27. **Jacob MP.** Extracellular matrix remodeling and matrix metalloproteinases in the vascular wall during aging and in pathological conditions. *Biomed Pharmacother* 57: 195-202, 2003.
28. **Kitoh T, Kawai Y, and Ohhashi T.** Effects of collagenase, elastase, and hyaluronidase on mechanical properties of isolated dog jugular veins. *American Journal of Physiology - Heart and Circulatory Physiology* 265: H273-H280, 1993.
29. **Krahn KN, Bouten CV, van Tuijl S, van Zandvoort MA, and Merckx M.** Fluorescently labeled collagen binding proteins allow specific visualization of collagen in tissues and live cell culture. *Anal Biochem* 350: 177-185, 2006.
30. **Lanir Y.** Constitutive equations for fibrous connective tissues. *J Biomech* 16: 1-12, 1983.
31. **Lanir Y.** A structural theory for the homogeneous biaxial stress-strain relationships in flat collagenous tissues. *J Biomech* 12: 423-436, 1979.
32. **Lillie MA, Chalmers GW, and Gosline JM.** The effects of heating on the mechanical properties of arterial elastin. *Connect Tissue Res* 31: 23-35, 1994.
33. **Lokshin O, and Lanir Y.** Micro and macro rheology of planar tissues. *Biomaterials* 30: 3118-3127, 2009.
34. **O'Connell MK, Murthy S, Phan S, Xu C, Buchanan J, Spilker R, Dalman RL, Zarins CK, Denk W, and Taylor CA.** The three-dimensional micro- and nanostructure of

- the aortic medial lamellar unit measured using 3D confocal and electron microscopy imaging. *Matrix Biol* 27: 171-181, 2008.
35. **Pope AJ, Sands GB, Smaill BH, and LeGrice IJ.** Three-dimensional transmural organization of perimysial collagen in the heart. *American Journal of Physiology - Heart and Circulatory Physiology* 295: H1243-H1252, 2008.
  36. **Rachev A, and Hayashi K.** Theoretical study of the effects of vascular smooth muscle contraction on strain and stress distributions in arteries. *Ann Biomed Eng* 27: 459-468, 1999.
  37. **Roach MR, and Burton AC.** The reason for the shape of the distensibility curves of arteries. *Canadian journal of biochemistry and physiology* 35: 681-690, 1957.
  38. **Rowe AJ, Finlay HM, and Canham PB.** Collagen biomechanics in cerebral arteries and bifurcations assessed by polarizing microscopy. *J Vasc Res* 40: 406-415, 2003.
  39. **S. Allender, Scarborough P, Peto V, and al. e.** European Cardiovascular disease statistics 2008. edited by European Heart Network B2008.
  40. **Sacks MS.** Incorporation of experimentally-derived fiber orientation into a structural constitutive model for planar collagenous tissues. *J Biomech Eng* 125: 280-287, 2003.
  41. **Snowhill P, and Silver F.** A Mechanical Model of Porcine Vascular Tissues-Part II: Stress-Strain and Mechanical Properties of Juvenile Porcine Blood Vessels. *Cardiovascular Engineering* 5: 157-169, 2005.
  42. **Wuyts FL, Vanhuysse VJ, Langewouters GJ, Decraemer WF, Raman ER, and Buyle S.** Elastic properties of human aortas in relation to age and atherosclerosis: A structural model. *Phys Med Biol* 40: 1577-1597, 1995.
  43. **Zoumi A, Lu X, Kassab GS, and Tromberg BJ.** Imaging coronary artery microstructure using second-harmonic and two-photon fluorescence microscopy. *Biophys J* 87: 2778-2786, 2004.
  44. **Zulliger MA, Fridez P, Stergiopoulos N, and Hayashi K.** A strain energy function for arteries accounting for wall composition and structure. *J Biomech* 37: 989-1000, 2004.
  45. **Zulliger MA, and Stergiopoulos N.** Structural strain energy function applied to ageing and hypertension. *Arch Physiol Biochem* 112: 67, 2004.
  46. **Zulliger MA, Stergiopoulos N, and Rachev A.** A constitutive formulation of arterial mechanics including vascular smooth muscle tone. *Am J Physiol Heart Circ Physiol* 287: H1335-1343, 2004.





# Chapter 1

---



# A Structural Model of the Venous Wall Considering Elastin Anisotropy

Rana Rezakhaniha and Nikos Stergiopoulos

Hemodynamics and Cardiovascular Technology Laboratory  
School of Life Sciences-Institute of Bioengineering  
Ecole Polytechnique Fédérale de Lausanne (EPFL)  
Station 15, CH-1015 Lausanne

## Abstract

The three-dimensional biomechanical behavior of the vascular wall is best described by means of strain energy functions (SEF). Significant effort has been devoted lately into the development of structure-based models of the vascular wall, which account for the individual contribution of each major structural component (elastin, collagen, vascular smooth muscle). However, none of the currently proposed structural models succeeds in describing simultaneously and accurately both the pressure-radius and pressure-longitudinal force curves. We have hypothesized that shortcomings of the current models are, in part, due to unaccounted anisotropic properties of elastin. We extended the previously developed biomechanical model of Zulliger et al. (2004) to account for elastin anisotropy. The experimental data were obtained from inflation-extension tests on facial veins of five young white New Zealand rabbits. Tests have been carried out under a fully relaxed state of smooth muscle state for longitudinal stretch ratios ranging from 100% to 130% of the *in vivo* length. The experimental data (pressure-radius, pressure-force and zero-stress-state geometry) provided a complete biaxial mechanical characterization of rabbit facial vein and served as the basis for validating the applicability and accuracy of the new biomechanical model of the venous wall. When only the pressure-radius curves were fitted, both the anisotropic and the isotropic models gave excellent results. However, when both pressure-radius and pressure-force curves are fitted simultaneously, the model with isotropic elastin shows an average weighted residual sum of squares (WRSS) of 8.94 and 23.9, in the outer radius and axial force, respectively, as compared to an average of 6.07 and 4.00, when anisotropic elastin is considered. Both the Akaike information criterion (AIC) and Schwartz Criterion (SC) show that the model with the anisotropic elastin is more successful in predicting the data for a wide range of longitudinal stretch ratios. We conclude that anisotropic description of elastin is required for a full 3-D characterization of the biomechanics of the venous wall.

**Keywords:** rabbit veins, biomechanical properties, longitudinal stretch, elastin, anisotropy

Published in:

Journal of Biomechanical Engineering, 2008, 130 (3), art. no. 031017-1

## Introduction

The vessel wall exhibits relatively strong nonlinear properties during both loading and unloading procedures [1-6]. It has been shown that collagen and elastin fibers are the major passive components that support mechanical forces in the vessel wall [3]. Low strain characteristics are dominated by elastin fibers, whereas at high strains the progressive recruitment of much stiffer collagen fibers shifts the balance to a collagen-dominated regime [3, 5, 7]. Elastin, collagen and vascular smooth muscle content of vascular tissue can differ from one vessel to the other and from veins to arteries: veins have thinner walls, higher contents of collagenous (fibrous) tissue and lower contents of smooth muscle cells compared to arteries [8].

Identification of an appropriate strain energy function (SEF) is the preferred method to describe the complex nonlinear elastic properties of vascular tissues [9]. Once the strain energy function is known, the constitutive stress-strain relationships can be directly obtained from the SEF. Early formulations of SEFs were purely phenomenological, in the sense that parameters involved in the mathematical expression of the SEF had little physiological meaning [10, 11]. Lately, significant effort has been put into developing structure-based or constituent-based SEF, where the parameters of the strain energy function represent some identifiable physical and structural characteristics of the different components of the vessel wall, such as elastic constants of elastin and collagen, fiber structural characteristics of the collagen network, volume fraction of elastin, collagen and vascular smooth muscle cells, etc. An example of a SEF which considers some structural properties, i.e. the orientation of the collagen fibers relative to the arterial wall's circumferential direction is the model by Holzapfel and colleagues [4]. The Holzapfel et al.'s model has been subsequently modified and extended by Zulliger et al. to take the waviness of collagen fibers into account [9] and later to include vascular tone [12].

The structure-based SEFs did provide a significant improvement over the previous phenomenological ones, as this was evidenced via a better description of experimentally measured pressure-radius ( $P-r_0$ ) curves [9]. SEFs are meant, however, to provide for a complete 3-D description of the stress-strain field. For an axisymmetric vessel, this translates into a good description of both the pressure-radius ( $P-r_0$ ) and the pressure-longitudinal force ( $P-F_z$ ) curves, as those are measured in a typical inflation-extension experiment. However, all of the above structure-based models do a relatively poor job when are forced to describe simultaneously both the  $P-r_0$  and the  $P-F_z$  curves. This was true for arteries [9] as well as for veins (present study). Although the reason for this poor description is not clear, we hypothesize that one contributing factor is likely to be the anisotropic properties of elastin. Indeed, in previously proposed structure-based models, wall anisotropy has been assigned only to the collagen component and was modeled by taking into account the spatial dispersion or distribution of collagen fiber directions [4, 9, 13]. Further, all of the aforementioned structure-based models have assumed only isotropic properties for elastin, despite published observations of elastin anisotropy [14-18]. So, there is reasonable ground to suggest that accounting for the anisotropic properties for both elastin and collagen may be indeed necessary for better description of the 3-D biomechanical characteristics of the vascular wall. The present study was thus set to extend the structure-based SEF by Zulliger et al. in order to take into account the anisotropic properties of elastin and to quantify its improvement over previous SEFs using data derived from standard pressure-inflation tests.

## Methods

### Experimental setup

Five facial veins were harvested from white New Zealand rabbits weighing  $3 \pm 0.1$  kg. Their *in vivo* length as well as the length after excision was measured to determine the *in vivo* stretch ratios. The segments were transferred to the laboratory in flasks containing phosphate buffered saline (PBS) solution kept on ice. Immediately after arrival, the veins were cleaned and adventitia was removed manually. The segments were then mounted on our inflation-extension biomechanical testing device (Fig. 1) and bathed with PBS at  $37^\circ\text{C}$ . The segments were stretched to longitudinal stretch ratios corresponding to 100%, 115% and 130% of their *in vivo* stretch ratio.

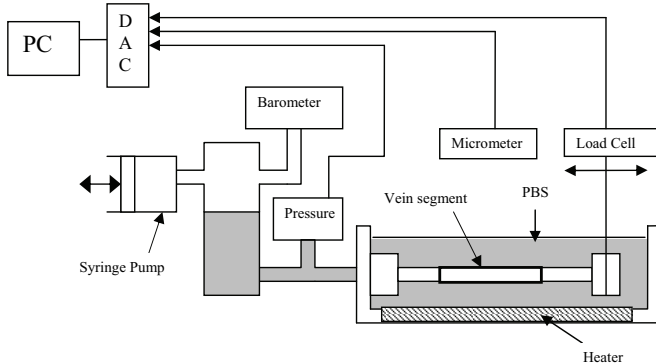


**Fig. 1: Schematic diagram of the experimental setup**

At each longitudinal stretch ratio, 10 preconditioning cycles were carried out to eliminate the transient and strain softening effects, resulting in a reproducible pressure-diameter curve. Next, the pressure-radius and pressure-longitudinal force curves were obtained by inflation of the vessels in the range of 0-14 mmHg at the rate of  $0.50 \pm 0.1$  mmHg/s. The external diameter was measured by a CDD micrometer (Keyence, LS-7030MT) and the longitudinal force by a load cell force transducer (FORT10, World Precision Instruments). Tests were carried out under a fully relaxed smooth muscle state, achieved by adding  $80 \mu\text{mol/L}$  of sodium nitro prusside (SNP) to the bath.

After the inflation-extension experiments, rings of  $0.4 \pm 0.1$  mm in thickness, were cut off from the middle part of the segments to measure the zero-load state (ZLS) geometry (Fig. 2a). Rings were kept at  $37^\circ\text{C}$  in a Petri dish with PBS for 20 min to reach an equilibrium state, and photographs were taken to measure ZLS parameters. The rings were subsequently cut longitudinally and kept for another 20 min in PBS at  $37^\circ\text{C}$  to measure the zero-stress state (ZSS) geometry, namely the radii  $R_i$  and  $R_o$  as well as the opening angle  $\Theta$  (Fig. 2a). Measurements were performed on images taken by an upright microscope (Axioplan 2 Imaging, Carl Zeiss Inc.). To approximate the fraction area ratios of the different components of the vessel wall, veins were fixed by 4% buffered Paraformaldehyde and stained by the Van Gieson and Resorcin-Fuchsin staining.

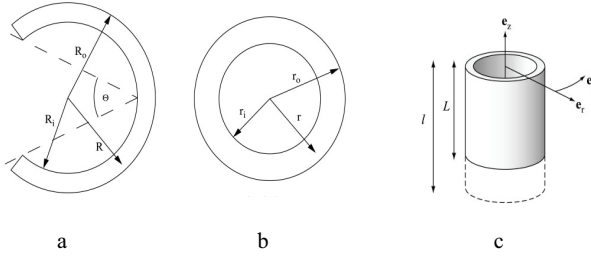


**Fig. 2: Schema of a) the Zero Stress State (ZSS) , b) the Zero Load State (ZLS) of a vessel and c) the choice of the coordinate system**

## Theoretical considerations

We consider the vessel as a hollow cylinder and assign the cylindrical coordinate system shown in Fig. 2c. The principal stretch ratios are defined by the following equation based on the zero stress state (ZSS) configuration of the vessel [19]:

$$\lambda_r = \frac{\partial r}{\partial R}, \quad \lambda_\theta = \frac{\pi}{\pi - \Theta} \frac{r}{R}, \quad \lambda_z = \frac{l}{L} \quad (1)$$

$\Theta$  is the opening angle,  $R$  the radius to a point in the ZSS, and  $r$  the radius to the same material point in the loaded state (Fig. 2),  $L$  the axial length of the segment in the zero stress state and  $l$  the loaded axial length. By considering material incompressibility, we obtain:

$$\lambda_\theta \lambda_z \lambda_r = 1 \quad (2)$$

Substituting relations (1) into (2) and integrating we obtain:

$$r = \sqrt{r_o^2 - \frac{(\pi - \Theta)L}{\pi l} (R_o^2 - R^2)} \quad (3)$$

Equation (3) provides with a mapping from any point in the ZSS to the corresponding point in the zero load state.

## Estimation of mean values of stresses and strains

In order to obtain an insight to the general behavior of the vessel wall, the mean values of stresses ( $\bar{\sigma}_\theta$  and  $\bar{\sigma}_z$ ) and strains ( $\bar{\lambda}_\theta$  and  $\bar{\lambda}_z$ ) are considered based on the formulae:

$$\bar{\sigma}_\theta = \frac{Pr_i}{h} \quad (4)$$

$$\bar{\sigma}_z = \frac{F_z + P\pi r_i^2}{2\pi \bar{r}h} \quad (5)$$

$$\bar{\lambda}_\theta = \frac{\pi}{\pi - \Theta} \frac{\bar{r}}{\bar{R}} \quad (6)$$

Where  $P$  is the intraluminal pressure,  $h$  the thickness of the vessel,  $F_z$  the longitudinal measured force,  $\bar{r}$  the mean radius of the vein, and  $\bar{R}$ , the mean radius in ZSS.

## Strain energy functions

We consider the vascular tissue as a thick-walled circular cylinder undergoing extension-inflation experiments, assuming finite hyperelastic stress response for the material.

In cylindrical coordinates and in the absence of torsion in inflation-extension tests,  $\lambda_r$ ,  $\lambda_\theta$  and  $\lambda_z$ , are the principal stretches of the deformation associated with the radial, circumferential and axial direction in the absence of twist which is the case in the extension-inflation test conditions. In this case, the off-diagonal terms of  $\mathbf{C}$ , the Right Cauchy-Green deformation tensor, and  $\mathbf{E}$ , the Green strain tensor vanish. (for more details see, for example, Holzapfel et al [4]). Expressed in cylindrical coordinates, principal stretch ratios and  $\mathbf{C}$ , the Right Cauchy-Green deformation tensor, relate to each other as:

$$C_{11} = \lambda_r^2 \quad C_{22} = \lambda_\theta^2 \quad C_{33} = \lambda_z^2 \quad (7)$$

Green strains are given by:

$$E_k = \frac{1}{2}(\lambda_k^2 - 1) \quad k = \theta, z, r \quad (8)$$

which form the diagonal elements of Green strain tensor defined as:

$$\mathbf{E} = \frac{1}{2}(\mathbf{C} - \mathbf{I}) \quad (9)$$

According to the objectivity condition, the SEF must be independent of the chosen coordinate system. Employing  $\mathbf{C}$  and its invariants automatically satisfies this condition.  $I_1$ , the first invariant of Cauchy-Green tensor, is defined as:

$$I_1 = \text{tr}(\mathbf{C}) \quad (10)$$

To incorporate the structural aspects of the collagen fiber network into the model, we introduce  $I_4$ , defined as a pseudo-invariant of the Cauchy-Green tensor with respect to the unit vector  $\vec{v}_\alpha$ , which defines the fiber orientation:

$$I_4 = \vec{v}_\alpha \cdot \mathbf{C} \cdot \vec{v}_\alpha \quad (11)$$

Assuming no torsion and  $\alpha$  being the angle between  $\vec{v}_\alpha$  and the  $e_\theta$  ( $\vec{v}_\alpha$  is assumed in the  $e_\theta$ - $e_z$  plane), we obtain:

$$I_4 = \lambda_\theta^2 \cos^2 \alpha + \lambda_z^2 \sin^2 \alpha \quad (12)$$

As seen from the above equation,  $I_4$  represents the square of the stretch in the direction of the collagen fibers. For a given SEF,  $\Psi$ , stresses are calculated as:

$$\sigma_k = -p + \lambda_k^2 \frac{\partial \Psi}{\partial E_k} \quad k = \theta, z, r \quad (13)$$

where  $p$  is the Lagrange multiplier associated with the incompressibility constraint and is referred to as the *arbitrary hydrostatic pressure* [20]. Boundary conditions are defined as:

$$\sigma_r(r_i) = -P \quad , \quad \sigma_r(r_o) = 0 \quad (14)$$

where  $P$  is the luminal pressure applied to the vessel. By integrating the equations across the vessel wall and applying the boundary conditions:

$$P = \int_{r_i}^{r_o} (\sigma_\theta - \sigma_r) \frac{1}{r} dr \quad (15)$$

$$F_z = \int_{r_i}^{r_o} \sigma_z 2\pi r dr - P_l \pi r_i^2 \quad (16)$$

$F_z$  represents the longitudinal force required to maintain longitudinal stretch applied to the vessel.

### Strain energy function with anisotropic elastin properties

Our work is an extension of the structure based SEF by Zulliger et al. [9, 12]. The model takes into account both the fraction of the total wall cross-section area composed of elastin,  $f_{elast}$ , and the corresponding fraction area composed of collagen,  $f_{coll}$ , to give the appropriate weight to the contribution of each constituent to the total SEFs.

$$\Psi_{passive} = f_{elast} \Psi_{elast} + f_{coll} \Psi_{coll} \quad (17)$$

Where  $\Psi_{passive}$  stands for the passive SEF, which assumes that vascular smooth muscle cells (VSMCs) are totally passive (no active tone),  $\Psi_{elast}$  the SEF for elastin and  $\Psi_{coll}$  the SEF for collagen.

In most of structural SEFs, as well as in Zulliger et al. model, elastin is considered to have isotropic properties. This is also the case in Holzapfel et al. [4], although Holzapfel et al. did not specifically attribute isotropy to elastin only. Gundiah et al. [21] proposed an orthotropic material symmetry for arterial elastin, comprising two equivalent orthogonal families of fibers, but a mathematical model accounting for this orthotropy was not developed. Further, earlier experimental work has shown that elastin possesses anisotropic-nonlinear properties [15, 22]. Our observations suggested a higher elastic modulus for elastin in the longitudinal direction as compared to the circumferential direction (see Results section). We have thus chosen a transversely isotropic SEF for elastin to account for its anisotropy. To describe the properties of the transversely isotropic material, we consider a material constructed from one family of axially oriented fibers continuously distributed in an isotropic matrix. To achieve this, we assumed that the wall elastin component has been divided into two parts. The first part, which constitutes our isotropic component, is assumed to be a randomly distributed network of elastin fibrils. The second part, which represents our anisotropic component, is an ensemble of elastin fibers oriented in the longitudinal direction. The total SEF will be the sum of the isotropic and anisotropic part:

$$\Psi_{elast} = \Psi_{iso}(I_1) + \Psi_{amiso}(I_4^n) \quad (18)$$

where,

$$I_4^n = e_z \cdot C \cdot e_z = \lambda_z^2 \quad (19)$$

For the isotropic component of elastin, we use the same SEF as in the Zulliger et al.'s model [9],

$$\Psi_{iso} = c_{elast}^i (I_1 - 3)^{3/2} \quad (20)$$



where  $c_{elast}^i$  represents the modulus for the isotropic elastin component. As for the anisotropic component, we assume the one dimensional form of an incompressible Neo-Hookean material for each fiber, undergoing a uniform cross-section deformation when stretched in the fiber direction. This brings us to the following formulation for the anisotropic part of the SEF:

$$\Psi_{aniso} = c_{elast}^a (I_4^n + \frac{2}{\sqrt{I_4^n}} - 3) \quad (21)$$

where  $c_{elast}^a > 0$  is an elastic constant enabling us to obtain a higher modulus for elastin in the z-direction.

As for the collagen, we keep the same definition as proposed by Zulliger et al [9, 12], which is presented in brief in the Appendix. Using the proposed anisotropic function for elastin and the original one for the collagen, the following SEF is obtained for the passive properties of the wall:

$$\Psi_{passive} = f_{elast} (c_{elast}^i (I_1 - 3)^{3/2} + c_{elast}^a (I_4^n + \frac{2}{\sqrt{I_4^n}} - 3)) + f_{coll} (\frac{1}{2} \Psi_{coll} (\frac{I_4 - 1}{2}) + \frac{1}{2} \Psi_{coll} (\frac{I_4' - 1}{2})) \quad (22)$$

For an incompressible material, the chosen SEF has to meet the following conditions [23]:

1. *Objectivity*: the material properties should be independent of chosen coordinates. This condition is automatically fulfilled by defining SEFs as a function of invariants of C (Right Cauchy-Green deformation tensor)
2. *Stress free reference*: The reference geometry should be stress free.
3. *Convexity*:  $\Psi = 0$  should be a global minimum at zero stress strain conditions. This is fundamental for the existence and uniqueness of the solution.

Zulliger et al. have demonstrated the convexity of their SEF function. The present SEF is formed by simply adding one extra term,  $\Psi_{aniso}$  yielding the following form:

$$\Psi_{passive} = \Psi_{passive}^Z + \Psi_{aniso} \quad (23)$$

where  $\Psi_{passive}^Z$  is the SEF of Zulliger et al.. As seen in Eq. 21,  $\Psi_{aniso}$  represents a Neo-Hookean material and therefore is by default convex for  $c_{elast}^a > 0$ . By using the additivity concept [24], one may deduce that the new SEF,  $\Psi_{passive}$  is also convex. Moreover, it is clear that in zero strain conditions i.e  $I_1 = 3$ ,  $I_4 = I_4' = I_4^n = 1$ , the SEF has a zero value.

## Numerical fitting of experimental data

Radius-pressure and longitudinal force-pressure curves were fitted to experimental data by minimizing the following function:

$$\Phi = \frac{1}{2} \frac{1}{mn} \sum_{i,j}^{m,n} \left( \frac{r_{ij}^{mod} - r_{ij}^{exp}}{\sigma_{ij}^r} \right)^2 + \frac{1}{2} \frac{1}{mn} \sum_{i,j}^{m,n} \left( \frac{F_{ij}^{mod} - F_{ij}^{exp}}{\sigma_{ij}^F} \right)^2 \quad (24)$$

In the above formulation,  $m$  is the number of experimental points measured at different pressures at a given longitudinal stretch ratio and  $n$  is the number of different longitudinal stretch ratios. Superscript *mod* denotes the values predicted by the mathematical model whereas superscript *exp* denotes those measured experimentally. Indices  $i$  and  $j$  denote the pressure and longitudinal elongation at which the corresponding outer radius,  $r$ , and longitudinal force,  $F$ , were obtained.  $\sigma$  is the standard deviation of the experimental mean value of radius or force at a given pressure and longitudinal stretch ratio. It is used as a weighting factor, giving more weight to the points with the least variation.

The fitting procedure yields the best estimates for five parameters. These include the two elastic constants  $c_{elast}^r$  and  $c_{elast}^a$  for elastin, two variables describing the engagement distribution function of collagen ( $k$  and  $b$ ) and the fiber orientation of collagen ( $\alpha$ ). The elastic constant of collagen was chosen as  $c_{coll} = 200$  MPa, a reasonable value taken from the literature and in accordance to Zulliger et al. [9].

In order to check the goodness of the fit, the weighted residual sum of squares for radius and force,  $WRSS^r$  and  $WRSS^F$  have been calculated based on the following formulae:

$$WRSS^k = \sum_i^m \left( \frac{k_i^{mod} - k_i^{exp}}{\sigma_i^k} \right)^2 \quad k = r, F \quad (25)$$

A measure of the mean values of  $WRSS$  over different stretch ratios is given by:

$$\overline{WRSS^k} = \frac{1}{n} \sum_j^n WRSS_j^k \quad k = r, F \quad (26)$$

### Comparison of the anisotropic and isotropic model

The present anisotropic model contains one more parameter when compared to the previous isotropic Zulliger et al.'s model. It is therefore expected that the  $WRSS$  will be smaller in the anisotropic one. To account for this difference in the number of free parameters, the Akaike and Schwarz criteria have been used to compare the two models. In both of these criteria, there is a 'penalty' function proportional to the number of free parameters ( $L$ ) in the model so that the  $WRSS$  is appropriately adjusted for the amount of free parameters used in the fitting process. The Akaike and Swartz criteria are computed as [25]:

$$AIC = m \ln(WRSS) + 2L \quad (27)$$

$$SC = m \ln(WRSS) + L \ln(m) \quad (28)$$

In the above equations,  $L$  denotes the number of free parameters in the model. The model with the smallest  $AIC$  and  $SC$  is considered superior.

## Results

### Zero stress state data

The average opening angle was  $\Theta = 115 \pm 12^\circ$ . The average inner and outer arc length were found to be  $L_i = 9.72 \pm 0.83$  mm and  $L_o = 10.8 \pm 0.83$  mm, respectively. The mean *in vivo* stretch ratio was  $\lambda_c = 1.62 \pm 0.09$ .

## Pressure-radius and longitudinal force-pressure data

The experimental results from our inflation-extension tests for 100% to 130% of *in vivo* longitudinal stretch ratio are shown in Fig. 3. The pressure-diameter curves exhibit a typical S-shape, with the elastin-dominated zone (convex part of the curve) being limited to pressures between 0 and 3 mmHg. At higher physiological pressures, collagen fibers begin to engage, limiting the maximal diameter extension. This diameter limitation appears to be more abrupt at lower longitudinal stretch ratios as opposed to more gradual at higher values of  $\lambda_z$ .

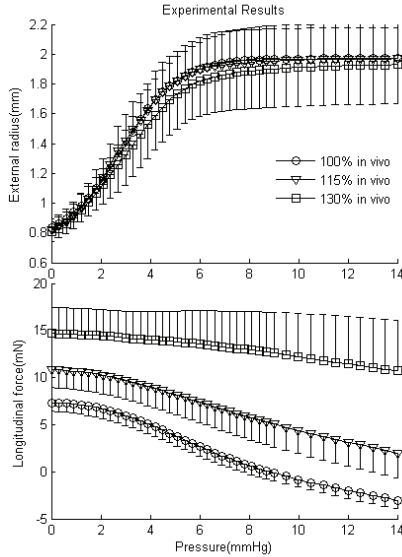


**Fig. 3 :** Experimental diameter-pressure and longitudinal force-pressure data of the rabbit facial veins at different stretch ratios. Error bars denote standard deviations.

It can be also seen in Fig. 3 that the longitudinal stretch of the veins from 100% to 130% of their *in vivo* longitudinal length decreases the diameter over the entire pressure range. Longitudinal force appears to be fairly constant in the low-pressure zone ( $p < 3$  mmHg), despite a significant diameter (therefore circumferential strain) increase within the same low pressure range (0 to 3 mmHg), where the diameter attains about half of its maximal increase.

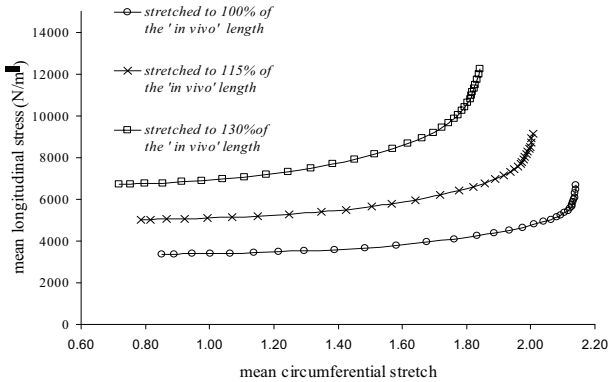


**Fig. 4: The longitudinal stress versus the circumferential stretch for different longitudinal stretch ratios.**

To get a better insight into the potential anisotropic behavior of the venous wall, graphs of mean longitudinal stress  $\bar{\sigma}_z$  versus the mean circumferential stretch ratio  $\bar{\lambda}_\theta$  (Fig. 4) and vs. longitudinal stretch ratio  $\bar{\lambda}_z$  (Fig. 5) were obtained. These figures suggest that at low strains, longitudinal stress is fairly independent of circumferential strain. Moreover, based on Fig. 5, for low circumferential strains ( $\bar{\lambda}_\theta < 1.2$ ), the relationship between  $\bar{\sigma}_z$  and  $\bar{\lambda}_z$  is almost linear, over the entire range of  $\bar{\lambda}_z$ . Therefore, venous tissue shows an anisotropic behavior in not only high strain region (due to collagen) but also in low strain region where elastin is the main functional component. This strengthened our hypothesis (see Methods) that, in the low strain region, elastin, which is the dominant constituent, may be modeled as a composite material with a family of fibers in z-direction with linear stress-strain relationship. This approach is mainly based on the fact that  $\sigma_z$  depends fairly linearly on  $\lambda_z$  and is almost independent of  $\lambda_\theta$  in this region.

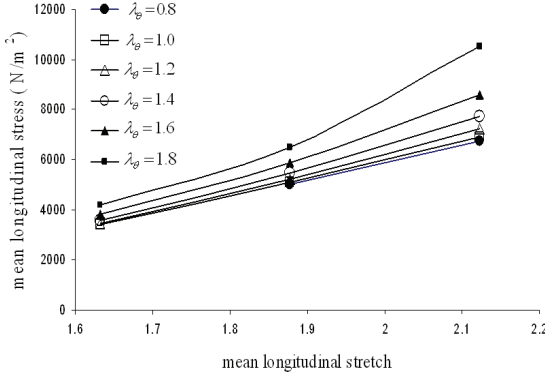


**Fig. 5: longitudinal stress versus longitudinal stretch ratio for different circumferential stretch ratios.**

## Radius-pressure and longitudinal force-pressure data as fitted by the isotropic and anisotropic model

Fig. 6a illustrates the data which was fit based on the Zulliger et al.'s SEF only when the radius-pressure data have been considered in the fit and no weight is assigned to the  $P-F_z$  data. In this case, the Zulliger et al.'s model resulted in an excellent fit ( $\overline{WRSS}^F = 4.150$ ) for the  $P-r_o$  data, however, it underestimated substantially the  $P-F_z$  curve ( $\overline{WRSS}^F = 57.7$ ) as seen in the figure. Figure 6.b shows the result when both the  $P-r_o$  and  $P-F_z$  have been fitted simultaneously using original Zulliger et al.'s model. While the quality of  $P-F_z$  fit is improved ( $\overline{WRSS}^F = 28.5$ ), there are still problems fitting both curves to the data at the same time. This shows that although the original Zulliger et al. model can describe very well the  $P-r_o$  data on its own, it falls short when both the  $P-r_o$  and  $P-F_z$  data are included. Fig. 6.c shows fits of the data based on our proposed model ( $\overline{WRSS}^r = 3.77$ ,  $\overline{WRSS}^F = 1.16$ ). It can be seen that the proposed anisotropic model can very well describe both  $P-r_o$  and  $P-F_z$  data simultaneously.

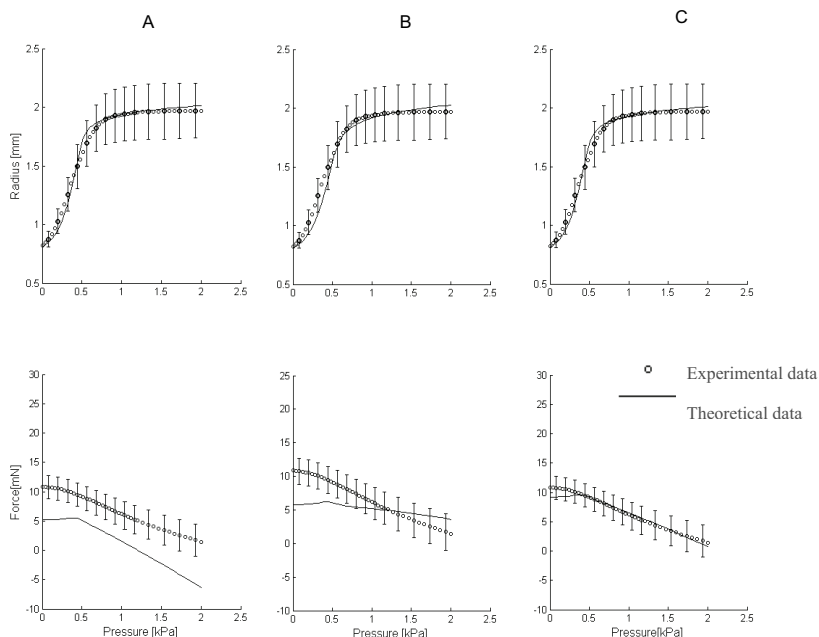


**Fig. 6: Fit of the experimental pressure-radius (top row) and pressure-longitudinal force (bottom row) curves by the isotropic and anisotropic model under 115% of *in vivo* longitudinal stretch ratio. Column (a) shows the fit of the isotropic model when only the radius-pressure data are used to fit the data. Column (b) shows the fit of the isotropic model when both the radius-pressure and force-pressure curves are fit. Column (c) shows the fit of the model with anisotropic elastin properties when fit to both pressure-radius and pressure-force data**

**Table 1: parameters used in minimizing  $\Phi$** 

strain energy function	original model	modified model
fitted parameters	$c_{elast} = 7120 \text{ Pa}$	$c_{elast}^i = 6302 \text{ Pa}$
	$k = 11.1$	$c_{elast}^a = 9076 \text{ Pa}$
	$b = 2.77$	$k = 11.6$
	$\alpha = 0.68 \text{ rad}$	$b = 2.82$
		$\alpha = 0.57 \text{ rad}$
experimentally defined parameters	$f_{elas} = 0.101$	$f_{elas} = 0.101$
	$f_{coll} = 0.482$	$f_{coll} = 0.482$
imposed on model	$c_{coll} = 200 \text{ MPa}$	$c_{coll} = 200 \text{ MPa}$
$\Phi$	0.48640	0.1616

The influence of longitudinal stretch on the goodness of fit of both the isotropic and anisotropic model is shown in Fig. 7 and 8, respectively. The fitted data set included all pressure-radius and pressure-longitudinal force data for longitudinal stretch ratios of 100%, 115% and 130% of the *in vivo* value. The fit of the isotropic model yielded  $\overline{WRSS^r} = 8.94$ ,  $\overline{WRSS^F} = 23.9$  and  $\Phi = 0.486$ . The fit based on the modified model with anisotropic elastin for the same longitudinal stretch ratios gave smaller weighted residual sum of squares ( $\overline{WRSS^r} = 6.07$ ,  $\overline{WRSS^F} = 4.00$ ) as well as a smaller overall cost function value  $\Phi = 0.162$ . From Fig. 8, it can be seen that the suggested model is able to fit well both the radius and longitudinal force data at the same time. The goodness of fit was confirmed over a wide range of stretch ratios. The parameters obtained from the fit are shown in Table 1 for both the original and modified models.

Values for quantifying the goodness of fits (WRSS) as well as those used for comparison of two models (*AIC* and *SC* numbers) for each longitudinal stretch ratio and their average over the total range are given in Table 2. Based on this table, both *AIC* and *SC* values favor the new model with the anisotropic elastin term. Take for instance values corresponding to experimental data from longitudinal stretch ratio of 115% of *in vivo* state. The *WRSS* for radius and axial force has been reduced by 53% and 94%, respectively, while, at the same time, the Schwarz criteria shows a reduction of 27% and 82% for radius and longitudinal force. Similar reduction applies also to the Akaike criterion, showing that, despite the penalty paid for the extra parameter, the “adjusted” *WRSS* is lower in the new model.

**Table 2: Comparison of two models**

100% of <i>in vivo</i> stretch ratio	Original model			Modified Model		
number of free parameters	4			5		
	radius	force	total	radius	force	total
<i>WRSS</i>	4.93	37.8		4.06	10.6	
<i>AIC</i>	76.6	164		70.3	112	
<i>SC</i>	83.7	171		79.1	120	
$\Phi$			0.462			0.187
115% of <i>in vivo</i> stretch ratio	Original model			Modified Model		
number of free parameters	4			5		
	radius	force	total	radius	force	total
<i>WRSS</i>	8.06	20.4		3.77	1.16	
<i>AIC</i>	97.8	138		67.0	16.5	
<i>SC</i>	105	145		75.8	25.4	
$\Phi$			0.338			0.0817
130% of <i>in vivo</i> stretch ratio	Original model			Modified Model		
number of free parameters	4			5		
	radius	force	total	radius	force	total
<i>WRSS</i>	13.8	13.3		10.4	0.238	
<i>AIC</i>	121	119		110	-51.7	
<i>SC</i>	128	127		119	-42.9	
$\Phi$			0.324			0.129
all the stretch ratios	Original model			Modified Model		
number of free parameters	4			5		
	radius	force	total	radius	force	total
<i>WRSS</i>	8.94	23.9		6.07	4.00	
<i>AIC</i>	98	140		82.6	25.5	
<i>SC</i>	105	147		91.4	34.3	
$\Phi$			0.486			0.162



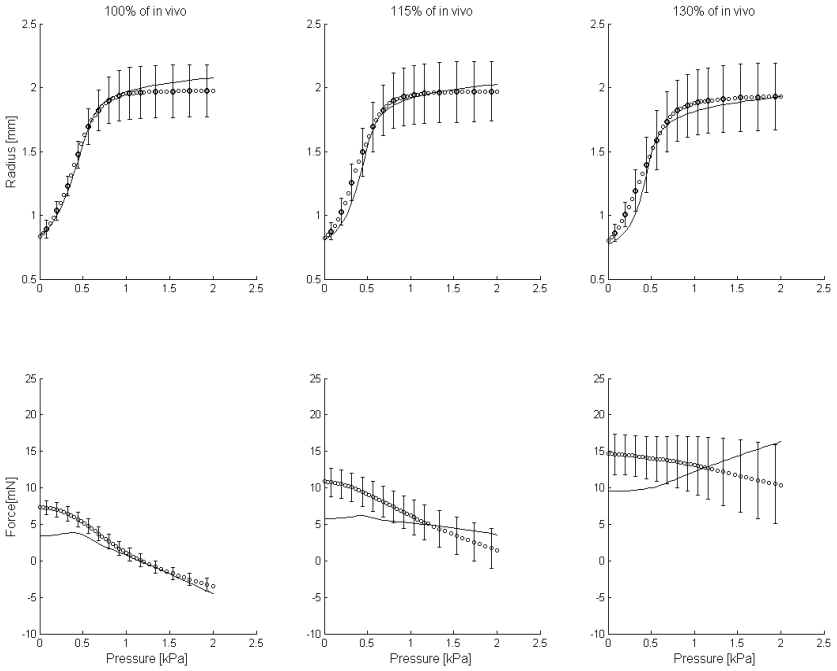


**Fig. 7: Fit of the original isotropic SEF to the entire experimental data set, including three different stretch ratios. The top row shows the radius-pressure data and the lower row the longitudinal force-pressure data.**

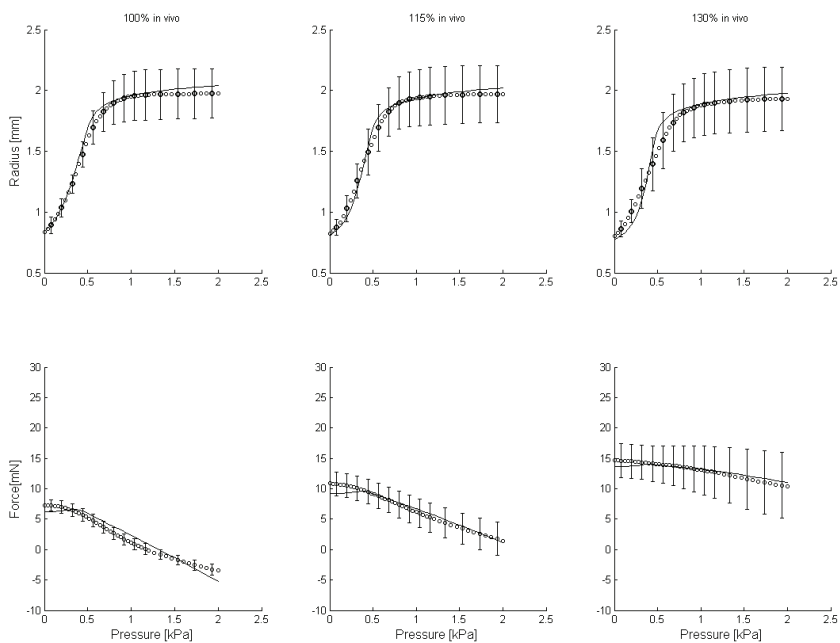


**Fig. 8:** Fit of the new anisotropic SEF to the entire experimental data set, including three different stretch ratios. The top row shows the radius-pressure data and the lower row the longitudinal force-pressure data.

## Discussion

There are a significant number of earlier studies on the biomechanical properties of vascular tissues and their mathematical descriptions. Most of these studies focus on the properties in the circumferential direction, often neglecting the longitudinal behavior of the vessel wall. However, the longitudinal characteristics of vessels are altered in many pathophysiological conditions such as aging [26, 27], hypertension [28] and atherosclerosis [29, 30] and play an important role in the overall biomechanical behavior of the vascular wall. In this study, we develop a structural strain energy function that describes simultaneously both the circumferential and longitudinal properties of the vascular wall.

To describe the mechanical behavior of soft tissue using a SEF, two general approaches exist: phenomenological and structural. In phenomenological approaches, the general mathematical form of the SEF is appropriately chosen to reflect the biomechanical behavior of the wall but the parameters of the SEF do not necessarily have any physical meaning. In structural or constituent-based approaches, care is taken so that each wall constituent is accounted explicitly for its contribution to the SEF and that parameters correspond to some physical properties of the tissue (i.e. wall fractions of elastin and collagen, elastic modulus, angle of orientation of collagen fibers, etc.). The present model is an extension of the structural model of Zulliger et al. [9], where elastin and collagen contribute in parallel and independently to the overall SEF. Vascular smooth muscle (VSM) is neglected here. As for the collagen part, the model follows the original approach of Zulliger et al., in which each collagen fiber is modeled as an elastic material and the engagement of fibers is taking place gradually and according to some stochastic distribution of the collagen fiber waviness. The form of the log-logistic distribution function of the collagen engagement is somehow arbitrary and certainly not unique, the choice been motivated by the goodness of the fit to a wide range of experimental data [9, 12, 31-33]. For the sake of simplicity and for keeping the number of free parameters of the model to a minimum, we fixed the elastic constant of a single collagen fiber to  $c_{\text{coll}} = 200$  MPa, which is in accordance to values reported in the literature. Another important parameter describing collagen properties is the collagen fiber orientation angle  $\alpha$ . Experimental assessment of the collagen fiber orientation within the tissue is difficult. In our study, the angle that best fit the experimental data was  $32.6^\circ$ . Holzapfel et al. have chosen a similar angle of  $29^\circ$  in their original model [4], Driessen et al. have taken  $\alpha=30^\circ$  for the media layer [13]. Zulliger et al. found this angle to be  $35.0^\circ$  in porcine carotid arteries [9]. Therefore, the angle obtained here seems to lie within the range of previously reported studies. In order to assess the sensitivity of the fit to the collagen fiber angle, this parameter was allowed to vary within the physiological range of  $25^\circ$  to  $35^\circ$ . Table 3 displays values of  $\Phi$  for different angles. This data shows a maximum change of 3% in  $\Phi$ , for an angle variation of 5% around the optimal value (ranging from  $31^\circ$  to  $34^\circ$ ), suggesting that changes of the angle in this range does not alter significantly the quality of the fit. Although further changes in the angle may lead to relatively weaker quality of the fit. For instance at  $35^\circ$ ,  $\Phi$  shows already an increase of 9% in its value.

**Table 3: Sensitivity of the quality of fit to changes in collagen fiber angle**

collagen fiber angle	goodness of fit ( $\Phi$ )
25	0.253
27	0.217
29	0.187
31	0.167
32.6	0.162
33	0.163
35	0.177

To quantify the degree of elastin anisotropy and to facilitate the comparison with other studies, we have linearized the stress-strain relationship around a physiological operational point ( $P = 3.6 \text{ mmHg} = 300 \text{ Pa}$ ), in order to obtain the Young's modulus from our model parameters. The stress-strain relationship for elastin in circumferential direction is given by:

$$\sigma_{\theta} = -p + \lambda_{\theta}^2 \frac{\partial \Psi_{elast}}{\partial E_{\theta}} \quad (29)$$

We fix  $\lambda_z$  to the mean *in vivo* longitudinal stretch ratio of 1.62, which for a pressure  $P = 3 \text{ mmHg}$  gives a  $\lambda_{\theta} = 1.68$ . By linearizing Eq. 28 with respect to  $\lambda_{\theta}$ , setting  $c_{elast}^i = 6302 \text{ Pa}$  and  $c_{elast}^a = 9076 \text{ Pa}$  (Table 1), we obtain the elastin modulus in the circumferential direction as being equal to 136 kPa.

Similarly, for the longitudinal direction we have:

$$\sigma_z = -p + \lambda_z^2 \frac{\partial \Psi_{elast}}{\partial E_z} \quad (30)$$

By fixing  $\lambda_{\theta} = 1.68$  as above and linearizing with respect to  $\lambda_z$  to get the Hooke's law at the *in vivo* longitudinal stretch ratio of 1.63, we find an elastic modulus of about 196 kPa for the longitudinal direction. Published data for the elastin Young modulus of ligamentum nuchae vary between 100 kPa to 1 MPa [34, 35]. Studies on porcine vascular tissue under low strain conditions suggest an elastin Young modulus between 30 to 300 kPa [17, 35, 36]. Therefore, our estimates for the circumferential and longitudinal Young's modulus of elastin are within the range previously published in the literature.

Different formulations have been attributed to the isotropic constituent of vascular tissue, which in some studies, was not identified solely as elastin (see, for instance, Holzapfel et al.[4]). Zulliger et al. considered an isotropic part of the arterial wall for elastin alone [9]. Their SEF was nonlinear with respect to  $I_1$  (first invariant of Cauchy-Greens strain tensor). In our work, we have adopted the Zulliger et al.'s nonlinear form for the elastin SEF. We have, however, attempted to use a simpler New Hookean function for the isotropic term of elastin

and fit the model to our experimental data, but this simpler approach failed to reproduce faithfully the initial phase of both the pressure-radius and pressure-longitudinal force data simultaneously. It is also worth mentioning that the improvement observed on the fit quality of Zulliger et al.'s model after including anisotropy for elastin was also observed on other vascular wall models. For example, when the same type of anisotropy for elastin was applied to Holzapfel et al.'s model (one family of fibers in the z-direction as given by equation (21)), a significant improvement in the quality of fit was observed with  $\Phi$  being reduced by 75%.

It should be noted, nevertheless, that the choice of collagen SEF may affect the success of the global fit for a given SEF form of elastin. This may mean that, despite a good global fit, our SEF may not necessarily be the absolute best model for the elastin alone. In a recent study, Gundiah et al. [21], have observed that a neo-Hookean model gives excellent results for pure elastin. One possible reason for this effect is that collagen may contribute in the low-pressure (strain) region, thus affecting the supposedly elastin dominated region and forcing the elastin SEF to take a form somewhat different from that of a pure elastin. Moreover, the choice for the exponent (3/2) in the elastin SEF was purely empirical and was based on the best fit results.

The choice of isotropic versus anisotropic strain energy function for elastin based on its 3D ultrastructure has been a controversial issue. While in some species, including man, the individual fibers appear to coalesce to form continuous, uninterrupted sheets, other studies in the pig aorta show that the medial elastic fibers retain their individuality and do not form sheets [18, 37]. Furthermore, the low strain modulus of porcine vascular tissue obtained from aorta, carotid, iliac and vena cava is reported to be different in the transversal and longitudinal directions [17], suggesting the existence of anisotropy in the low strain region, where elastin is the dominant component. In contrast, earlier studies have reported random coil structure [38, 39] as well as elastin isotropy [40]. Moreover, as mentioned above, Gundiah et al. have shown recently that purified elastin from pig thoracic arteries can be described by an isotropic strain energy function [21]. The somewhat contradicting results presented above may suggest that the anisotropy observed in elastin could be species, artery and location dependent.

We have considered transversely isotropic properties for elastin. The structural origins of this anisotropy are not well defined. It is known that elastin filaments orient themselves in the direction of the applied force upon stretching [14, 41]. This property of elastin explains, to some extent, the apparent anisotropy as well as higher elastic modulus in the longitudinal direction. The inflation-extension tests were performed under longitudinal stretch ratios ranging from 100% to 130% of the *in vivo* longitudinal stretch ratio. The average *in vivo* stretch ratio was  $\bar{\lambda}_z = 1.63$ , thus the longitudinal stretch ratios under which the experiments were done ranged from 1.6 to 2.6. Therefore, at low pressures, the relatively high longitudinal stretch ratios might have lead to the axial orientation of fibers, yielding the anisotropy observed in this experiment. Furthermore, in 3D observations of vascular elastin scaffolds using scanning electron microscopy, elastin network was shown to be porous, with pores being mostly spindle shaped [42]. This porous structure, in particular the orientation of the spindle shape pores, may also contribute to the anisotropic properties of vascular elastin. The aforementioned hypotheses on the origin of elastin anisotropy needs to be tested experimentally, ideally through high-resolution 3D microstructure imaging modalities obtained at different levels of tissue inflation/extension.

Our model and testing methods are subject to a number of limitations. First of all, the results are vessel specific, i.e., they pertain to rabbit facial veins and may not apply to other veins of

the same or other animals species [3, 43]. Extension to arterial wall properties is not straightforward, since the arterial wall structure is substantially different [3, 44]. Our SEF function is applicable to vascular tissues with stiffer properties in the longitudinal direction than the transversal direction in low strain region. If this is not the case, the use of an orthotropic function for the low strain part may be necessary. SEFs considering more than one family of fibers or defining an alternative fiber direction to describe the orthotropic properties may be used to address this problem. VSM is neglected on the basis that its passive elastic modulus is reported to be about one order of magnitude less than that of elastin [45]. Based on recent studies on decellularized porcine common arteries, removal of cells from the matrix causes changes in mechanical properties of arteries even in their fully passive state [32]. The same study of Roy et al. also suggests that a part of elastin is connected in series with VSM. Experiments on rabbit carotids, whereby elastin was selectively destroyed by elastase, showed that when elastin is dissolved this leads to changes collagen engagement properties, which further supports the argument of structural interdependence between the two scleroproteins [33].

To our knowledge, this study is the first one to take into account, in a concise biomechanical framework, the anisotropy of elastin. Despite its limitations, our SEF fits well both the experimental longitudinal force-pressure and radius-pressure curves. This fit has been achieved by adding only one extra parameter to the previous model with isotropic elastin. The improvement over the previous models was quantified and judged essential. Thus we conclude that a model with anisotropic elastin may offer a better description of the biomechanical properties of the vascular wall.

## Acknowledgements

We would like to thank Tyler Thacher for proofreading an earlier version of this document. This work was supported by the Swiss National Science Foundation (grant # 310A0-100423).

## Nomenclature

$C$	Cauchy–Green tensor
$c_{\text{elast}}^i$	an elastic constant for isotropic elastin component
$c_{\text{elast}}^a$	an elastic constant for anisotropic elastin component
$E$	Local green strain along a collagen fiber
$e_0, e_r, e_z$	local base of cylindrical coordinate system
$f_{\text{elast}}$	area fraction of load bearing elastin
$f_{\text{coll}}$	area fraction of load bearing collagen
$F_z$	longitudinal force
$F_{ij}^{\text{mod}}$	longitudinal force as given by model
$F_{ij}^{\text{exp}}$	axial force as measured experimentally
$h$	thickness of the wall
$I$	identity tensor
$I_1$	first invariant of $C$
$I_4$	forth invariant of $C$ ; relative to the vector $v_\alpha$
$l$	the longitudinal length (loaded state)
$L$	$L$ the longitudinal length of the segment (zero stress state)

$L_f$	number of free parameters in a model
$m$	number of experimental points measured at different pressures
$p$	local wall stresses in principal directions
$P$	intraluminal pressure
$r$	radius of a wall point (loaded state)
$r_i$	inner radius (loaded state)
$r_o$	outer radius (loaded state)
$r_{ij}^{\text{mod}}$	internal radius as given by model
$r_{ij}^{\text{exp}}$	internal radius as measured experimentally
$R$	radius of a wall point (zero stress state)
$R_i$	inner radius (zero stress state)
$R_o$	outer radius (zero stress state)
$V_\alpha$	vector defining collagen fiber orientation
$\lambda_\theta, \lambda_z, \lambda_r$	circumferential, longitudinal, and radial stretch ratios
$\alpha$	angle of fiber vector $v_\alpha$ to $e_\theta$ in the $e_\theta$ - $e_z$ plane
$\Theta$	opening angle
$\rho^{\text{fiber}}$	collagen fiber engagement strain distribution
$\bar{\sigma}_\theta, \bar{\sigma}_z$	mean tangential and axial stresses
$\sigma_\theta, \sigma_z, \sigma_r$	local wall stresses in principal directions
$\sigma_{ij}^f$	standard deviation of the measured mean longitudinal force
$\sigma_{ij}^F$	standard deviation of the measured mean internal radius
$\Psi^{\text{iso}}$	strain energy function representing isotropic matrix
$\Psi^{\text{aniso}}$	strain energy function representing the anisotropic term
$\Psi^{\text{elast}}$	strain energy function representing elastin
$\Psi^{\text{coll}}$	strain energy function representing collagen
$\Psi_{\text{coll}}^f$	strain energy function representing a family of collagen
$\Psi^{\text{fiber}}$	strain energy function representing an individual collagen fiber
$\Psi_z^{\text{passive}}$	strain energy function representing passive part from Zulliger et al.'s model

## Appendix: Structure-based Strain Energy Function for Vascular Collagen

Zulliger et al.'s model consists of an isotropic term accounting for elastin fibers  $\Psi^{\text{elast}}$  and an anisotropic term representing collagen fibers  $\Psi^{\text{coll}}$  [9, 12]. The model takes into account both the fraction of the total wall cross-section area composed of elastin,  $f_{\text{elast}}$ , and the corresponding fraction area composed of collagen,  $f_{\text{coll}}$ , to give the appropriate weight to the contribution of each constituent to the total SEFs (see equation 17).

In order to define the structure-based SEF for collagen, both the waviness and the orientation of fibers have been taken into account. A log-logistic distribution function ( $\rho^{\text{fiber}}$ ) describes the gradual engagement of the collagen fibers as a function of the fiber strain:

$$\rho_{fiber}(E) = \begin{cases} 0 & \text{for } E \leq 0 \\ \frac{k}{b} \frac{\left(\frac{E}{b}\right)^{k-1}}{\left[1 + \left(\frac{E}{b}\right)^k\right]^2} & \text{for } E > 0 \end{cases} \quad (\text{a.1})$$

$E$  is the local strain in the direction of the fiber,  $b > 0$  is a scaling parameter and  $k > 0$  defines the shape of the distribution. The contribution of the ensemble of collagen fibers to the SEF is given by:

$$\Psi_{coll}^f(E) = \Psi_{fiber} * \rho_{fiber} = \int_{-\infty}^{\infty} \rho_{fiber}(E^*) \Psi_{fiber}(E - E^*) dE^* \quad (\text{a.2})$$

where  $\Psi_{coll}^f$  is the strain energy function for a family of fibres with  $\Psi_{fiber}$  being the strain energy function for each individual fiber, described as:

$$\Psi_{fiber}(E) = \begin{cases} 0 & \text{for } E \leq 0 \\ c_{coll} \frac{1}{2} E^2 & \text{for } E > 0 \end{cases} \quad (\text{a.3})$$

Assuming that collagen fibers are at an angle  $\alpha$  to the circumferential direction in the  $e_z - e_\theta$  plane, the stretch ratio to which the fiber ensemble is submitted is:

$$\lambda = \sqrt{I_4} = \sqrt{\lambda_\theta^2 \cos^2 \alpha + \lambda_z^2 \sin^2 \alpha} \quad (\text{a.4})$$

The local strain in the direction of fiber  $E$  is then defined as:

$$E = \frac{\lambda^2 - 1}{2} \quad (\text{a.5})$$

Half of the fibers have been considered with an  $\alpha$  angle while the other half with an angle of  $-\alpha$  which leads to  $I_4'$  and  $E'$  corresponding to the negative values of  $\alpha$ . The final SEF for collagen becomes:

$$\Psi_{coll} = \frac{1}{2} \Psi_{coll}^f \left( \frac{I_4 - 1}{2} \right) + \frac{1}{2} \Psi_{coll}^f \left( \frac{I_4' - 1}{2} \right) \quad (\text{a.6})$$



## References

- [1] Vito, R. P., and Dixon, S. A., 2003, "Blood Vessel Constitutive Models-1995-2002," *Annual Review Of Biomedical Engineering*, **5**, pp. 413-439.
- [2] Fung, Y. C., and Liu, S. Q., 1995, "Determination of the Mechanical Properties of the Different Layers of Blood Vessels in Vivo," *Proceedings of the National Academy of Sciences of the United States of America*, **92**(6), pp. 2169-2173.
- [3] Silver, F. H., Snowhill, P. B., and Foran, D. J., 2003, "Mechanical Behavior of Vessel Wall: A Comparative Study of Aorta, Vena Cava, and Carotid Artery," *Annals of Biomedical Engineering*, **31**(7), pp. 793-803.
- [4] Holzapfel, G. A., Gasser, T. C., and Ogden, R. W., 2000, "A New Constitutive Framework for Arterial Wall Mechanics and a Comparative Study of Material Models," *Journal of Elasticity*, **61**(1-3), pp. 1-48.
- [5] Holzapfel, G. A., Gasser, T. C., and Stadler, M., 2002, "A Structural Model for the Viscoelastic Behavior of Arterial Walls: Continuum Formulation and Finite Element Analysis," *European Journal of Mechanics, A/Solids*, **21**(3), pp. 441-463.
- [6] Monos, E., Berczi, V., and Nadasy, G., 1995, "Local Control of Veins: Biomechanical, Metabolic, and Humoral Aspects," *Physiological Reviews*, **75**(3), pp. 611-666.
- [7] Zulliger, M. A., Kwak, N. T. M. R., Tsapikouni, T., and Stergiopoulos, N., 2002, "Effects of Longitudinal Stretch on Vsm Tone and Distensibility of Muscular Conduit Arteries," *American Journal of Physiology - Heart and Circulatory Physiology*, **283**(6 52-6).
- [8] Marieb, E. N., 2007, *Human Anatomy & Physiology*, Pearson Benjamin Cummings, San Fransisco.
- [9] Zulliger, M. A., Fridez, P., Stergiopoulos, N., and Hayashi, K., 2004, "A Strain Energy Function for Arteries Accounting for Wall Composition and Structure," *Journal of Biomechanics*, **37**(7), pp. 989-1000.
- [10] Chuong, C. J., and Fung, Y. C., 1983, "3-Dimensional Stress-Distribution in Arteries," *Journal Of Biomechanical Engineering-Transactions Of The Asme*, **105**(3), pp. 268-274.
- [11] Takamizawa, K., and Hayashi, K., 1987, "Strain-Energy Density-Function and Uniform Strain Hypothesis for Arterial Mechanics," *Journal Of Biomechanics*, **20**(1), pp. 7-17.
- [12] Zulliger, M. A., Stergiopoulos, N., and Rachev, A., 2004, "A Constitutive Formulation of Arterial Mechanics Including Vascular Smooth Muscle Tone," *American Journal of Physiology - Heart and Circulatory Physiology*, **287**(3 56-3).
- [13] Driessen, N. J. B., Bouten, C. V. C., and Baaijens, F. P. T., 2005, "A Structural Constitutive Model for Collagenous Cardiovascular Tissues Incorporating the Angular Fiber Distribution," *Journal of Biomechanical Engineering*, **127**(3), pp. 494-503.
- [14] Pasquali Ronchetti, I., Alessandrini, A., Bacarani Contri, M., Fornieri, C., Mori, G., Quaglino Jr, D., and Valdre, U., 1998, "Study of Elastic Fiber Organization by Scanning Force Microscopy," *Matrix Biology*, **17**(1), pp. 75-83.
- [15] Sherebrin, M. H., Song, S. H., and Roach, M. R., 1983, "Mechanical Anisotropy of Purified Elastin from the Thoracic Aorta of Dog and Sheep," *Canadian Journal of Physiology and Pharmacology*, **61**(6), pp. 539-545.
- [16] Lillie, M. A., David, G. J., and Gosline, J. M., 1998, "Mechanical Role of Elastin-Associated Microfibrils in Pig Aortic Elastic Tissue," *Connective Tissue Research*, **37**(1-2), pp. 121-141.

- [17] Snowhill, P., and Silver, F., 2005, "A Mechanical Model of Porcine Vascular Tissues-Part II: Stress-Strain and Mechanical Properties of Juvenile Porcine Blood Vessels," *Cardiovascular Engineering*, **5**(4), pp. 157-169.
- [18] Clark, J. M., and Glagov, S., 1985, "Transmural Organization of the Arterial Media - the Lamellar Unit Revisited," *Arteriosclerosis*, **5**(1), pp. 19-34.
- [19] Fung, Y. C., 1990, *Biomechanics: Motion, Flow, Stress and Growth*, Springer-Verlag New York Inc., New York.
- [20] Holzapfel, G. A., and Ogden, R. W., 2003, *Biomechanics of Soft Tissue in Cardiovascular Systems*, Springer Wien New York, Udine.
- [21] Gundiah, N., B Ratcliffe, M., and A Pruitt, L., 2007, "Determination of Strain Energy Function for Arterial Elastin: Experiments Using Histology and Mechanical Tests," *Journal of Biomechanics*, **40**(3), pp. 586-594.
- [22] Lillie, M. A., and Gosline, J. M., 2002, "Unusual Swelling of Elastin," *Biopolymers*, **64**(3), pp. 115-126.
- [23] Pioletti, D. P., and Rakotomanana, L. R., 2000, "Non-Linear Viscoelastic Laws for Soft Biological Tissues," *European Journal of Mechanics, A/Solids*, **19**(5), pp. 749-759.
- [24] Rockafellar, R. T., 1997, *Convex Analysis*, Princeton University Press, Princeton, New Jersey.
- [25] Landaw, E. M., and DiStefano Iii, J. J., 1984, "Multiexponential, Multicompartmental, and Noncompartmental Modeling. II. Data Analysis and Statistical Considerations," *American Journal of Physiology - Regulatory Integrative and Comparative Physiology*, **15**(5), p. R665.
- [26] Schulze-Bauer, C. A. J., Mörth, C., and Holzapfel, G. A., 2003, "Passive Biaxial Mechanical Response of Aged Human Iliac Arteries," *Journal of Biomechanical Engineering*, **125**(3), pp. 395-406.
- [27] Gaballa, M. A., Jacob, C. T., Raya, T. E., Liu, J., Simon, B., and Goldman, S., 1998, "Large Artery Remodeling During Aging: Biaxial Passive and Active Stiffness," *Hypertension*, **32**(3), pp. 437-443.
- [28] Lichtenstein, O., Safar, M. E., Poitevin, P., and Levy, B. I., 1995, "Biaxial Mechanical Properties of Carotid Arteries from Normotensive and Hypertensive Rats," *Hypertension*, **26**(1), pp. 15-19.
- [29] Doriot, P. A., and Dorsaz, P. A., 2005, "Estimation of the Axial Wall Strains Induced by an Arterial Stenosis at Peak Flow," *Medical Physics*, **32**(2), pp. 360-368.
- [30] Doriot, P. A., 2003, "Estimation of the Supplementary Axial Wall Stress Generated at Peak Flow by an Arterial Stenosis," *Physics in Medicine and Biology*, **48**(1), pp. 127-138.
- [31] Zulliger, M. A., and Stergiopoulos, N., 2004, "Structural Strain Energy Function Applied to Ageing and Hypertension," *Archives of Physiology and Biochemistry*, **112**(SUPPL.), p. 67.
- [32] Roy, S., Silacci, P., and Stergiopoulos, N., 2005, "Biomechanical Proprieties of Decellularized Porcine Common Carotid Arteries," *American Journal of Physiology - Heart and Circulatory Physiology*, **289**(4 58-4), pp. H1567-H1576.
- [33] Fonck, E., Prod'hom, G., Roy, S., Augsburg, L., Rufenacht, D., and Stergiopoulos, N., 2007, "Effect of Elastin Degradation on Carotid Wall Mechanics as Assessed by a Constituent-Based Biomechanical Model," *American Journal of Physiology - Heart and Circulatory Physiology*, **292**(6), pp. H2754-H2763.
- [34] Milnor, W. R., 1989, *Hemodynamics*, Williams & Wilkins, Baltimor.

- [35] Bank, A. J., Wang, H., Holte, J. E., Mullen, K., Shammass, R., and Kubo, S. H., 1996, "Contribution of Collagen, Elastin, and Smooth Muscle to in Vivo Human Brachial Artery Wall Stress and Elastic Modulus," *Circulation*, **94**(12), pp. 3263-3270.
- [36] Sokolis, D. P., Zarbis, N., Dosios, T., Papalouka, V., Papadimitriou, L., Boudoulas, H., and Karayannacos, P. E., 2005, "Post-Vagotomy Mechanical Characteristics and Structure of the Thoracic Aortic Wall," *Annals of Biomedical Engineering*, **33**(11), pp. 1504-1516.
- [37] Grut, W., Edwards, J., and Evans, E. J., 1977, "Scanning Electron Microscopy of Freeze-Dried Aortic Elastin," *J Microsc*, **110**(3), pp. 271-275.
- [38] Hoeve, C. A., and Flory, P. J., 1974, "The Elastic Properties of Elastin," *Biopolymers*, **13**(4), pp. 677-686.
- [39] Dorrington, K., Grut, W., and McCrum, N. G., 1975, "Mechanical State of Elastin," *Nature*, **255**(5508), pp. 476-478.
- [40] Gosline, J. M., 1980, *The Elastic Properties of Rubber-Like Proteins and Highly Extensible Tissues*, cambridge university press, cambridge.
- [41] Pasquali-Ronchetti, I., Fornieri, C., Baccarani-Contri, M., and Quaglino, D., 1995, "Ultrastructure of Elastin," *Ciba Foundation symposium*, **192**, pp. 31-42.
- [42] Lu, Q., Ganesan, K., Simionescu, D. T., and Vyavahare, N. R., 2004, "Novel Porous Aortic Elastin and Collagen Scaffolds for Tissue Engineering," *Biomaterials*, **25**(22), pp. 5227-5237.
- [43] Silver, F. H., Horvath, I., and Foran, D. J., 2001, "Viscoelasticity of the Vessel Wall: The Role of Collagen and Elastic Fibers," *Critical Reviews in Biomedical Engineering*, **29**(3), pp. 279-302.
- [44] Monson, K. L., Goldsmith, W., Barbaro, N. M., and Manley, G. T., 2005, "Significance of Source and Size in the Mechanical Response of Human Cerebral Blood Vessels," *Journal of Biomechanics*, **38**(4), pp. 737-744.
- [45] VanDijk, A. M., Wieringa, P. A., van der Meer, M., and Laird, J. D., 1984, "Mechanics of Resting Isolated Single Vascular Smooth Muscle Cells from Bovine Coronary Artery," *The American journal of physiology*, **246**(3 Pt 1), pp. C277-287.



## Chapter 2

---



# Role of Elastin Anisotropy in Structural Strain Energy Functions of Arterial Tissue

R. Rezakhaniha<sup>1</sup>, E. Fonck<sup>1</sup>, C. Genoud<sup>2</sup>, N. Stergiopoulos<sup>1</sup>

1. Laboratory of Hemodynamics and Cardiovascular Technology, Ecole Polytechnique Federale de Lausanne, 1015 Lausanne, Switzerland

2. Friedrich Miescher Institute for Biomedical Research, Basel, Switzerland

## Abstract

The vascular wall exhibits nonlinear anisotropic mechanical properties. The identification of a strain energy function (SEF) is the preferred method to describe its complex nonlinear elastic properties. Earlier constituent-based SEF models, where elastin is modeled as an isotropic material, failed in describing accurately the tissue response to inflation-extension loading. We hypothesized that these shortcomings are partly due to unaccounted anisotropic properties of elastin. We performed inflation-extension tests on common carotid of rabbits before and after enzymatic degradation of elastin and applied constituent-based SEFs, with both an isotropic and an anisotropic elastin part, on the experimental data. We used transmission electron microscopy (TEM) and serial block-face scanning electron microscopy (SBF-SEM) to provide direct structural evidence of the assumed anisotropy. In intact arteries, the SEF including anisotropic elastin, with one family of fibers in the circumferential direction, fitted better the inflation-extension data than the isotropic SEF. This was supported by TEM and SBF-SEM imaging, which showed interlamellar elastin fibers in the circumferential direction. In elastin-degraded arteries, both SEFs succeeded equally well in predicting anisotropic wall behavior. In elastase-treated arteries fitted with the anisotropic SEF for elastin, collagen engaged earlier than in intact arteries. We conclude that constituent-based models with an anisotropic elastin part, characterize more accurately the mechanical properties of the arterial wall as compared to models with simply an isotropic elastin. Microstructural imaging based on electron microscopy techniques provided evidence for elastin anisotropy. Finally, based on our model, there is a clear functional interaction between elastin and collagen component that is often neglected in constituent-based SEFs.

**Keywords:** arterial wall biomechanics, anisotropy, elastin, ultrastructure, rabbit carotid artery, constitutive equations

Submitted to:

Biomechanics and Modeling in Mechanobiology, 2009

## Introduction

Vascular tissue shows a nonlinear anisotropic behavior, as a result of material properties, structural arrangements and interconnections of its main constituents i.e. elastin, collagen and vascular muscle cells (Silver et al. 2003; Vito and Dixon 2003; Zhou and Fung 1997). Significant effort has been put into developing constituent-based or structural strain energy functions (SEFs) for the vascular tissue, which take into account the individual mechanical contribution of each intramural element (Driessen et al. 2005; Gasser et al. 2006; Gundiah et al. 2009; Holzapfel et al. 2000; Zulliger et al. 2004; Zulliger et al. 2004) and therefore provide a solid base to study mechanical properties of the tissue in health and disease.

SEFs should provide a complete 3-D description of the stress-strain field. For an axisymmetric vessel, this translates into a good description (fit) of both the pressure-radius ( $P-r_o$ ) and the pressure-longitudinal force ( $P-F_z$ ) curves, as those are measured in a typical inflation-extension experiment. Most of the previously published constituent-based SEFs have considered that collagen is the only wall element contributing to the material anisotropy (Holzapfel et al. 2000; Zulliger et al. 2004; Zulliger et al. 2004). Although these SEFs successfully describe  $P-r_o$  curves of vessels, they fail to describe simultaneously both the  $P-r_o$  and the  $P-F_z$  curves, in veins (Rezakhaniha and Stergiopulos 2008) as well as in arteries (Zulliger et al. 2004). In a recent study on veins, we have suggested an anisotropic SEF for elastin with fibers in the longitudinal direction, which, in conjunction with an isotropic collagen description, significantly improved the quality of the  $P-r_o$  and  $P-F_z$  curves (Rezakhaniha and Stergiopulos 2008). Yet, as the anisotropy observed in the mechanical behavior of elastin could be different in arteries and veins, the present study was designed to focus on the existence and nature of elastin anisotropy in arteries. We hypothesized that a SEF with both elastin and collagen as anisotropic materials provides a better description of the mechanical properties of the arterial wall compared to traditional SEFs with anisotropic collagen and isotropic elastin components. Furthermore, we searched for direct micro-structural evidence to support our hypotheses by studying the structural organization of elastin within the arterial wall. Finally, we applied our suggested SEF, with an elastin anisotropic term, on both intact and elastase-treated arteries to obtain more information about structural links and resulting functional interactions between collagen and elastin structures in the arterial wall.

## Methods

### Experimental data

#### Biological specimens

Six common carotids were excised from young white New Zealand rabbits ( $3\pm 0.4$  kg) from a local abattoir. The length of the arteries was measured before and after the excision to determine the *in vivo* longitudinal stretch of the vessels. The arteries were submerged in phosphate buffered saline (PBS) and transported on ice to the laboratory. Right after arrival, the arteries were cleaned from surrounding tissue. The common carotid arteries were typically 50-60 mm from which two 16 mm segments were excised. One segment was used as a control artery and the other for the elastase treatment.



## **Biochemical treatment**

We followed the procedure described in detail in an earlier study performed in our laboratory (Fonck et al. 2007). In summary, the artery segments were submerged in a PBS bath and stretched to their *in vivo* longitudinal stretch. Elastase was gradually added to the bath to reach a final concentration of 6.85 U/ml. Each artery was left in the bath for 30 min at 37°C and washed afterwards with fresh PBS. To inhibit the elastase trapped in the arterial wall, the arteries were left for 30 min in a bath of 2U/ml aprotinin (Elastin). The artery was then washed with PBS.

## **Geometric measurements**

Before running inflation-extension experiments, rings of 0.4±0.1 mm thickness were cut from the end of the segments to measure the opening angle, wall thickness, and inner and outer diameter. Rings were placed in a Petri dish with PBS for 20 min at 37°C to reach an equilibrium state, and photographs were taken under an upright microscope at x20 magnification (Axioplan2; Carl Zeiss Inc.). The rings were subsequently cut open and placed in PBS for 30 min at 37°C to measure the opening angle.

## **Biomechanical testing**

Arteries were tested by an inflation-extension device described in detail in our previous study (Rezakhaniha and Stergiopulos 2008) following the protocol described by Fonck et al. (Fonck et al. 2007). In summary, the arteries were stretched to their *in vivo* length and then submitted to preconditioning cycles of inflation-extension (pressure range: 0-180 mmHg approximate rate: 1.5 mmHg/s) to ensure repeatability of the curve. External diameter data was measured with a CCD micrometer (model LS-7030, Keyence). Pressure was recorded with a blood pressure transducer (BLPR, World Precision Instruments) and the longitudinal force by a load cell force transducer (FORT10, World Precision Instruments). The passive arterial state was achieved by adding sodium nitroprusside to the bath (SNP, 10<sup>-4</sup>M).

## **Transmission electron microscopy**

Two intact carotid arteries were removed from the animal postmortem. These were then immersed in a solution of 2.5 % glutaraldehyde and 2.0 % paraformaldehyde in 0.1M phosphate buffer, pH 7.4 for a total time of 4 hours at 4°C. The arteries were initially pressurized at 70 mmHg for ten minutes, then pressure was released and to ensure good fixation, the arteries were cut into small rings (width<3 mm). After fixation the arteries were washed thoroughly with cacodylate buffer (0.1M, pH 7.4), postfixed for 40 minutes in 1.0 % osmium tetroxide, then 40 minutes in 5 % tannic acid followed by 60 minutes in palladium chloride (1 % in water). They were finally stained for 60 minutes in 1% uranyl acetate in water before being dehydrated through increasing concentrations of alcohol and then embedded in Durcupan ACM (Fluka, Switzerland) resin. The resin was hardened for 24 hours in a 65°C oven. Semi-thin sections, 1 micron thick, were cut from the trimmed blocks using glass knives to check the orientation of the vessels, and quality of the tissue, and then, thin 50 nm thick sections were cut using a diamond knife (Diatome, Switzerland) and ultramicrotome (Leica UCT). These thin sections were further contrasted with lead citrate (Reynold's stain) and images captured digitally on a CCD camera (SIS Morada, Munich) inside a Philips CM10 transmission electron microscope at a filament voltage of 80kV.

## **Serial block-face scanning electron microscopy (SBF-SEM)**

We used the same resin blocks prepared for the TEM. Image stacks were obtained using serial block-face scanning electron microscopy SBF-SEM developed by Denk and

Horstmann (Denk and Horstmann 2004). The equipment is composed of a scanning electron microscope (SEM) (FEI Quanta 200 VP-FEG) combined with an ultramicrotome (3View, GATAN Inc). The ultramicrotome repeatedly removes uniform sections from the specimen surface and therefore exposes subsequent surfaces for block-face imaging by the SEM. Because the tissue block position is fixed, image registration is inherent and image distortion is absent, greatly simplifying volume reconstruction (Denk and Horstmann 2004). Images were done on three different sites in the media at the accelerating voltage of 3.5keV and in the low vacuum mode (0.35 Torr). The section thickness was 50 nm and the obtained images were 2048x2048 pixels with 8.9 nm per pixel.

## Mathematical model

### Background

The mathematical model presented in this work is an extension of our work on venous tissue (Rezakhaniha and Stergiopulos 2008). We considered the artery as a thick wall circular cylinder which undergoes inflation-extension experiments and shows nonlinear, anisotropic and incompressible behavior. The material behavior is assumed to be pseudo-elastic i.e. loading and unloading curves can be represented by separate elastic laws as proposed by Fung (Fung et al. 1979). In the absence of vascular tone, we considered only passive properties of the arterial wall and therefore separated our constituent-based strain energy function into two parts representing the elastin and collagen components:

$$\Psi_{passive} = f_{elast} \Psi_{elast} + f_{coll} \Psi_{coll} \quad (1)$$

Where  $f_{elast}$  and  $f_{coll}$  are the fractions of the wall cross-section area composed of elastin and collagen and  $\Psi_{passive}$ ,  $\Psi_{elast}$  and  $\Psi_{coll}$  represent the SEF for artery in the passive state, the SEF for the network of elastin and the SEF for the network of collagen, respectively.

To define the collagen SEF, we followed the same approach as Zulliger et al. and assumed collagen as a collection of wavy fibers arranged in two helical families of fibers at angles  $\alpha$  and  $-\alpha$  to the circumferential direction. A detailed description of the method can be found in the study of Zulliger et al. (Zulliger et al. 2004). In short, the engagement of collagen fibers is assumed to take place in a statistical manner and represented by a log logistic distribution:

$$\rho_{fiber}(E) = \begin{cases} 0 & \text{for } E \leq 0 \\ k \frac{\left(\frac{E}{b}\right)^{k-1}}{b \left[1 + \left(\frac{E}{b}\right)^k\right]^2} & \text{for } E > 0 \end{cases} \quad (2)$$

$E$  is the local strain in the direction of the fiber,  $b > 0$  is a scaling parameter and  $k > 0$  defines the shape of the distribution. The mode (peak value) of this statistical distribution is situated at  $b \left(\frac{k-1}{k+1}\right)^{1/k}$ . Larger  $b$  results in a later engagement and larger scale parameter  $k$  results in a more spread out distribution. The strain energy function of an individual collagen fiber is defined by:

$$\Psi_{fiber}(E) = \begin{cases} 0 & \text{for } E \leq 0 \\ c_{coll} \frac{1}{2} E^2 & \text{for } E > 0 \end{cases} \quad (3)$$

where  $c_{coll}$  is an elastic constant associated with collagen fibers. The contribution of the ensemble of collagen fibers to the SEF is therefore given by:

$$\Psi_{coll}^f(E) = \Psi_{fiber} * \rho_{fiber} = \int_{-\infty}^{\infty} \rho_{fiber}(E^*) \Psi_{fiber}(E - E^*) dE^* \quad (4)$$

where  $\Psi_{coll}^f$  is the strain energy function for the ensemble of the fibres. Assuming that collagen fibres are at an angle  $\alpha$  to the circumferential direction in the  $e_\theta$ - $e_z$  plane and their direction is represented by the unit vector  $v_\alpha$ , we can define  $I_4$ , an invariant of the Cauchy-Green tensor  $\mathbf{C}$  with respect to  $v_\alpha$ , as :

$$I_4 = v_\alpha \cdot \mathbf{C} \cdot v_\alpha = \lambda^2 = \lambda_\theta^2 \cos^2 \alpha + \lambda_z^2 \sin^2 \alpha \quad (5)$$

Similarly, we can define the invariant  $I_4'$  in respect to a vector  $v_\alpha'$  having the angle  $-\alpha$  with the circumferential direction. As we assumed that fibers are organized symmetrically around the longitudinal direction,  $I_4'$  and  $I_4$  are equal in this case.

Thus the collagen SEF, with half of the fibres at angle  $\alpha$  and the other half at  $-\alpha$  to the circumferential direction, becomes:

$$\Psi_{coll} = f_{coll} \left( \frac{1}{2} \Psi_{coll}^f \left( \frac{I_4 - 1}{2} \right) + \frac{1}{2} \Psi_{coll}^f \left( \frac{I_4' - 1}{2} \right) \right) \quad (6)$$

## Anisotropic strain energy function for elastin

To define the SEF for elastin, we propose a combination of an orthotropic model, accounting for a subset of elastin fibers oriented in the circumferential direction and an isotropic model, accounting for the remaining elastin matrix:

$$\Psi_{elast} = \Psi_{iso}(I_1) + \Psi_{aniso}(I_4'') \quad (7)$$

where  $I_1$  is the first invariant of the Cauchy-Green deformation tensor  $\mathbf{C}$  and  $I_4''$  is an invariant of  $\mathbf{C}$  with respect to  $e_\theta$  defined as:

$$I_4'' = e_\theta \cdot \mathbf{C} \cdot e_\theta = \lambda_\theta^2 \quad (8)$$

$e_\theta$  is the unit vector in the circumferential direction.

For the isotropic component of elastin, we used a neo-Hookean SEF:

$$\Psi_{iso} = c_{elast}^i (I_1 - 3) \quad (9)$$

where  $c_{elast}^i$  represents the modulus for the isotropic elastin component. As for the anisotropic component, we assumed the one dimensional form of an incompressible neo-Hookean material for each fiber, undergoing a uniform cross-section deformation when stretched in the fiber direction. This results in the following formulation for the anisotropic part of the SEF:

$$\Psi_{aniso} = c_{elast}^a \left( I_4^n + \frac{2}{\sqrt{I_4^n}} - 3 \right) \quad (10)$$

where  $c_{elast}^a > 0$  is an elastic constant enabling us to obtain a higher modulus for elastin in the  $\theta$ -direction.

Combining the individual SEF for collagen and elastin, we obtain the global SEF of the artery at its passive (no vascular tone) state as:

$$\Psi_{passive} = f_{elast} \left( c_{elast}^i (I_1 - 3) + c_{elast}^a \left( I_4^n + \frac{2}{\sqrt{I_4^n}} - 3 \right) \right) + f_{coll} \left( \frac{1}{2} \Psi_{coll} \left( \frac{I_4 - 1}{2} \right) + \frac{1}{2} \Psi_{coll} \left( \frac{I_4 - 1}{2} \right) \right) \quad (11)$$

## Fit function

Pressure-radius and pressure-longitudinal force curves were fitted to the experimental data by minimizing the following function:

$$\Phi = \frac{1}{2} \frac{1}{m} \sum_i^m \left( \frac{r_i^{mod} - r_i^{exp}}{\sigma_i^r} \right)^2 + \frac{1}{2} \frac{1}{m} \sum_i^m \left( \frac{F_i^{mod} - F_i^{exp}}{\sigma_i^F} \right)^2 \quad (12)$$

$m$  is the number of experimental points measured at different pressures. Superscript *mod* denotes the values predicted by the mathematical model whereas superscript *exp* those measured experimentally. The index  $i$  denotes the pressure at which the corresponding outer radius,  $r$ , and longitudinal force,  $F$ , were obtained.  $\sigma$  is the standard deviation of the experimental mean value of radius or force at a given pressure and longitudinal stretch ratio. It is used as a weighting factor, giving more weight to the points with the least variation.

In order to check the fit quality, the weighted residual sum of squares for radius and force,  $WRSS^r$ ,  $WRSS^F$  have been calculated based on the following formulae:

$$WRSS^k = \sum_i^m \left( \frac{k_i^{mod} - k_i^{exp}}{\sigma_i^k} \right)^2 \quad k = r, F \quad (13)$$

## Results

P- $r_o$  and P- $F_z$  curves from inflation-extension experiments on intact arteries and elastase-treated arteries are plotted in Fig. 1. As seen from the P- $r_o$  curves, the vessel inflates more abruptly at lower pressures in elastase-treated arteries than the intact arteries and the final diameter, reached at 20 kPa, is higher in elastase-treated arteries (1.76mm) than intact arteries (1.46 mm). In addition, based on P- $F_z$  curves, the elastin degradation causes a decrease in the measured longitudinal force at low pressures (between 0 and 10 kPa) and at higher pressures, makes the curve less steep.

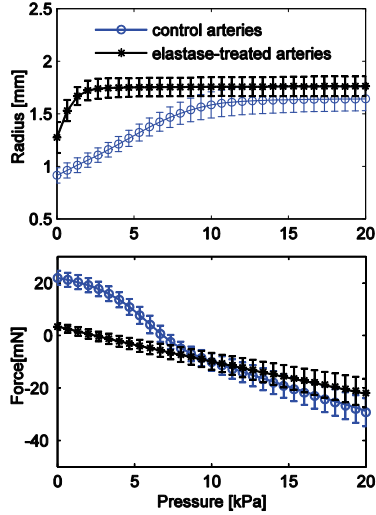


Fig. 1 Experimental data from control and elastase-treated arteries

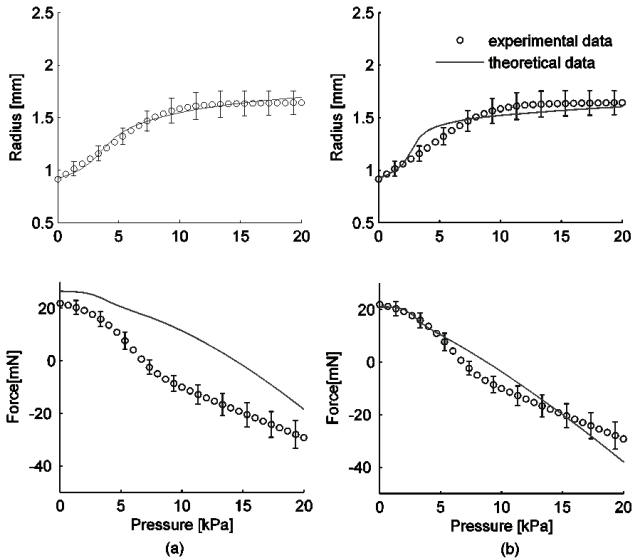
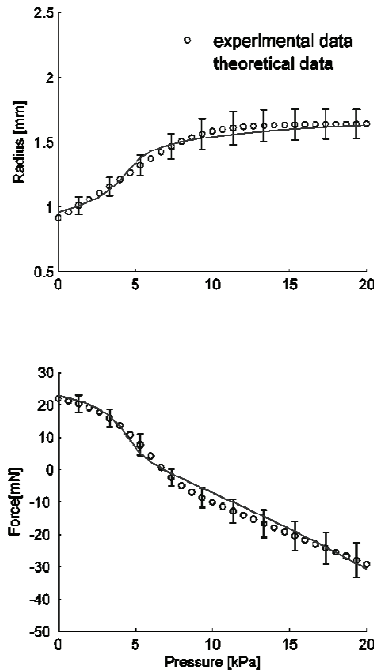


Fig. 2 Original model of Zulliger et al., with isotropic term for elastin, applied on intact arteries a) when only  $P-r_0$  is fitted and b) when both  $P-r_0$  and  $P-F_z$  are fitted.

Fig.2 shows the  $P-r_o$  and  $P-F_z$  curve fits based on the original model, with an isotropic elastin term. Column (a) presents the fit from original Zulliger et al. model, when only the  $P-r_o$  curve was considered to fit the data and no importance was given to the  $P-F_z$  curve in the fitting process. In this case, the model closely fit the  $P-r_o$  curve ( $WRSS^r=3.72$ ), yet gave a relatively poor fit for the  $P-F_z$  curve ( $WRSS^f=643$ ). When the  $P-r_o$  and  $P-F_z$  curves were both considered in the fitting process, i.e. function  $\Phi$  was optimized, this resulted in  $\Phi=1.189$  and the fit is shown in column (b). The quality of the fit for the  $P-F_z$  curve was improved and  $WRSS^f$  was reduced to 55.26 at the expense of the quality of the  $P-r_o$  fit ( $WRSS^r=23.23$ ).

Fig. 3 presents the fits of the modified model with an anisotropic elastin component applied on the experimental data of intact arteries. The fit was considerably improved compared to the one resulted from the original model with an isotropic elastin ( $WRSS^r=3.65$ ,  $WRSS^f=9.04$  for the modified model compared to  $WRSS^r=23.23$ ,  $WRSS^f=55.26$  in original model). The fit function  $\phi$  was reduced to 0.1909 compared to 1.189 from the best fit of the original model (Fig. 2b).



**Fig. 3 Modified model of Zulliger et al., with an anisotropic SEF for elastin, applied to intact arteries when both  $P-r_o$  and  $P-F_z$  are fitted.**

The parameters used in minimizing  $\Phi$  in the fit procedure are listed in Table 1 for the original model with an isotropic elastin component and the modified model with an anisotropic elastin component having fibers in the  $\theta$ -direction. The model resulted in  $WRSS^r=157$  and  $WRSS^f=8377$  when the same parameters as for the best fit of the modified model from Table 1 were applied on the experimental data of elastase-treated arteries (Fig. 4a). To improve the quality of the fit,  $b$  and  $\alpha$  were allowed to vary freely, while other parameters were held constant which resulted in  $b=0.832$  and  $\alpha=0.80$  rad compared to the original values of  $b=1.63$  and  $\alpha=0.68$  rad. The result of the new fit is plotted in Figure 3b ( $WRSS^r=7.85$  and  $WRSS^f=32.23$ ) and the parameters used are indicated in Table 2.

The probability density function of the log logistic distribution assumed for collagen engagement is plotted in Fig. 4 for two sets of parameters, first,  $k=6.63$  and  $b=1.63$  (parameters related to the best fit on the data of intact arteries) and second,  $k=6.63$  and  $b=0.832$  (related to the best fit of elastase-treated arteries). As seen from Fig.5, in elastase treated arteries, collagen engages at lower values of strain compared to the intact artery. The collagen engagement is more abrupt, the distribution is extended between  $E=0.2$  and 2, while in intact arteries collagen engages between  $E=0.5$  and 3.5.

**Table 1** parameters used in minimizing  $\Phi$  in intact arteries

strain energy function	original model (with isotropic elastin)	modified model (with anisotropic elastin)
fitted parameters	$c_{elast}^i=17.99 \text{ KPa}$ $k=5.35$ $b=1.96$ $\alpha=0.60 \text{ rad}$	$c_{elast}^j=18.39 \text{ KPa}$ $c_{elast}^a=13.59 \text{ KPa}$ $k=6.64$ $b=1.63$ $\alpha=0.68 \text{ rad}$
Experimentally-defined parameters	$f_{elast}=0.3$ $f_{coll}=0.3$	$f_{elast}=0.3$ $f_{coll}=0.3$
imposed on model	$c_{coll}=200 \text{ MPa}$	$c_{coll}=200 \text{ MPa}$
$\Phi$	1.189	0.1909

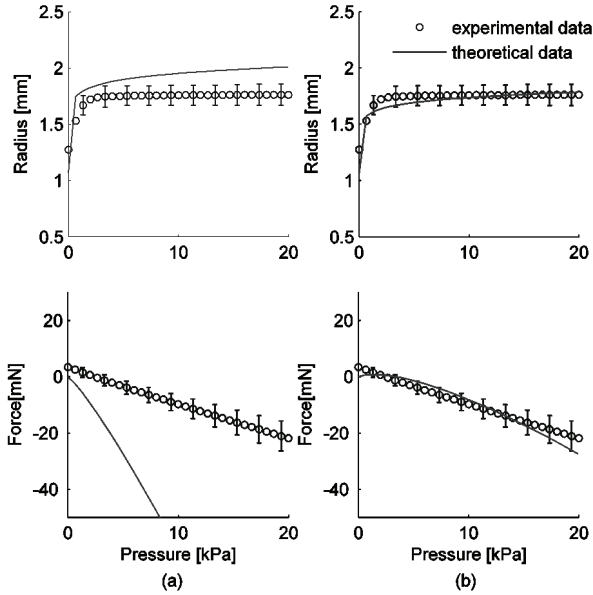


**Fig. 4** Modified model of Zulliger et al., with an anisotropic term for elastin, applied on elastase-treated arteries a) with same parameters as optimized for the intact arteries (based on table 1) and b) when parameters  $b$  and  $\alpha$  are optimized

**Table 2** Parameters used in Figure 3 for elastase-treated arteries

	Parameters from the best fit of intact arteries	$k$ and $\alpha$ optimized for elastase-treated arteries
Fixed parameters	$c_{elast}^i = 18.39 \text{ KPa}$ $c_{elast}^a = 13.59 \text{ KPa}$ $c_{coll} = 200 \text{ MPa}$ $k = 6.64$ $b = 1.63$ $\alpha = 0.68 \text{ rad}$ $f_{elast} = 0.01$ $f_{coll} = 0.3$	$c_{elast}^i = 18.39 \text{ KPa}$ $c_{elast}^a = 13.59 \text{ KPa}$ $c_{coll} = 200 \text{ MPa}$ $k = 6.64$ $f_{elast} = 0.01$ $f_{coll} = 0.3$
Free parameters	<i>no optimization</i>	$b = 0.832$ $\alpha = 0.80 \text{ rad}$
$\Phi$	129.1	0.456



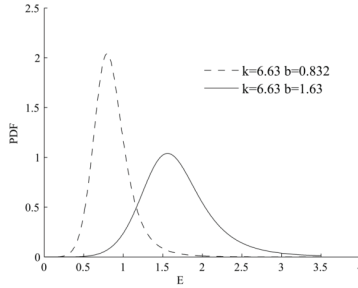


**Fig. 5 Probability density functions of the log-logistic collagen distribution for a) parameters  $k=6.63$ ,  $b=1.63$  (—) as extracted from the best fit for intact arteries and b)  $k=6.63$ ,  $b=0.832$  (- - - -) as fitted to elastase-treated arteries when  $b$  and  $\alpha$  were allowed to vary**

Fig.6 shows a TEM image of the arterial cross section in the media. Elastin, smooth muscle cells, and collagen fibers are depicted in dark, medium and light grey respectively. In the arterial cross sections, interlamellar elastin fibers (IEF) (arrows) made links between elastin lamina (asterisks) and SMCs and were oriented in the similar direction as the SMCs. Fig. 7 indicates a 2D SBF-SEM image of the arterial cross section where the same pattern was observed but with the elastin in light grey and collagen in dark grey. Fig. 8 illustrates an example of 3D SBF-SEM images. An intralamellar elastin feature is marked with arrows in the image. In Fig. 9 one could follow the same IEF structure in 3D by choosing proper planes of views. As seen from the planes A and B, the IEF runs obliquely in the  $\theta$ - $r$  plane making a slight angle (around  $2.5^\circ$ ) with the lamellar elastin (i.e. the circumferential direction) and does not extend in the  $z$  direction. In addition, 3D SBF-SEM images were examined at three different sites. IEFs appear mainly in the circumferential direction in all layers; however they become less organized when located in layers closer to the intima compared to those closer to the adventitia. Moreover, moving from the intima to the adventitia, IEFs become more abundant and thicken in diameter.

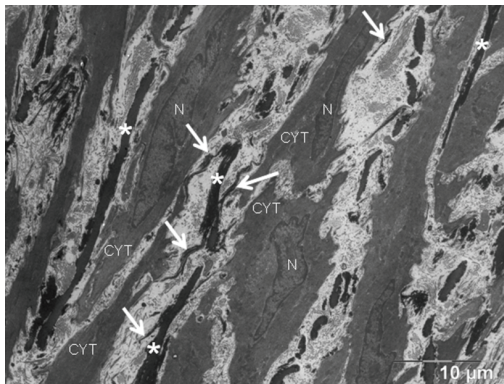


**Fig. 6 A TEM image of arterial cross section showing SMC's nucleus (N) and cytoplasm (CYT), elastin lamina (Asterisks) and intralamellar elastin fibers (arrows)**

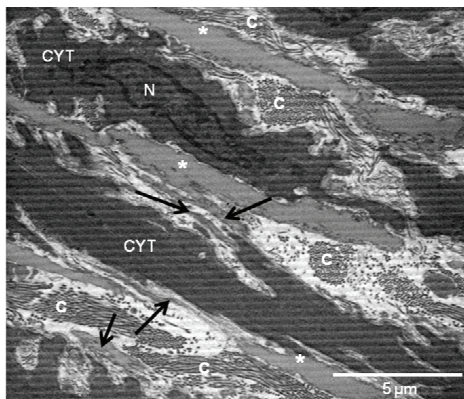


**Fig. 7** A 2D SBF-SEM image of the arterial cross section showing SMC's nucleus (N) and cytoplasm (CYT), collagen fibers (C), elastin laminas (Asterisks) and intralamellar elastin fibers (arrows)

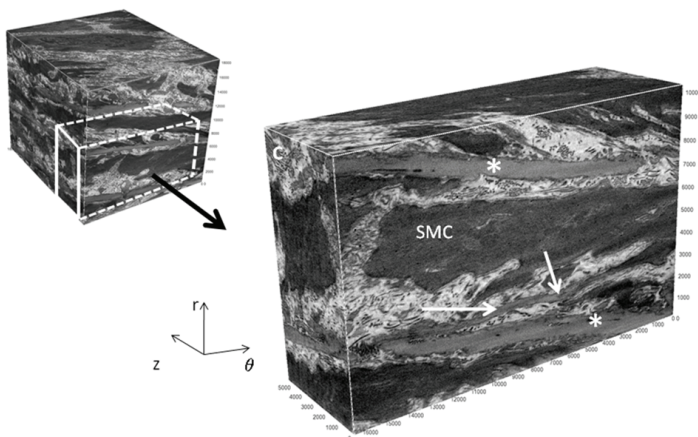


**Fig. 8** 3D SFBSEM images showing an arterial volume, IEFs (arrows) and Elastin lamella (\*) can be seen on the images. IEFs run obliquely, spread from elastic lamella and end in SMCs. volume dimensions are 18μm, 10 μm and 5 μm.

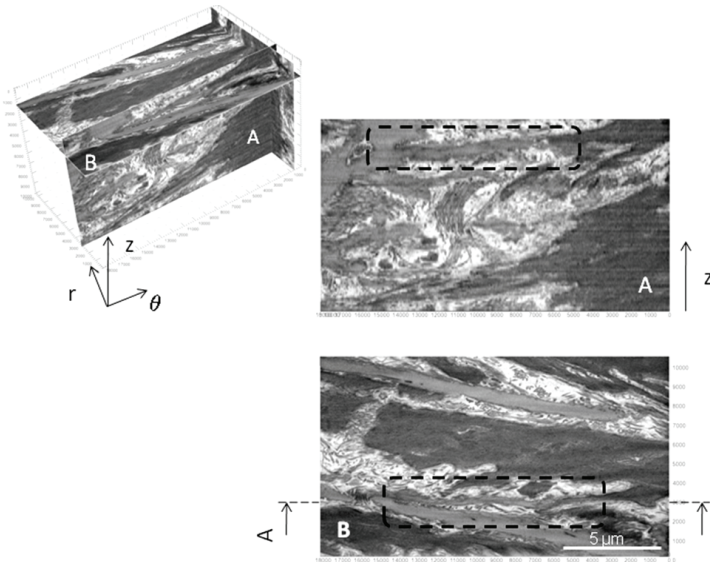


**Fig. 9** An interlamellar elastin structure as seen by 3D SFBSEM images. The intersection of planes A and B have been chosen to align with an IEF structure. The IEF does not extend in the  $z$  direction and is almost parallel with elastin laminae thus in the circumferential direction.

## Discussion

Our results showed that including an anisotropic formulation for the SEF of elastin, with one family of fibers in the circumferential direction, could significantly improve the quality of  $P-r_0$  and  $P-F_z$  curve fits ( $\Phi$  value was reduced from 1.189 to 0.1909). Assessment of arterial tissue ultrastructure, based on scanning microscopy techniques, revealed interlamellar elastin fibers running in the circumferential direction between the elastin lamellar sheets, thereby providing substantial evidence for this anisotropy. These ultrastructural features were formulated in an anisotropic strain energy function for elastin, which included an isotropic part, representing the elastin lamellar sheets, and an anisotropic part for the family of fibers in the circumferential direction. The results also indicated that in the absence of a structurally functional elastin, collagen engages more abruptly and the angle of collagen fibers is altered, suggesting an interaction between elastin and collagen constituents, an important feature often neglected in the definition of arterial SEFs.

## Elastin in constituent-based SEFs

In the present study, we have suggested a transversely isotropic SEF for arterial elastin with elastin as a fiber-reinforced material having one family of fibers in the circumferential direction. Table 3 summarizes characteristics of some constituent-based SEFs previously reported in the literature. The table provides the properties of each mural constituent

considered for the formulation of the SEF and the type of experimental data used to validate these SEFs. In both the SEF of Holzapfel et al. (Holzapfel et al. 2000) and the model of Zulliger et al. (Zulliger et al. 2004), collagen is the only constituent which contributes to the anisotropic properties of the vascular tissue, and elastin is considered as an isotropic material. These models were validated using P-r<sub>0</sub> curves of intact arteries. However, when forced to fit the P-r<sub>0</sub> and P-F<sub>z</sub> curves simultaneously, they provided a poor fit (Rezakhaniha and Stergiopoulos 2008; Zulliger et al. 2004). Our results suggest that the shortcomings of these models to fit the multidimensional data are mainly due to the elastin definition in their constituent-based SEF. The collagen term in their SEF seems to be appropriate, because it can successfully fit both the P-r<sub>0</sub> and the P-F<sub>z</sub> curves simultaneously in the absence of elastin (Fig. 4.b).

The present study indicates that an anisotropic formulation for elastin can improve the match between SEF and experimental measurements. In a former study on isolated arterial elastin (autoclaved and alkali-treated), Gundiah and colleagues tested pig thoracic aortas using a biaxial stretcher system. They proposed an orthotropic material symmetry for arterial elastin, but suggested that an isotropic SEF could successfully describe the biaxial data (Gundiah et al. 2007; Gundiah et al. 2009). Since the microstructure and mechanical behavior of normal arterial wall varies with location along the vascular tree and species (Humphrey 2002), the observed difference in mechanical behavior of elastin could be species/location dependent (pig thoracic aorta vs rabbit common carotid). In addition, the study of Gundiah et al. was based on techniques of collagen digestion. Digestion techniques can affect the mechanical properties of the resulting network. For example hot alkali treatment causes fragmentation of the elastin network (Daamen et al. 2001; Lillie and Gosline 1990). Finer features, such as IEFs, might also be degraded while larger features remain. The damage to fine structures could affect the degree of elastin anisotropy, but this needs to be verified through careful ultrastructural assessment with appropriate imaging techniques.

**Table 3 A summary of existing constituent-based SEFs**

	Experimental data used for validation	Elastin	Collagen	SMCs
(Holzapfel et al. 2000)	Various intact arteries	<ul style="list-style-type: none"> <li>• Isotropic</li> </ul>	<ul style="list-style-type: none"> <li>• Anisotropic</li> <li>• Two family of fibers</li> <li>• Orientation of fibers</li> </ul>	-----
(Zulliger et al. 2004)	Various intact arteries	<ul style="list-style-type: none"> <li>• Isotropic</li> </ul>	<ul style="list-style-type: none"> <li>• Anisotropic</li> <li>• Two family of fibers</li> <li>• Orientation of fibers</li> <li>• Waviness of fibers</li> </ul>	Contraction state
(Gundiah et al. 2007)	Autoclaved and alkali-extracted porcine thoracic arteries	<ul style="list-style-type: none"> <li>• Isotropic (two orthogonal family of fibers with same material properties)</li> </ul>	-----	-----
(Rezakhaniha and Stergiopoulos 2008)	Intact rabbit facial veins	<ul style="list-style-type: none"> <li>• Anisotropic (one family of fibers in the longitudinal direction)</li> </ul>	<ul style="list-style-type: none"> <li>• Anisotropic</li> <li>• Two family of fibers</li> <li>• Orientation of fibers</li> <li>• Waviness of fibers</li> </ul>	-----

In a recent study on rabbit facial veins, we have suggested an anisotropic SEF considering elastin as a fiber reinforced material with one family of fibers in the longitudinal direction (Rezakhaniha and Stergiopulos 2008). In the current study on arteries, we observed likewise that an anisotropic formulation for elastin could improve the quality of fits. However, contrary to the longitudinal orientation of elastin fibers in veins, we had to consider the fibers in the circumferential direction to obtain the best fit in arteries. In the present study, the circumferential direction of fibers was justified by the circumferential direction of IEF structures in arteries (Fig. 9). In the study on veins, no histological reason for fiber direction was investigated and the results were only based on the quality of the fits. Assuming that the direction of IEFs dictates the direction of fibers in the SEF, one can imagine axially oriented IEFs for the studied veins. A more detailed study of elastin structure in veins and arteries could be helpful to clarify the subject.

The present model assumes that all elastin fibers are oriented in the circumferential direction. This assumption is supported by visual inspection of microscopic images of the wall structure. Yet, realistically, the fibers are distributed around some mean direction. Consequently, the dispersion of fiber orientation could influence the overall behavior of the model. Based on our results, the model with only one family of fibers in circumferential direction could fit successfully the experimental data. Therefore, we believe that considering all the fibers in an effective circumferential direction is an acceptable assumption. A detailed future study on the angular distribution of IEFs would be needed to validate our assumption and to define in greater detail the structural properties of the elastin fiber network.

As for the isotropic part of elastin, we have chosen a neo-Hookean SEF, suggested by Holzapfel and Weizsacker (Holzapfel and Weizsacker 1998). This was different from our previous study on veins (Rezakhaniha and Stergiopulos 2008) where the SEF suggested by Zulliger et al. was utilized (Zulliger et al. 2004):

$$\Psi_{iso} = c_{elast}^i (I_1 - 3)^{3/2} \quad (14)$$

The model by Zulliger et al. was based on an improved fit to the gross mechanical response of arteries. Watton et al. recently compared the model of Zulliger et al. for elastin with the neo-Hookean model and concluded that the neo-Hookean model captures more accurately the mechanical response of elastin (Watton et al. 2009). In summary, they observed that the model suggested by Zulliger et al. does not yield a good fit to (uniaxial) experimental data within the physiological range of stretches. Furthermore, the infinitesimal shear modulus is zero in the linear limit and therefore, violates a basic requirement of continuum mechanics. Finally, the SEF is not well defined for  $(I_1 - 3) < 0$ , i.e. if the material is slightly compressible. Therefore, the Zulliger et al. SEF may give rise to numerical difficulties in finite element applications. If, on the other hand, elastin is modelled as a rubber like material, the neo-hookean formulation has a sound theoretical basis (Treloar 1942).

In addition, it should be mentioned that the equation 11 could be also presented in an alternative form as,

$$\Psi_{passive} = f_{elast}^i \left( c_{elast}^i (I_1 - 3) \right) + f_{elast}^a \left( c_{elast}^a \left( I_4^a + \frac{2}{\sqrt{I_4^a}} - 3 \right) \right) + f_{coll} \left( \frac{1}{2} \Psi_{coll} \left( \frac{I_4 - 1}{2} \right) + \frac{1}{2} \Psi_{coll} \left( \frac{I_4 - 1}{2} \right) \right) \quad (15)$$

where  $f_{elast}^i$  and  $f_{elast}^a$  represent the volume fraction of the isotropic and anisotropic elastin components, respectively and  $c_{elast}$  is the elastic constant of elastin from a neo-Hookean

description. In this way, the strain energy function could be directly related to the elastin structure.

### **Elastin 3D ultrastructure in arteries**

By definition, constituent-based SEFs need to contain the structural information of each constituent. In this study, we tried to explain the suggested form of the elastin anisotropy based on its 3-D structure. The 3-D structure of arterial elastin has been subject to some controversial studies. While in some species, including man, the individual fibers appear to coalesce to form continuous, uninterrupted sheets, other studies in the pig aorta indicate that the medial elastic fibers retain their individuality and do not form sheets (Clark and Glagov 1985; Grut et al. 1977). Most of these previous microstructural studies have used the information from 2D views in which complex features can easily be misinterpreted. Recently, Denk and Colleagues developed a new technique called the serial block-face scanning electron microscopy (SBF-SEM) to produce nanostructural information in three dimensions (Briggman and Denk 2006; Denk and Horstmann 2004). O'Connell et al. used this novel technique to obtain 3D volumetric information of aortic medial microstructure and described in detail the 3D organization of each wall element in rat abdominal aorta (O'Connell et al. 2008). In the present study, we have used SBF-SEM as well as transmission electron microscopy (TEM) to access the structural organization of elastin in arteries. These techniques provide a basis to define the form of the suggested anisotropic SEF for arterial elastin.

In our study, TEM and SBF-SEM images suggested a nearly circumferential direction of interlamellar elastin fibers. Using TEM, we observed elastin fibers going from lamella to SMCs in a nearly circumferential direction between elastin sheets. These structures were not found in transversely cut sections and we could only detect a cross sectional view of elastin fibers, suggesting that interlamellar elastin structures don't continue in the longitudinal plane and are limited to the circumferential-radial plane. This was confirmed by the 3D SBF-SEM images (Fig. 9). These results constitute the structural basis for the suggested anisotropic form of the arterial elastin, derived from the family of fibers in the circumferential direction.

Our results are in accordance with earlier ultrastructural studies of arteries (Clark and Glagov 1979; Clark and Glagov 1985; Dingemans et al. 2000; O'Connell et al. 2008). Specifically, in a recent study, O'Connell et al. described in detail the medial ultrastructure of rat abdominal aorta using SBF-SEM and confocal microscopy techniques. They reported three unique forms of elastin in the aorta: lamellae, IEFs and radial elastin struts. Of the total elastin volume, lamellae comprised 71%, IEFs 27% and radial elastin struts the remaining 2%. Similar to the current study, O'Connell and colleagues reported that IEFs and SMC nuclei were preferentially oriented in the circumferential direction, which is in agreement with our findings.

### **Collagen's engagement pattern and angle in absence of elastin**

To study interlinks between collagen and elastin structures, we have applied our suggested SEF on experimental data from intact and elastin degraded arteries. Experimental data from vascular tissues, where selectively one of the wall constituents is altered, could be useful in assessing the material behavior of each constituent, their functional coupling and interlinks between different wall elements. These data are therefore helpful to develop the SEF of different wall constituents. Among models with selectively altered constituents, elastase-treated arteries offer an attractive model to access the biomechanical properties of arteries after elastin degradation, as seen in pathologies such as aortic stiffening with age and

aneurysm formation (Dobrin 1989; Dobrin and Canfield 1984; Hayashi et al. 1987). Recently, Fonck et al. studied the collagen engagement profile in intact and elastase-treated arteries by applying the SEF proposed by Zulliger et al. on P-r<sub>o</sub> curves and suggested a clear interaction between collagen and elastin in the arterial wall (Fonck et al. 2007). Following the same approach, in the present study, we extended the work of Fonck et al, first by using both P-r<sub>o</sub> and P-F<sub>z</sub> curves from intact and elastase-treated arteries and second by applying the newly proposed SEF including the elastin anisotropic term.

Our results showed a different pattern for the engagement of collagen before and after enzymatic degradation of elastin. In elastase-treated arteries, collagen appeared to be engaged earlier than in intact arteries and the engagement was more abrupt. The log-logistic form of the distribution function for collagen engagement is somehow arbitrary and certainly not unique, the choice has been motivated by the goodness of the fit to a wide range of experimental data (Fonck et al. 2007; Roy et al. 2005; Zulliger et al. 2004; Zulliger et al. 2004). In the log-logistic distribution (eq. 2), parameters  $k$  and  $b$  characterize the distribution:  $k$  is a shape parameter and  $b$  is a scale or statistical dispersion parameter. The distribution becomes concentrated for smaller values of  $b$  and gets more spread out for larger ones. The mode (peak value) of this statistical distribution is situated at  $b \left( \frac{k-1}{k+1} \right)^{1/k}$ . Therefore, if  $k$  is kept constant, the peak value happens earlier for smaller values of  $b$ . In elastase-treated arteries, for constant  $k=6.63$ , value of  $b$  reduced by 49% from its initial value of 1.63 in intact arteries. Based on Fig. 5, the PDF of elastase-treated arteries is more concentrated and reaches its peak value earlier than the PDF of intact arteries, suggesting earlier and more abrupt collagen engagement pattern.

Fonck et al. studied elastase-treated rabbit carotids and found the same tendency in the engagement of collagen, however reported different values for  $k$  and  $b$  (Fonck et al. 2007). Based on the model of Fonck et al., the peak value happens at  $E=0.912$  in control arteries and 0.869 in elastase-treated arteries compared to the corresponding 1.557 and 0.794 in the current study. Fonck et al. assumed a circumferential direction for collagen fibers and used only P-r<sub>o</sub> curves to fit the data. On the contrary, we let free the angle of collagen fibers, which was necessary to fit simultaneously both P-r<sub>o</sub> and P-F<sub>z</sub> curves. The choice of angle of collagen fibers may have led to different values of  $k$  and  $b$  in these studies. More importantly, we used a neo-Hookean SEF,  $(I_1-3)$ , as the isotropic term for elastin. Fonck et al. applied a different SEF suggested by Zulliger et al.,  $(I_1-3)^{3/2}$ , which makes the elastin stiffer at higher strains and therefore alters engagement parameters of collagen.

Based on Table 2, the angle of collagen fibers ( $\alpha$ ) was increased by 18% after degradation of elastin. Only by allowing  $\alpha$  to vary could we fit both the P-r<sub>o</sub> and P-F<sub>z</sub> curves simultaneously in both intact and elastase degraded arteries. We reported an angle of 0.68 rad (39 degrees) for collagen fibers in intact arteries. Holzapfel et al. have chosen an angle of 29° in their original model (Holzapfel et al. 2000), Driessen et al. have taken  $\alpha=30^\circ$  for the media layer (Driessen et al. 2005). Zulliger et al. found this angle to be 35.0° in porcine carotid arteries (Zulliger et al. 2004). Thus, the angle obtained in the present study is within the range of previously reported values.

The changes in collagen engagement pattern and angle of collagen fibers suggest a mechanical interaction between elastin and collagen. Furthermore, the degradation of elastin appears to alter anisotropic properties of the tissue not only in the elastin-dominated region (low circumferential stretch range) but also in the collagen-dominated region (high circumferential stretch range).

## Limitations

The vascular smooth muscle (VSM) plays an important role in the mechanical properties of the wall. We have neglected the contribution of VSM, because we intended to look only at the “passive” components of the wall, which are principally elastin and collagen and to do so we tested arteries under maximally dilated vascular smooth muscle (VSM). This was achieved in our study by adding a high dose of Sodium Nitroprusside, which according to earlier studies and literature guarantees maximal vasodilation. Maximally dilated VSM is assumed to have a negligible effect on mechanical properties of elastic arteries at its passive state. The assumption has been on the basis that its passive elastic modulus is reported to be about one order of magnitude less than that of elastin (VanDijk et al. 1984). We acknowledge the potential shortcoming of our model, which derives from the fact that other wall components (proteoglycans, ground substance, etc.) were also assumed to have a negligible mechanical effect when compared to the principal structural components, i.e., elastin and collagen.

Electron microscopy images show that smooth muscle cells are oriented in the same direction as interlamellar elastin fibers (IEFs) and thus could contribute to the mechanical properties in the same direction as IEFs. Therefore, the fact that we attribute anisotropy of elastin solely to IEF may not be entirely true and anisotropy at low strains could be also the result of the combined effect of the in-series ensemble of IEF and VSM. Earlier experimental (Roy et al. 2005) and theoretical work (Roy et al. 2008) from our laboratory points towards this direction.

The model suggested in this study is a one-layer model and structural properties have been homogenized throughout the arterial wall. Clearly this does not reflect reality, knowing that the adventitia is primarily comprised of collagen. However, the artery considered in this study (rabbit common carotid) is an elastic artery with the adventitia occupying only about 10% of the wall. Therefore, although a two-layer model could more correctly capture the structural properties of the rabbit common carotid, the error of using a one layer model may be not so significant. Of course, even within the media alone, we have a multi-layer structure (lamellar units) and our model falls again short in that respect providing a simplified description of reality.

## Conclusion

We conclude that in addition to collagen, arterial elastin plays an important role in anisotropic behavior of the tissue in a direct and an indirect manner. The direct role of elastin is a result of its 3D structure, as observed by electron microscopy techniques, which affects the arterial mechanics in the elastin-dominated region. On the other hand, elastin plays an indirect role due to its interlink with collagen and by influencing the collagen engagement, thus affecting the anisotropic properties of the artery in the collagen-dominated region.

## Acknowledgements

The authors would like to thank Dr. Graham Knott and Stephanie Rosset at EPFL’s SV electron microscopy facilities for the assistance with specimen preparation and imaging, Alessandra Griffa and J.C. Sarria at EPFL’s BIOP facilities for their assistance in image analysis and Dr. Bryn Martin for proofreading of the text. This work was supported by the Swiss National Science Foundation (Grant No. 325230-125445).



## References

- Briggman KL, Denk W (2006) Towards neural circuit reconstruction with volume electron microscopy techniques. *Curr. Opin. Neurobiol.* 16:562-570
- Clark JM, Glagov S (1979) Structural Integration Of The Arterial-Wall .1. Relationships And Attachments Of Medial Smooth-Muscle Cells In Normally Distended And Hyper-Distended Aortas. *Lab. Invest.* 40:587-602
- Clark JM, Glagov S (1985) Transmural Organization Of The Arterial Media - The Lamellar Unit Revisited. *Arteriosclerosis* 5:19-34
- Daamen WF, Hafmans T, Veerkamp JH, Van Kuppevelt TH (2001) Comparison of five procedures for the purification of insoluble elastin. *Biomaterials* 22:1997-2005
- Denk W, Horstmann H (2004) Serial block-face scanning electron microscopy to reconstruct three-dimensional tissue nanostructure. *PLoS Biol* 2:e329
- Dingemans KP, Teeling P, Lagendijk JH, Becker AE (2000) Extracellular matrix of the human aortic media: an ultrastructural histochemical and immunohistochemical study of the adult aortic media. *Anat. Rec.* 258:1-14
- Dobrin PB (1989) Patho-Physiology and Pathogenesis of Aortic-Aneurysms - Current Concepts. *Surg. Clin. North Am.* 69:687-703
- Dobrin PB, Canfield TR (1984) Elastase, Collagenase, and the Biaxial Elastic Properties of Dog Carotid-Artery. *Am. J. Physiol.* 247:H124-H131
- Driessen NJB, Bouten CVC, Baaijens FPT (2005) A structural constitutive model for collagenous cardiovascular tissues incorporating the angular fiber distribution. *Journal Of Biomechanical Engineering-Transactions Of The Asme* 127:494-503
- Driessen NJB, Bouten CVC, Baaijens FPT (2005) A structural constitutive model for collagenous cardiovascular tissues incorporating the angular fiber distribution. *J. Biomech. Eng.* 127:494-503
- Fonck E, Prod'hom G, Roy S, Augsburg L, Rufenacht D, Stergiopoulos N (2007) Effect Of Elastin Degredation on carotid wall mechanics as assessed by a constituent-based biomechanical model *American Journal of Physiology - Heart and Circulatory Physiology* 292:H2754-H2763
- Fung YC, Fronek K, Patitucci P (1979) Pseudoelasticity of Arteries and the Choice of Its Mathematical Expression. *Am. J. Physiol.* 237:H620-H631
- Gasser TC, Ogden RW, Holzapfel GA (2006) Hyperelastic modelling of arterial layers with distributed collagen fibre orientations. *Journal Of The Royal Society Interface* 3:15-35
- Grut W, Edwards J, Evans EJ (1977) Scanning electron microscopy of freeze-dried aortic elastin. *J. Microsc.* 110:271-275
- Gundiah N, Ratcliffe M, Pruitt L (2007) Determination of strain energy function for arterial elastin: Experiments using histology and mechanical tests. *J. Biomech.* 40:586-594
- Gundiah N, Ratcliffe MB, Pruitt LA (2009) The biomechanics of arterial elastin. *Journal of the Mechanical Behavior of Biomedical Materials* 2:288-296

Hayashi K, Takamizawa K, Nakamura T, Kato T, Tsushima N (1987) Effects of Elastase on the Stiffness and Elastic Properties of Arterial-Walls in Cholesterol-Fed Rabbits. *Atherosclerosis* 66:259-267

Holzappel GA, Gasser TC, Ogden RW (2000) A new constitutive framework for arterial wall mechanics and a comparative study of material models. *Journal of Elasticity* 61:1-48

Holzappel GA, Weizsacker HW (1998) Biomechanical behavior of the arterial wall and its numerical characterization. *Comput. Biol. Med.* 28:377-392

Humphrey JD (2002) *Cardiovascular Solid Mechanics: cells, tissues and organs*. Springer-Verlag New York New York

Lillie MA, Gosline JM (1990) The effects of hydration on the dynamic mechanical properties of elastin. *Biopolymers* 29:1147-1160

O'Connell MK, Murthy S, Phan S, Xu C, Buchanan J, Spilker R, Dalman RL, Zarins CK, Denk W, Taylor CA (2008) The three-dimensional micro- and nanostructure of the aortic medial lamellar unit measured using 3D confocal and electron microscopy imaging. *Matrix Biol.* 27:171-181

Rezakhaniha R, Stergiopoulos N (2008) A structural model of the venous wall considering elastin anisotropy. *J. Biomech. Eng.* 130: Doi:10.1115/1.111.2907749

Roy S, Silacci P, Stergiopoulos N (2005) Biomechanical properties of decellularized porcine common carotid arteries. *American Journal of Physiology - Heart and Circulatory Physiology* 289:H1567-H1576

Roy S, Tsamis A, Prod'homme G, Stergiopoulos N (2008) On the in-series and in-parallel contribution of elastin assessed by a structure-based biomechanical model of the arterial wall. *J. Biomech.* 41:737-743

Silver FH, Snowhill PB, Foran DJ (2003) Mechanical behavior of vessel wall: A comparative study of aorta, vena cava, and carotid artery. *Ann. Biomed. Eng.* 31:793-803

Treloar LRG (1942) Thermodynamic study of the elastic extension of rubber. *Trans. Faraday Soc.* 293-298

VanDijk AM, Wieringa PA, van der Meer M, Laird JD (1984) Mechanics of resting isolated single vascular smooth muscle cells from bovine coronary artery. *The American journal of physiology* 246:C277-287

Vito RP, Dixon SA (2003) Blood vessel constitutive models-1995-2002. *Annual Review Of Biomedical Engineering* 5:413-439

Watton PN, Ventikos Y, Holzappel GA (2009) Modelling the mechanical response of elastin for arterial tissue. *J. Biomech.* 42:1320-1325

Zhou J, Fung YC (1997) The degree of nonlinearity and anisotropy of blood vessel elasticity. *Proc. Natl. Acad. Sci. U. S. A.* 94:14255-14260

Zulliger MA, Fridez P, Stergiopoulos N, Hayashi K (2004) A strain energy function for arteries accounting for wall composition and structure. *J. Biomech.* 37:989-1000

Zulliger MA, Stergiopoulos N, Rachev A (2004) A constitutive formulation of arterial mechanics including vascular smooth muscle tone. *Am J Physiol Heart Circ Physiol* 287:H1335-1343

## Chapter 3

---



# **A Structural Constitutive Model for Vascular Wall Considering Angular Dispersion and Waviness of Collagen Fibers**

R. Rezakhaniha, N. Stergiopoulos

Laboratory of Hemodynamics and Cardiovascular Technology  
Institute of Bioengineering  
Ecole Polytechnique Federale de Lausanne  
1015 Lausanne, Switzerland

## **Abstract**

Structural constitutive models of the vascular wall integrate information on composition and structural arrangements of tissue. We have previously developed a model which considers the waviness of collagen fibers. In this study, we have suggested a structural strain energy function that incorporates not only the waviness but also the angular dispersion of fibers. We studied the effect of parameters related to the orientational distribution on macro-mechanical behavior of tissue during inflation-extension tests. The model was further applied on experimental data from rabbit facial veins. Our parametric study showed the model is less sensitive to the orientational dispersion when fibers are mainly oriented circumferentially. The macro-mechanical response is less sensitive to changes in the mean orientation when fibers are more dispersed. The model accurately fitted the experimental data of veins, while not improving the quality of the fit compared to the model without dispersion. Our results showed that the orientational dispersion of collagen fibers could be compensated by a less abrupt and shifted to higher strain collagen engagement pattern. This should be considered when the model is fitted to experimental data and model parameters are used to study structural modifications of collagen fiber network in physiology and disease.

**Keywords:** strain energy functions, constitutive modeling, veins, vascular collagen, orientation distribution, waviness distribution, structural modeling

Submitted to:

Annals of Biomedical Engineering, 2010

## Introduction

Constitutive modeling of vascular tissue has been a challenging area for several decades<sup>13,18</sup>. Structural constitutive models, in particular, attempt to integrate information on composition and structural arrangements of tissue to avoid ambiguities in material characterization. In this way, they offer an insight into the function, structure and mechanics of the principal wall components i.e. elastin, collagen and vascular smooth muscle cells (VSMCs). Structural constitutive models have been developed for a variety of tissues and tissue components including blood vessels<sup>16,28,30</sup>, skin<sup>23</sup>, pericardium<sup>27</sup>, heart valves<sup>9</sup>, tendons and ligaments<sup>19</sup>.

In blood vessels, collagen fibers appear in coiled and wavy bundles in their unloaded state<sup>6,8</sup> and the individual collagen fibers have a deviation from their mean orientations<sup>4,11</sup>. In the media, collagen fibers are strongly co-aligned<sup>11</sup>. Canham et al. reported the angular standard deviation of fibers in the media as  $5.2^\circ$  in brain arteries and  $5.6^\circ$  in coronary arteries<sup>5</sup>. However, within the adventitia layer, collagen fibers have large angular dispersion<sup>11</sup>. A complete structural constitutive model for vascular collagen should incorporate both waviness and orientational distribution of fibers.

Perhaps the most complete framework for structural modeling of fibrous tissue has been presented by Lanir et al.<sup>20-22</sup>. In this framework, the total strain energy function (SEF) is assumed to be a result of the collective contribution of the individual fibers linked with tensor transformations from the fiber coordinates to the global tissue coordinates. A number of previous studies have followed this approach and have incorporated waviness<sup>29,31</sup> or orientational distribution of collagen fibers<sup>1,9,27</sup>, to study the effects of collagen micro-organization on the macroscopic behavior of vascular tissue. Other studies have followed a different approach and involved the use of invariants<sup>15,29,31</sup>. Yet, currently, there is no SEF for the vascular wall, which includes both waviness and angular distribution of collagen fibers and which has been verified using standard inflation-extension tests. We have therefore set as goals of this study to, first, extend our previously developed model<sup>29,31</sup> to include both waviness and angular distribution of collagen fibers, second, to perform a parametric study to analyze the effects of orientational distribution parameters on the macro-mechanical behavior of the vascular tissue and, third, to assess the suitability and importance of including fibers' orientational distribution by applying the model to experimental data from inflation-extension tests.

## Methods

### Experimental database

We have used the experimental set of data from inflation-extension tests, previously reported in our study on rabbit facial veins<sup>25</sup>. The methods were described in detail in the reported manuscript. Briefly, facial veins of rabbits were excised from young animals, the veins were cleaned from the surrounding tissue and the adventitia was removed mechanically. The veins were then mounted on our inflation-extension device and stretched to their *in vivo* length ( $\lambda_z=1.62\pm 0.09$ ). After 10 preconditioning cycles, each vein was inflated in the range of 0-15mmHg and the outer diameter, luminal pressure and longitudinal force were measured. Tests were carried out after adding  $80 \mu\text{mol/L}$  of sodium nitroprusside (SNP) to the bath to relax smooth muscle cells. The geometry of the zero load state and zero stress state were measured directly on intact and cut-open vascular rings and the volumetric fractions of each wall component i.e. elastin, collagen and vascular muscle cells were assessed histologically.

## Mathematical model

The mathematical model presented in this work is an extension of our work on venous tissue<sup>25</sup>. We considered the blood vessel as a thick wall circular cylinder which undergoes inflation-extension tests. To develop the model, time dependent effects were ignored and only the pseudo-elastic loading response was considered. Furthermore, the material was assumed to be incompressible.

To formulate the strain energy function and in the absence of vascular tone, we considered only passive properties of the arterial wall and therefore separated our constituent-based strain energy function into two parts representing the elastin and collagen components:

$$\Psi_{\text{passive}} = f_{\text{elast}} \Psi_{\text{elast}} + f_{\text{coll}} \Psi_{\text{coll}} \quad (1)$$

where  $f_{\text{elast}}$  and  $f_{\text{coll}}$  are the fractions of wall cross-section area composed of elastin and collagen, and  $\Psi_{\text{elast}}$  and  $\Psi_{\text{coll}}$  represent the SEF for the network of elastin and collagen fibers, respectively.

### Elastin SEF

We based our SEF of elastin on our previous work on rabbit veins. We modeled elastin as an anisotropic material, with one family of fibers in the longitudinal direction, embedded in an isotropic matrix with neo-Hookean material properties. We modeled fibers as a one-dimensional material that bears load only along its axis.

$$\Psi_{\text{elast}} = c_{\text{elast}}^i (I_1 - 3) + c_{\text{elast}}^a \left( I_4'' + \frac{2}{\sqrt{I_4''}} - 3 \right) \quad (2)$$

where  $c_{\text{elast}}^i$  and  $c_{\text{elast}}^a$  represent the moduli for the isotropic and anisotropic elastin components.  $I_1$  is the first invariant of the Cauchy-Green deformation tensor  $C$  and  $I_4''$  is an invariant of  $C$  with respect to  $e_z$  defined as:

$$I_4'' = e_z \cdot C \cdot e_z = \lambda_z^2 \quad (3)$$

$e_z$  being the unit vector in the axial direction.

### Collagen SEF

The constitutive model for collagen used here is based on the work by Lokshin and Lanir on fibrous connective tissue<sup>20,21,23</sup>. The framework is therefore founded on the assumption that the gross behavior of the tissue results from the collective contribution of the individual components.

Schematically, the model for collagen is shown in Fig. 1. Collagen fibers are considered to be wavy in their unloaded state and arranged in two symmetric families of fibers in the circumferential-longitudinal plane. Each fiber is characterized (in the unstrained state) by its directional vector  $\mathbf{u}$  and its local straightening strain  $E^*$ . The  $\mathbf{u}$  coincides with the overall direction of the fiber<sup>21</sup> and makes an angle  $\theta$  with respect to the circumferential direction. In each family of fibers, we assume that individual fibers follow a distribution around their mean orientation  $\alpha$  in a statistical manner, with  $R(\theta)$  being the angular distribution of a family of fibers. Therefore,  $R(\theta)d\theta$  is the fraction of fibers oriented between  $\theta$  and  $\theta+d\theta$ .

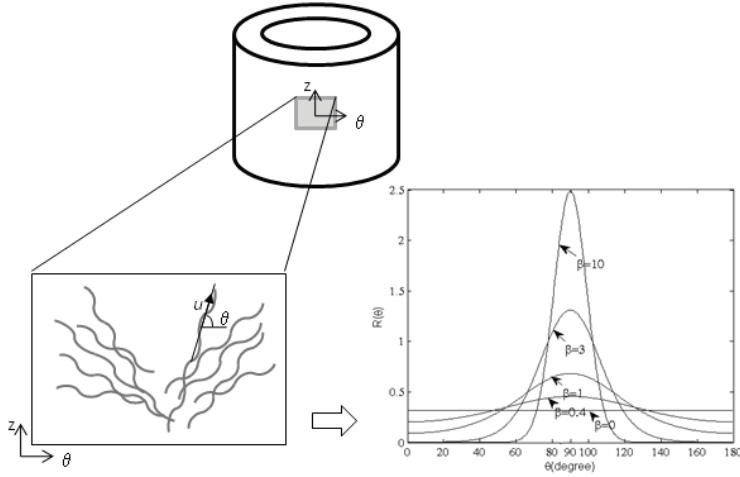


**Figure 1. A schema of the angular distribution of collagen fibers**

The collagen fibers are undulated. We assume that the load required to straighten fibers is negligible when compared to the load transmitted by the stretched fibers. Hence, collagen fibers transmit load only if stretched beyond the point where undulations disappear. This point is represented by  $E^*$ , the engagement strain in the direction of fibers, defined as:

$$E^* = \frac{(\lambda^*)^2 - 1}{2} \quad (4)$$

where  $\lambda^*$  is the stretch along the fiber at which the fiber straightens. We assume that for all fibers in the direction  $\theta$ , the engagement of the collagen fibers happens in some statistical manner<sup>7, 28</sup>. A log-logistic probability distribution function<sup>29, 31</sup> ( $\rho_{fiber}$ ) is chosen to account for the distribution of the engagement strain  $E^*$ :

$$\rho_{fiber}(E^*) = \begin{cases} 0 & \text{for } E^* < 0 \\ k \frac{\left(\frac{E^*}{b}\right)^{k-1}}{b \left[1 + \left(\frac{E^*}{b}\right)^k\right]^2} & \text{for } E^* \geq 0 \end{cases} \quad (5)$$

$b > 0$  is a scaling parameter and  $k > 0$  defines the shape of the distribution.

As stated above, we assume that fibers carry load only when stretched. For a bundle of straight fibers with the same overall direction, the strain energy function is defined by:

$$\Psi_{fiber}(E^f) = \begin{cases} 0 & \text{for } E^f < 0 \\ \frac{1}{2} c_{coll} (E^f)^2 & \text{for } E^f \geq 0 \end{cases} \quad (6)$$



where  $c_{coll}$  is an elastic constant and  $E^f$  is the local Green strain with respect to the fiber's straight configuration.

We assume that the distribution of the engagement pattern is independent of fiber orientation. This means that fibers oriented in any direction  $\theta$ , engage following the same probability density function  $\rho_{fibers}$ , as defined earlier. Let us consider a family of fibers oriented in the direction  $\theta$  with respect to the circumferential direction. The green strain in the main direction of fibers is:

$$E = E_\theta \cos^2 \theta + E_z \sin^2 \theta \quad (7)$$

$E_\theta$  and  $E_z$  are Green strains in the circumferential and longitudinal directions, respectively. The deformations have been calculated considering a circular cylindrical vessel whose zero-stress state is a circular sector<sup>14,29</sup>.

At a certain Green strain along the fibers  $E$ , the true strain in the fiber, with the straightening strain  $E^*$ , will be  $(E-E^*)/(1+2E^*)$  as explained in detail by Lokshin and Lanir<sup>23</sup>. Thus, the contribution of the fibers oriented between  $\theta$  and  $\theta+d\theta$  becomes:

$$\Psi_{coll}^\theta(E) = \int_0^E \rho_{fiber}(E^*) \Psi_{fiber} \left( \frac{E-E^*}{1+2E^*} \right) dE^* \quad (8)$$

Consequently, the SEF of the ensemble of a family of fibers is defined as:

$$\Psi_{coll}^f = \int_0^\pi \left( \int_0^E \rho_{fiber}(E^*) \Psi_{fiber} \left( \frac{E-E^*}{1+2E^*} \right) dE^* \right) R(\theta) d\theta \quad (9)$$

Thus the collagen SEF with half of the fibers having the angular distribution  $R(\theta)$  with mean angle  $\alpha$  and the other half having  $R'(\theta)$  with mean angle  $-\alpha$  to the circumferential direction becomes:

$$\Psi_{coll} = \frac{1}{2} \left( \int_0^\pi \left( \int_0^E \rho_{fiber}(E^*) \Psi_{fiber} \left( \frac{E-E^*}{1+2E^*} \right) dE^* \right) R(\theta) d\theta + \int_0^\pi \left( \int_0^E \rho_{fiber}(E^*) \Psi_{fiber} \left( \frac{E-E^*}{1+2E^*} \right) dE^* \right) R'(\theta) d\theta \right) \quad (10)$$

### Form of angular distribution $R(\theta)$

We assume that the orientation (main direction, as defined in Fig. 1) of collagen fibers is distributed according to a planar  $\pi$ -periodic von-Mises distribution:

$$R(\theta; \alpha, \beta) = \frac{1}{\pi I_0(\beta)} e^{\beta \cos(2(\theta-\alpha))} \quad \text{for } 0 \leq \theta < \pi \quad (11)$$

where  $I_0$  denotes the modified Bessel function of the first kind and order 0, which can be defined by:

$$I_0(\beta) = \frac{1}{2\pi} \int_0^{2\pi} e^{\beta \cos \theta} d\theta \quad (12)$$

The parameter  $\alpha$  is the mean direction and the parameter  $\beta$  is known as the concentration parameter.

The distribution is uni-modal and symmetrical about  $\theta=\alpha$ <sup>24</sup>.

There are various useful measures of dispersion and concentration of a distribution on the circle. The *circular variance*  $v$  of a random angle  $\theta$  is defined as:

$$v = 1 - \rho \quad (13)$$

where  $\rho$  is the *mean resultant length* and  $0 \leq v \leq 1$ .  $v=0$  if and only if the distribution is concentrated around the mean angle. If  $v=1$ , then the distribution can be regarded as so scattered that there is no concentration around any particular direction. The *circular standard deviation*  $\sigma$  is defined as<sup>24</sup>:

$$\sigma = \{-2 \log(1 - v)\}^{1/2} = \{-2 \log \rho\}^{1/2} \quad (14)$$

For the von-Mises distribution  $\rho$  is equal to  $A(\beta)$ <sup>24</sup>:

$$A(\beta) = \frac{I_1(\beta)}{I_0(\beta)} \quad (15)$$

Where  $I_l$  denotes the modified Bessel function of the first kind and order  $l$ :

$$I_l(\beta) = \frac{1}{2\pi} \int_0^{2\pi} \cos \theta e^{\beta \cos \theta} d\theta \quad (16)$$

The larger the value of  $\beta$ , the greater the clustering around the mode. As an example, the distribution is illustrated in Fig.1 for mean value of  $\alpha=90$  and  $\beta$  values of 0, 0.4, 1, 3 and 10. When  $\beta=0$ , the distribution  $R(\theta; \alpha, \beta)$  is uniform, meaning that there is no preferential angle for the ensemble of fibers. For larger values of  $\beta$ , the distribution becomes more concentrated around the mean angle  $\alpha$ .

Assuming that the two families of fibers are symmetric with respect to the longitudinal direction, we set  $\alpha'=-\alpha$  and we take the same concentration parameter  $\beta$ , as used for  $R(\theta)$ , for definition of  $R'(\theta)$ .

## Parametric study of effects of mean collagen fiber angle and angle dispersion

The parametric study was designed to elucidate the effect of concentration parameter  $\beta$  and mean direction  $\alpha$  of collagen fibers on the macro-mechanical behavior of a vascular tube, which undergoes inflation-extension tests. The geometry of the reference (zero stress) state has been taken from our recent study on rabbit facial veins<sup>25</sup>. The opening angle was  $115 \pm 12$  deg and average inner and outer arc lengths were  $9.72 \pm 0.83$  mm and  $10.8 \pm 0.83$  mm, respectively. Elastic constant  $c_{coll}$ ,  $c_{elast}^i$ ,  $c_{elast}^a$  and collagen engagement parameters  $k$  and  $b$  were taken from the best fit of the model with highly orientational fibers on the rabbit facial vein data<sup>25</sup>. Area fractions  $f_{elast}$  and  $f_{coll}$  were set to 0.10 and 0.48 as reported by the same study<sup>25</sup>. These parameters, used in the SEF, are listed in Table 1.

**Table 1. Values used for the parametric study**

parameter	Fitted value
$f_{elast}$	0.10
$f_{coll}$	0.48
$c_{coll}$	200 MPa
$c_{elast}^i$	12392 Pa
$c_{elast}^a$	7436 Pa
$k$	6.21
$b$	3.26

We studied the pressure-radius (P-r<sub>o</sub>) and pressure-longitudinal force (P-F<sub>z</sub>) response of the vessels using different sets of values for  $\alpha$  and  $\beta$ . The mean orientation angle  $\alpha=34.2^\circ$  reflects the best fit for the set of experimental data on our previous study<sup>25</sup>. Having set  $\alpha$  to  $34.2^\circ$ , we studied the effect of parameter  $\beta$  on vessel response. In addition to the ‘‘control value’’ i.e.  $\alpha=34.2^\circ$ , two other values of mean direction of fibers were chosen, a lower value  $\alpha=14.2^\circ$  and a higher value  $\alpha=54.2^\circ$ . These values stand in the physiological range. For each of these mean direction angles,  $\beta$  was set to  $\beta=0, 1, 10$  and  $1000$ .  $\beta=0$  shows the uniform distribution of fibers (isotropic case) and  $\beta=1000$  the highly concentrated distribution of fibers around the mean angle  $\alpha$ . For values of beta larger than 1000, we did not observe significant changes in the macro response of the tube (less than 1% difference), therefore, for all practical purposes, we will refer to  $\beta=1000$  as  $\beta=\infty$ .

### Fitting the model to experimental data

To assess the effect of including a dispersion parameter on the quality of fits for P-r<sub>o</sub> and P-F<sub>z</sub> curves, the new model including dispersion is fit to the experimental data on rabbit facial veins. Parameters  $c_{elast}^i$ ,  $c_{elast}^a$ ,  $k$ ,  $b$ ,  $\alpha$  and  $\beta$  were allowed to vary to be optimized in the curve fitting process. The elastic constant of collagen was chosen as  $c_{coll}=200$  MPa, a reasonable value taken from the literature and in accordance with Zulliger et al.<sup>29</sup>. Pressure-radius and pressure-longitudinal force curves were fitted to the experimental data by minimizing the following function using MATLAB R2007b (MATLAB, USA):

$$\Phi = \frac{1}{2} \frac{1}{m} \sum_i^m \left( \frac{r_i^{mod} - r_i^{exp}}{\sigma_i^r} \right)^2 + \frac{1}{2} \frac{1}{m} \sum_i^m \left( \frac{F_i^{mod} - F_i^{exp}}{\sigma_i^F} \right)^2 \quad (17)$$

$m$  is the number of experimental points measured at different pressures. Superscript *mod* denotes the values predicted by the mathematical model, whereas superscript *exp* shows those measured experimentally. Index  $i$  denotes the experimental points, i.e., the pairs of pressure and corresponding outer radius,  $r$ , and longitudinal force,  $F$ .  $\sigma$  is the standard deviation of the experimental mean value of radius or force at a given pressure and longitudinal stretch ratio. It is used as a weighting factor, giving more weight to the points with the least variation. The  $\Phi$  function has been used as a measure of the quality of the fit. Lower values of  $\Phi$  are representing higher fit qualities.

The quality of the fit, based on the new model including fiber dispersion, was compared with the one with perfectly aligned fibers (no dispersion)<sup>25</sup>. This model is equivalent to  $\beta=\infty$  referred to as the ‘original model’ in this article. For the model with no fiber angle dispersion,  $c_{coll}$  was also taken equal to 200 MPa and parameters  $c_{elast}^i$ ,  $c_{elast}^a$ ,  $k$ ,  $b$  and  $\alpha$  were allowed to vary freely to be optimized for best fit.

## Results

### Parametric analysis

Fig. 2 shows the effect of dispersion parameter  $\beta$  on P- $r_o$  and P- $F_z$  curves. Columns a, b and c represent the model predictions for  $\alpha$  equal to 14.2, 34.2 and 54.2 degrees respectively. The solid curve in Fig. 2 plots the response of the tube for  $\beta=0$  (the isotropic case in which orientation of collagen fibers is distributed uniformly). Our results showed that for values of  $\beta$  higher than 1000 (circular standard deviation  $\sigma$  less than 1.8°) the radius and longitudinal-force values changed only slightly (less than 1%). Therefore, the value  $\beta=1000$  has been used for the case of highly oriented fibers (dashed line ----) and referred to as  $\beta=\infty$  in the figures. The effect of concentration parameter  $\beta$  on P- $r_o$  and P- $F_z$  curves seemed to depend on the mean orientation. As seen from Fig. 2, for  $\alpha=14.2$ , the curves for  $\beta=10$  and  $\beta=\infty$  almost overlap. For instance, at P=2 KPa (15 mmHg),  $r_o$  is 1.781 for  $\beta=10$  compared to 1.780 mm for  $\beta=\infty$  showing a difference of less than 0.1%. The variations in  $F_z$  are also less than 1%. However, for  $\alpha=54.2$ , the effect of concentration parameter  $\beta$  becomes much more important. For the same pressure value (2 KPa), when  $\alpha$  is fixed to 54.2°,  $r_o$  is equal to 2.19 mm for  $\beta=10$  compared to 2.37 mm for  $\beta=\infty$  showing a decrease of around 8% in radius. As for the longitudinal force,  $F_z$  decreases from 9.17 mN for  $\beta=\infty$  to 2.88mN for  $\beta=10$ , a difference of more than 69%.

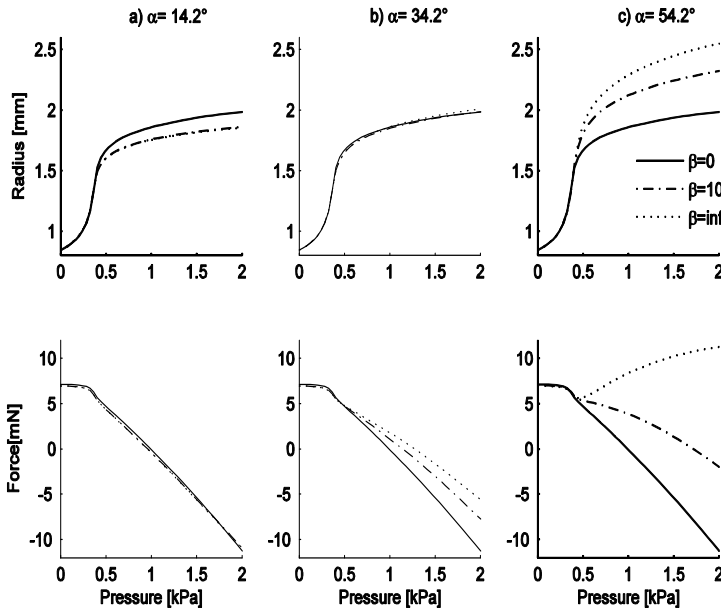


Figure 2. Effect of the concentration parameter  $b$  on P- $r_o$  and P- $F_z$  curves

$\beta=0$  is the equivalent of an isotropic distribution of the orientation of collagen fibers. Therefore, for  $\beta=0$  the different mean fiber orientations (indicated by different angles  $\alpha$ ) lose their meaning and the response of the tube is isotropic (solid curves in Fig. 2). On the contrary, for values of  $\beta=1, 10$  and  $1000 (\infty)$  plotted in Fig. 3 the macro-mechanical response of the tissue depends on the mean orientation of the fibers. Based on Fig. 3, the response of the material with highly oriented fibers ( $\beta=\infty$ ) depends strongly on the mean orientation angle  $\alpha$ . For example, at  $P=2$  KPa (15 mmHg) and  $\alpha=34.2^\circ$ , the radius and longitudinal pressure are  $r_o=1.90$  mm and  $F_z=0.323$  mN respectively. Increasing the mean alignment to  $\alpha=54.2^\circ$  gives values of  $r_o=2.37$  mm and  $F_z=9.17$  mN showing 25% increase in radius and 2740% increase in longitudinal force.

### Fitting the model to experimental data

Fig 4. Shows the best fit for the experimental data on the medial layer of rabbit facial veins using the original model (with all fibers in a family of fibers aligned in one direction) as well as the modified model, which includes the dispersion of collagen fibers. The values used to fit the data have been shown in Table 2. As seen from Fig. 4 and Table 2, for this set of data, the quality of fits is almost the same ( $\Phi=0.188$  for the original model compared to  $\Phi=0.181$  for the modified model), hence, for this particular vessel including dispersion in the collagen fibers does not seem to improve the quality of the fit.

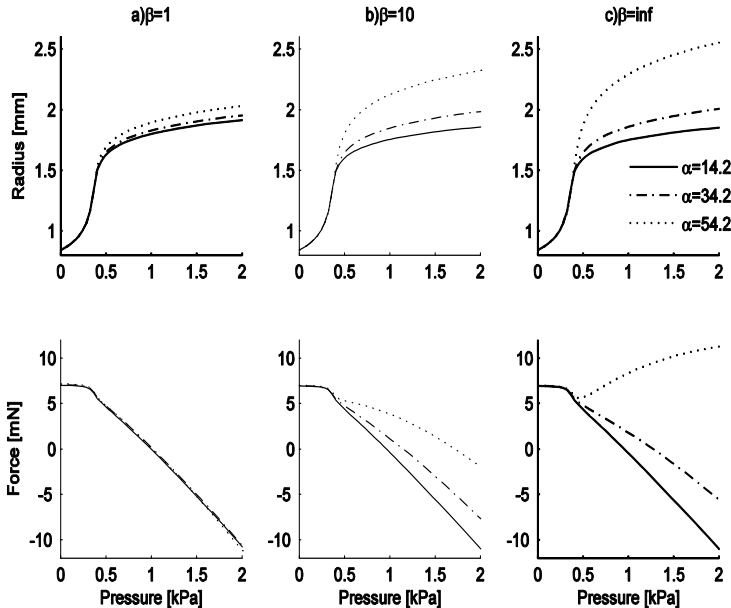


Figure 3. Effect of the angle parameter  $\alpha$  on  $P-r_o$  and  $P-F_z$  curves

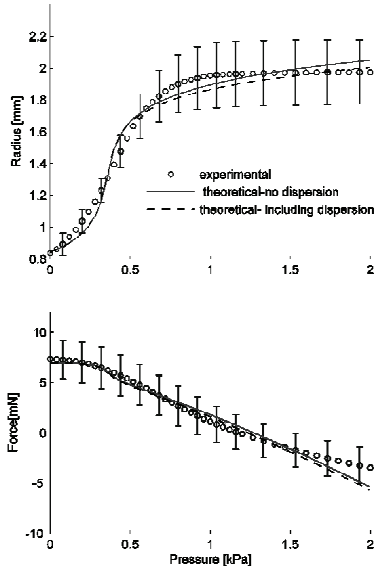


Figure 4. Best fit from the original model with no dispersion (\_\_\_\_) and the modified model including dispersion (-----) on experimental data from inflation-extension tests

Table 2. . Parameters used in minimizing  $\Phi$

Strain energy function		Original model (without dispersion)	modified model (with dispersion)
Fitted parameters		$c^i_{elast}=12392 Pa$ $c^a_{elast}=7436 Pa$ $k=6.21$ $b=3.26$ $\alpha=34.2^\circ$	$c^i_{elast}=12468 Pa$ $c^a_{elast}=7344 Pa$ $k=5.87$ $b=3.53$ $\alpha=36.2^\circ$ $\beta=217.73$
Experimentally defined parameters		$f_{elast}=0.101$ $f_{coll}=0.482$	$f_{elast}=0.101$ $f_{coll}=0.482$
Imposed on model		$c_{coll}=200 MPa$	$c_{coll}=200 MPa$
$\Phi$		0.188	0.181

## Discussion

In this study, a structural constitutive model for the macro-mechanical behavior of vascular tissue is presented based on the framework developed by Lanir et al. <sup>20,21</sup>. The new model incorporates both waviness and orientational distribution of collagen fibers. The waviness of fibers is modeled by a log-logistic distribution <sup>29,31</sup>. To account for the angular distribution of fibers, we suggested a planar  $\pi$ -periodic von-Mises distribution with mean orientation  $\alpha$  and concentration parameter  $\beta$ . We studied the effect of these parameters ( $\alpha$  and  $\beta$ ) on the macroscopic vessel response to inflation-extension tests, typically expressed as P-r<sub>0</sub> and P-F<sub>z</sub> curves. Finally, the new model was applied to fit experimental data of inflation–extension tests of rabbit facial veins in order to assess the usefulness or necessity of including the fiber angle dispersion in the model.

### The choice of strain energy function for collagen

Various structural energy functions have been developed previously to account for collagen microstructure in cardiovascular tissue. In this study, we modeled both waviness and orientational distribution of collagen fibers. Collagen fibers appear to be coiled and wavy in their unloaded state <sup>6,8</sup> and form two helically arranged families of fibers. The individual collagen fibers, in each family, show a deviation from their mean orientations <sup>4,11</sup>. Similar to our approach, some of previous studies also followed the work by Lanir et al. <sup>20,21</sup>. Billiar and Sacks proposed a model for aortic valve cusps and introduced the orientational distribution of collagen fibers to their model by means of a Gaussian Distribution <sup>1</sup>. Sacks extended the previous work and included further the pattern of recruitment of fibers in the model using a gamma distribution <sup>27</sup>. As for the orientational distribution of collagen fibers, differently from their earlier work, Sacks proposed a beta distribution and the modified model was applied on biaxial tests of Bovine pericardium. Other studies followed a different approach involving the use of invariants and introducing concepts of waviness, as the studies of Zulliger et al. and Cacho et al. <sup>2,31</sup>, or orientational distribution, as in the works of Gasser et al. and Driessen et al. <sup>9,15</sup>.

In the present study, we used a log-logistic distribution to account for waviness and the gradual engagement of the fibers, similar to the study of Zulliger et al. <sup>31</sup>. As Zulliger et al. have commented, the choice of the distribution function is fairly arbitrary. The present formulation to model the waviness is, however, slightly different from the one suggested by Zulliger et al. Zulliger and colleagues suggested that the waviness can be modeled by a convolution resulting in a  $\Psi^{\theta}_{coll}$  as:

$$\Psi^{\theta}_{coll}(E) = \rho_{fiber} * \Psi_{fiber} = \int_0^E \rho_{fiber}(E^*) \Psi_{fiber}(E - E^*) dE^* \quad (18)$$

On the contrary the present study models the waviness as:

$$\Psi^{\theta}_{coll}(E) = \int_0^E \rho_{fiber}(E^*) \Psi_{fiber} \left( \frac{E - E^*}{1 + 2E^*} \right) dE^* \quad (19)$$

The difference resides in the term  $(E-E^*)/(1+2E^*)$  which expresses the true strain in the group of fibers that are engaged at the Green strain  $E^*$ . For more details, please refer to the work by Lokshin and Lanir <sup>23</sup>.

As for the orientational distribution, we made the assumption that fibers are mainly in the circumferential-longitudinal plane and we have chosen a planar von-Mises probability

density function (PDF) to express the angular distribution of fibers. The assumption that collagen fibers lay preferentially in the circumferential-longitudinal plane seems reasonable based on values reported in the literature for the radial component of collagen fibers. Finlay et al. reported radial angle of around  $5^\circ$  in the adventitia and  $8^\circ$  in the media for collagen in human brain arteries fixed at 30 mmHg<sup>11</sup>. In addition, Canham et al. measured this value to be  $2^\circ$  in the media and  $1^\circ$  in the adventitia of human saphenous veins, fixed at 110 mmHg<sup>3</sup>. As for the choice of orientational distribution, Gasser et al. have used similarly the von-Mises distribution for orientational distribution of collagen fibers with the difference that they assumed a spatial distribution<sup>15</sup> while Billiar and Sakcs chose a Gaussian distribution<sup>1</sup>. The choice of Gaussian over von-Mises distribution does not seem to affect significantly the model since any von Mises distribution can be approximated by a (wrapped) Gaussian distribution<sup>24</sup>. Certainly, more experimental work on orientational distribution as well as the waviness of collagen fibers in various tissues is needed to quantify fibers' structure and clarify the type of the distributions to be used in structural models.

In this study, the vascular wall is for simplicity modeled as a one-layer material. However, the blood vessel is not composed of different layers and the composition and arrangement of intramural wall components differ from one layer to another. For instance, in the media, collagen fibers are circumferentially and coherently aligned, whereas in the adventitia, the pitch of the helically arrange fibers and the dispersity of the fiber distribution increases<sup>3,11</sup>. Obviously, the present model assumes homogenized properties throughout the arterial wall and therefore would be more accurate when only applied to single layer structures. In future studies, a two-layer structure should be developed. Furthermore, since collagen type in the media (primarily of Type I, III and V) is different from the adventitia (primarily of type I)<sup>17</sup>, future studies should also include a different collagen elastic constant for each layer.

### **Effect of orientational distribution parameters $\alpha$ and $\beta$ on gross material response**

The results of our parametric study showed that the effect of concentration parameter  $\beta$  on P- $r_0$  and P- $F_z$  curves depends on the mean orientation of fibers  $\alpha$  (Fig. 2). The model is less sensitive to adding orientational dispersion when fibers are located close to the circumferential direction (lower mean orientation of fibers  $\alpha$ ) than when fibers are located further from the circumferential direction (higher mean orientation of fibers). For instance, when  $\alpha$  was fixed at  $14.2^\circ$  and a circular standard deviation  $\sigma$  of  $18.6^\circ$  was applied ( $\beta=10$ ),  $r_0$  and  $F_z$  did not change more than 1% compared to the case without dispersion ( $\sigma=0$  i.e  $\beta=\infty$ ). However, at  $\alpha=54.2^\circ$ , the P- $r_0$  and P- $F_z$  curves deviated 8% in  $r_0$  and 69% in  $F_z$  compared to the case without dispersion.

The higher values of mean orientation of fibers  $\alpha$  are generally associated with the adventitia<sup>11</sup> while lower mean orientations are associated with the media<sup>4</sup>. Therefore, considering our results, one could conclude that in the presence of the adventitia, the model should include the information about the dispersion of collagen fibers and the effect of dispersion could not be neglected. While when the adventitia is removed (only the media is present), one could use a simpler model that does not include angular dispersion of collagen.

Our results showed that the material response is highly sensitive to the mean orientation of fibers  $\alpha$  when fibers are highly oriented (large values of  $\beta$  i.e. low values of  $\sigma$  which is the case in the media. On the other hand, when fibers are dispersed, which is the case in the adventitia, the material response is less sensitive to the mean orientation of fibers. Gasser et al. have observed the same effect in their study<sup>15</sup>.



## Fitting the model to experimental data

In the present study, the original model of Zulliger et al. (no dispersion,  $\sigma=0$ ) as well as our new model (including dispersion) were fitted to the set of experimental data from a previous study on rabbit facial veins in which the adventitia was removed mechanically<sup>25</sup>. When our model including dispersion was fitted to the data, the best fit was achieved with the concentration parameter  $\beta=144$  ( $\sigma=4.8^\circ$ ). As the adventitia was removed from the tissue, this value would represent the dispersion of collagen fibers in the media. Canham et al. have previously reported the circular standard deviation  $\sigma$  of fibers in the media to be  $5.2^\circ$  in brain arteries and  $5.6^\circ$  in coronary arteries<sup>5</sup>. The results value from our model are therefore similar and consistent with those of Canham et al..

Including dispersion of collagen fibers resulted in almost the same quality of the simultaneous fit of the  $P-r_0$  and  $P-F_z$  curves as the original model of Zulliger et al. ( $\Phi=0.188$  for the original model compared to  $\Phi=0.181$  for the modified model). However, the new model (including dispersion) resulted in a slightly higher (6%) mean orientation of fibers  $\alpha$  as well as an earlier and less abrupt engagement pattern of collagen fibers. The log-logistic probability distribution functions,  $\rho_{fibers}$ , for both models, with and without dispersion, have been plotted in Fig. 5 using the values of  $k$  and  $b$  from Table 2. The probability distribution function  $\rho_{fiber}$  becomes concentrated for smaller values of  $b$  and gets more spread out for larger ones. Based on Table 2, the value of  $b$  is smaller in the original model (without dispersion) than the modified one (including dispersion). Therefore, the original model without dispersion shows a more concentrated distribution and thus a more abrupt engagement.

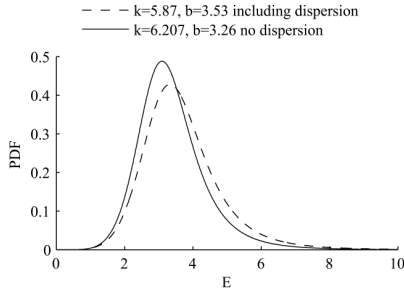


**Figure 5. Log-logistic probability density functions from the best fits using the original model without dispersion (—) and the modified model including dispersion (---), base on values in the table 2**

In addition, the mode (peak value) of the log-logistic distribution is situated at  $b \left( \frac{k-1}{k+1} \right)^{1/k}$ .

Therefore, the peak happens earlier (at  $E=3.09$ ) in the original model without dispersion than the modified one including dispersion (at  $E=3.45$ ), resulting in an earlier engagement of collagen fibers in the Zulliger et al. model than the modified one. The results suggest that including the orientational dispersion of collagen fibers changes the parameters of the collagen engagement pattern. This should be particularly considered when fit parameters are used to study changes in the engagement pattern<sup>12,26</sup> and/or orientational distribution of collagen fibers<sup>10</sup>. As an example, assume that the orientational distribution of collagen fibers

has been changed as a result of a mechanically induced remodeling. A model which does not include the dispersion of fibers could result in an ‘unrealistic’ change in parameters related to engagement pattern of collagen fibers.

## Conclusion

In summary, we developed a strain energy function for vascular tissue considering both waviness and orientational distribution of collagen fibers and studied effects of parameters related to the orientational distribution of collagen fibers. We conclude that including the dispersion of collagen fibers into the model, particularly when the adventitia is removed does not improve the quality of the fit of  $P-r_0$  and  $P-F_2$  curves from inflation-extension tests. However, it is very important to consider the dispersion of fibers when adventitia is included and when structural changes of collagen fibers, such as the collagen engagement pattern or orientation of fibers, are studied. Despite its limitations, the model offers possibilities to better understand the relation between structure and function in the vascular wall and to further study mechanically induced collagen remodeling in vascular tissue in health and disease. This can be achieved by relating fiber turnover, reorientation and waviness reorganization to the mechanical loading conditions.

## Acknowledgements

The authors would like to thank Dr. Tyler Thacher for proof reading of the article. This work was supported by the Swiss National Science Foundation (Grant No. 325230-125445).

## References

- <sup>1</sup> Billiar, K.L. and M.S. Sacks. Biaxial mechanical properties of the native and glutaraldehyde-treated aortic valve cusp: Part II--A structural constitutive model. *J. Biomech. Eng.* 122:327-335, 2000.
- <sup>2</sup> Cacho, F., P.J. Elbischger, J.F. Rodriguez, M. Doblare and G.A. Holzapfel. A constitutive model for fibrous tissues considering collagen fiber crimp. *International Journal of Non-Linear Mechanics.* 42:391-402, 2007.
- <sup>3</sup> Canham, P.B., H.M. Finlay and D.R. Boughner. Contrasting structure of the saphenous vein and internal mammary artery used as coronary bypass vessels. *Cardiovasc. Res.* 34:557-567, 1997.
- <sup>4</sup> Canham, P.B., H.M. Finlay, J.G. Dixon, D.R. Boughner and A. Chen. Measurements from light and polarised light microscopy of human coronary arteries fixed at distending pressure. *Cardiovasc. Res.* 23:973-982, 1989.
- <sup>5</sup> Canham, P.B., E.A. Talman, H.M. Finlay and J.G. Dixon. Medial collagen organization in human arteries of the heart and brain by polarized light microscopy. *Connect. Tissue Res.* 26:121-134, 1991.
- <sup>6</sup> Clark, J.M. and S. Glagov. Transmural Organization Of The Arterial Media - The Lamellar Unit Revisited. *Arteriosclerosis.* 5:19-34, 1985.
- <sup>7</sup> Decraemer, W.F., M.A. Maes and V.J. Vanhuyse. An elastic stress-strain relation for soft biological tissues based on a structural model. *J. Biomech.* 13:463-468, 1980.
- <sup>8</sup> Dingemans, K.P., P. Teeling, J.H. Lagendijk and A.E. Becker. Extracellular matrix of the human aortic media: an ultrastructural histochemical and immunohistochemical study of the adult aortic media. *Anat. Rec.* 258:1-14, 2000.
- <sup>9</sup> Driessen, N.J.B., C.V.C. Bouten and F.P.T. Baaijens. A structural constitutive model for collagenous cardiovascular tissues incorporating the angular fiber distribution. *J. Biomech. Eng.* 127:494-503, 2005.

- <sup>10</sup> Driessen, N.J.B., M.A.J. Cox, C.V.C. Bouten and F.P.T. Baaijens. Remodelling of the angular collagen fiber distribution in cardiovascular tissues. *Biomechanics and Modeling in Mechanobiology*. 2007.
- <sup>11</sup> Finlay, H.M., L. McCyllum and P.B. Canham. Three-dimensional collagen organization of human brain arteries at different transmural pressures. *J. Vasc. Res.* 32:301-312, 1995.
- <sup>12</sup> Fonck, E., G. Prod'homme, S. Roy, L. Augsburg, D. Rufenacht and N. Stergiopoulos. Effect Of Elastin Degredation on carotid wall mechanics as assessed by a constituent-based biomechanical model *American Journal of Physiology - Heart and Circulatory Physiology*. 292:H2754-H2763, 2007.
- <sup>13</sup> Fung, Y.C. *Biomechanics: Mechanical Properties of living tissues*. Springer-Verlag, 1981,
- <sup>14</sup> Fung, Y.C. *Biomechanics: motion ,flow, stress and growth*. New York:Springer-Verlag New York Inc. , 1990,
- <sup>15</sup> Gasser, T.C., R.W. Ogden and G.A. Holzapfel. Hyperelastic modelling of arterial layers with distributed collagen fibre orientations. *Journal Of The Royal Society Interface*. 3:15-35, 2006.
- <sup>16</sup> Holzapfel, G.A., T.C. Gasser and M. Stadler. A structural model for the viscoelastic behavior of arterial walls: Continuum formulation and finite element analysis. *European Journal of Mechanics, A/Solids*. 21:441-463, 2002.
- <sup>17</sup> Humphrey, J.D. *Cardiovascular Solid Mechanics: cells ,tissues and organs*. New York:Springer-Verlag New York 2002,
- <sup>18</sup> Humphrey, J.D. *Cardiovascular solid mechanics: cells, tissues, and organs*. New York Berlin Heidelberg: Springer-Verlag, 2002,
- <sup>19</sup> Hurschler, C., B. Loitz-Ramage and R. Vanderby, Jr. A structurally based stress-stretch relationship for tendon and ligament. *J. Biomech. Eng.* 119:392-399, 1997.
- <sup>20</sup> Lanir, Y. A structural theory for the homogeneous biaxial stress-strain relationships in flat collagenous tissues. *J. Biomech.* 12:423-436, 1979.
- <sup>21</sup> Lanir, Y. Constitutive equations for fibrous connective tissues. *J. Biomech.* 16:1-12, 1983.
- <sup>22</sup> Lanir, Y., O. Lichtenstein and O. Imanuel. Optimal design of biaxial tests for structural material characterization of flat tissues. *J. Biomech. Eng.* 118:41-47, 1996.
- <sup>23</sup> Lokshin, O. and Y. Lanir. Micro and macro rheology of planar tissues. *Biomaterials*. 30:3118-3127, 2009.
- <sup>24</sup> Mardia, K.V. and P.E. Jupp. *Directional statistics*. John Wiley 2000,
- <sup>25</sup> Rezakhanliha, R. and N. Stergiopoulos. A structural model of the venous wall considering elastin anisotropy. *J. Biomech. Eng.* 130: Doi:10.1115/1.111.2907749, 2008.
- <sup>26</sup> Roy, S., P. Silacci and N. Stergiopoulos. Biomechanical proprieties of decellularized porcine common carotid arteries. *American Journal of Physiology - Heart and Circulatory Physiology*. 289:H1567-H1576, 2005.
- <sup>27</sup> Sacks, M.S. Incorporation of experimentally-derived fiber orientation into a structural constitutive model for planar collagenous tissues. *J. Biomech. Eng.* 125:280-287, 2003.
- <sup>28</sup> Wuyts, F.L., V.J. Vanhuysse, G.J. Langewouters, W.F. Decraemer, E.R. Raman and S. Buyle. Elastic properties of human aortas in relation to age and atherosclerosis: A structural model. *Phys. Med. Biol.* 40:1577-1597, 1995.
- <sup>29</sup> Zulliger, M.A., P. Fridez, N. Stergiopoulos and K. Hayashi. A strain energy function for arteries accounting for wall composition and structure. *J. Biomech.* 37:989-1000, 2004.

<sup>30</sup> Zulliger, M.A. and N. Stergiopoulos. Structural strain energy function applied to ageing and hypertension. *Arch. Physiol. Biochem.* 112:67, 2004.

<sup>31</sup> Zulliger, M.A., N. Stergiopoulos and A. Rachev. A constitutive formulation of arterial mechanics including vascular smooth muscle tone. *Am J Physiol Heart Circ Physiol.* 287:H1335-1343, 2004.

## Chapter 4

---



# Experimental Investigation of Collagen Waviness and Orientation in the Adventitia

R. Rezakhaniha<sup>1</sup>, J.T.C Schrauwen<sup>2</sup>, A. Griffa<sup>3</sup>, D. Sage<sup>4</sup>, C.V. C. Bouten<sup>5</sup>, F.N. van De Vosse<sup>2</sup>, M. Unser<sup>4</sup>, N. Stergiopulos<sup>1</sup>

<sup>1</sup> Laboratory of Hemodynamics and Cardiovascular Technology, Institute of Bioengineering, EPFL, Lausanne, Switzerland

<sup>2</sup> Cardiovascular Biomechanics, Department of Biomedical Engineering, Eindhoven University of Technology, Eindhoven, the Netherlands

<sup>3</sup> Bioimaging and Optics Platform, Life Science Faculty, EPFL, Lausanne, Switzerland

<sup>4</sup> Biomedical Imaging Group, EPFL, Lausanne, Switzerland

<sup>5</sup> Soft Tissue Biomechanics & Engineering, Department of Biomedical Engineering, Eindhoven University of Technology, Eindhoven, the Netherlands

## Abstract

Mechanical properties of the adventitia are largely determined by the organization and material properties of collagen fibers. Therefore, measurements on the waviness and orientational organization of collagen, particularly at the zero stress state, are necessary in order to relate their structural organization to mechanical function. Using the fluorescence collagen marker CNA38-OG488 and confocal laser scanning microscopy, we imaged collagen fibers in adventitia of rabbit common carotids *ex vivo*. The arteries were cut open along their longitudinal axes to get the zero stress state. We used semi-manual and automatic techniques to measure parameters related to waviness and orientation of fibers. Our results showed that the straightness parameter (the ratio between the distances of endpoints of a fiber to the fiber length) was distributed with a beta distribution (mean value 0.72, variance 0.028) and this distribution did not depend on the mean angle orientation of fibers. Local angular density distributions revealed 4 axially symmetric families of fibers with mean directions of 0°, 90°, 43° and -43° and circular standard deviations of 40°, 47°, 37° and 37°, with respect to the axial direction, respectively. The distribution of local orientations was shifted to the circumferential direction when measured in arteries at the zero load state (intact), as compared to arteries at the zero stress state (cut open). Information on collagen fiber waviness and orientation, such as the one obtained in this study, could be used to develop structural models of the adventitia, thereby providing better means for analyzing and understanding the mechanical properties of the vascular wall.

**Keywords:** orientation distribution, waviness distribution, collagen fiber, arteries, common carotid, rabbit

To be submitted to:

Am J Physiol Heart Circ Physiol, 2010

## Introduction

Detailed biomechanical modeling of blood vessels should ideally be based on the structural properties of the main constituents of the wall with respect to its different layers. The adventitia is the outermost layer of blood vessels and its mechanical properties are determined mainly by the organization of collagen fibers in this layer. The two main features characterizing collagen fiber organization are its waviness and angular dispersion.

Different techniques such as polarized light microscopy (PLM) [6, 10, 17, 20, 28, 31], small angle light scattering (SALS) [4, 16, 30], transmitted light microscopy (TLM) [9, 14], fluorescence microscopy (FM) [1, 37], micro coherence tomography (Micro-CT) [36], optical coherence tomography (OCT) [19], small angle X-ray scattering (SAXS), second harmonic generation (SHG) [2, 5, 35] and electron microscopy (EM) [18, 24, 36] have been used to characterize collagen bundle orientation and/or crimp properties in soft tissue. Fewer studies have focused on the quantitative organization of collagen fibers within the arterial wall [9, 10, 12, 17, 31]. The studies on arteries have been mainly conducted on pressurized (loaded) and/or chemically fixed and embedded vessels. These procedures could modify structural organization of tissue components [13]. Structural models of the mechanical response of the arterial wall are ideally based on the knowledge of the true zero stress state (ZSS) of each wall constituent, preferably in wet fresh tissue where structural properties have not been changed. Krahn et al. have recently developed a new collagen specific fluorescence marker for tissues and live cell cultures [22] which enables high resolution 3D imaging of collagen fibers in wet fresh tissues [5].

In this study, we have used the fluorescent marker developed by Krahn et al. combined with confocal microscopy and image analysis techniques to quantify the waviness and angular the distribution of collagen fibers in adventitia of fresh arteries at their zero stress state. More specifically, this study was designed to a) quantify the waviness properties of collagen fibers, b) determine how the waviness distribution of fibers depends on their main orientation and c) measure the local angular distribution of collagen fibers in the adventitia of rabbit common carotids.

## Materials and Methods

### Tissue preparation

Fourteen common carotid arteries were excised post mortem from seven white New Zealand male rabbits from a local slaughterhouse. Arteries were transported on ice in phosphate buffered saline (PBS) to the laboratory and cleaned from the surrounding tissue. To visualize collagen fiber, the arteries were incubated over night at 37° in a 2 µM solution of CNA35-OG488 in PBS, which was used as the specific vital fluorescent marker for vascular collagen [22]. After incubation, the common carotid was cut into two equal segments of approximately 25-30 mm in length. One segment was used to measure collagen waviness and orientation in the zero stress state, which was achieved by cutting open carefully along the artery's axis (cut-open group) and then immersed in PBS for 30 minutes before imaging. The other group was kept intact (intact group). All measurements were done within 24 hours of excision.



## Confocal microscopy

We used an upright confocal microscope (Leica SP5 white laser, Leica, Germany) to visualize collagen fibers labeled with the fluorescent marker CNA35-OG488. Arteries were fixed by a pin on a silicon coated Petri dish filled with PBS, with the adventitia facing upwards (Figure 1). Two circumferential lines close to each border were marked by a blue Miller's elastic stain as shown in Figure 1. The distance between these lines was measured before and after fixing the tissue on the Petri dish to ensure that the arteries were not stretched. In addition, the field of view on the Petri dish was rotated in a way that the horizontal axis of images was parallel with the axial axis of the vessel. The fluorescent marker was excited at 488nm by an Argon laser and a photomultiplier tube (PMT) detector was defined at 498-550 nm to collect the emitted fluorescent signal. Ten arterial segments per group were scanned at 5 different locations along the longitudinal axis. At each location a z-stack with a step size of  $0.5 \mu\text{m}$  was obtained, resulting in a total image size of  $238\mu\text{m} \times 238 \mu\text{m} \times \sim 100\mu\text{m}$ . In total, 50 z-stacks were imaged for each group. Figure 1 shows an example of the image stack after 3D reconstruction by IMARIS software (Bitplane, Switzerland).

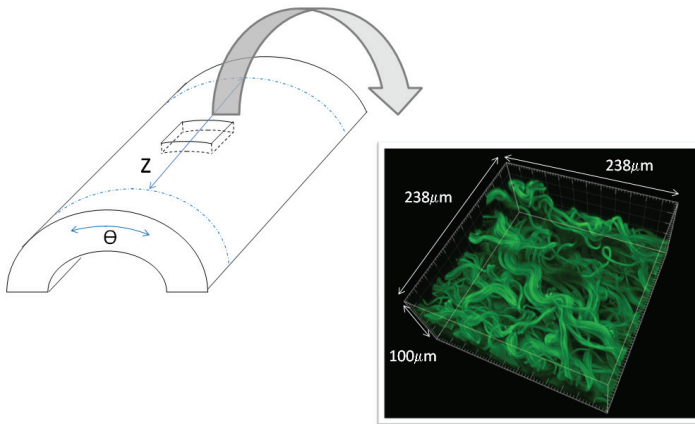


**Fig. 1** An example of the 3D reconstruction of outermost layer of adventitia

## Image analysis

### 3D measurement of angle fibers

The orientation of collagen bundles in two representative z-stacks from each group was measured by manually locating endpoints of each collagen bundle using IMARIS Software. Figure 2 shows an example of 3D reconstruction of collagen fibers from the z-stacks. Fibers have been manually traced and the global orientation of each fiber has been measured in a spherical coordinate system. The orientation of a fiber in 3D could be therefore described by the azimuthal angle  $\alpha$  (between  $-\pi/2$  and  $\pi/2$ ) and the latitude (radial) angle  $\varphi$  (between 0 and  $\pi$ ) as shown schematically in Figure 2.

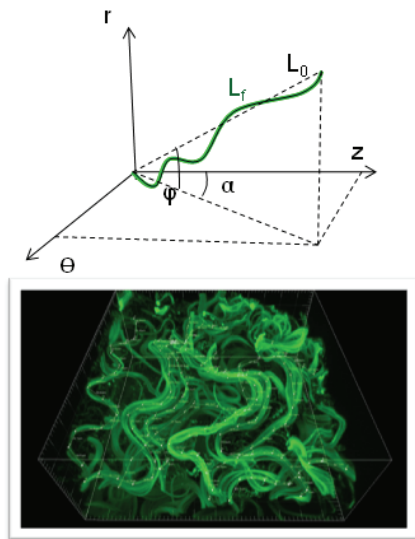


**Fig. 2** latitude (radial) angle  $\varphi$  measured by manual tracing of fibers in a representative 3D reconstruction of z-stacks

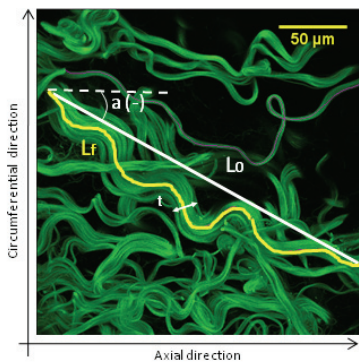


**Fig. 3** Definition of measured parameters i.e. global angle ( $a$ ), thickness ( $t$ ) and length ( $L_f$ ) of a fiber bundle as well as the length of a straight line connecting the ends of the measured fiber bundle.

## 2D image analysis

Based on the hypothesis that the radial angle  $\varphi$  is small and in order to facilitate the image analysis, the z-stacks were flattened using the maximum intensity projection (MIP) available in ImageJ software (NIH, Bethesda, Maryland, USA).

### *Measurement of waviness and global angle of collagen bundles*

To quantify the waviness characteristics and global angle of collagen bundles in the zero stress state, all 2D images from the cut-open group were analyzed semi-automatically. Figure 3 shows the parameters measured for each collagen bundle on the image i.e. the distance between endpoints of a collagen bundle ( $L_0$ ), the length of the fiber bundle ( $L_f$ ), the thickness ( $t$ ) measured in three different locations along each bundle and the global angle of bundles ( $a$ ) which is the angle between the main axis of the fiber and the axial direction  $z$  as specified in Figure 3. This angle could take values between  $-90$  and  $90$  degrees. These parameters were measured using NeuronJ, an ImageJ plug-in originally developed for Neurite tracing and analysis [27]. The plug-in facilitates following the fibers on a 2D image and gives as the output the fiber length ( $L_f$ ) as well as the coordinates of the endpoints. Most bundles are larger than the field of view. Therefore, we emphasize that these parameters are measured for the part of the bundle visible in the field of view.

To quantify the waviness of fibers, we introduced the *straightness parameter* ( $SP$ ) defined as,

$$SP = L_0 / L_f \quad (1)$$

$SP$  is bounded between 0 and 1. The lower the value of  $SP$ , the wavier the fiber is. A bundle with  $SP=1$  indicates a totally straight fiber.  $SP$  converges to zero where the fibers get very wavy. This parameter could be particularly useful for modeling the gradual engagement of wavy collagen fibers which will be discussed later. In addition, we estimated the size of the bundle by,

$$\tilde{S} = L_f \bar{t} \quad (2)$$

where  $\bar{t}$  is the mean thickness of collagen bundles. Each bundle could be therefore characterized with three parameters, i.e., a straightness parameter  $SP$ , a global angle  $a$  and an estimated size  $\tilde{S}$ . To give more importance to measurements from larger bundles than the smaller ones, in the estimation of mean straightness parameter  $SP$  and mean angle  $a$ , the individual bundle values of  $SP$  and  $a$  were weighted by the size  $\tilde{S}$  of the corresponding bundle.

### *Waviness distribution analysis*

To quantify the waviness characteristics of collagen fibers, we analyzed the distribution of the straightness parameter. First, we used a bi-variate histogram to visualize the frequency of straightness parameter  $SP$  and global angle  $a$ , based on the weighted dataset. Second, the dataset was used to plot a univariate probability density for the straightness parameter regardless of the global angle using MATLAB (The MathWorks, U.S.A.). This means that the probability density was extracted from all values of  $SP$  in the dataset. A beta and an extreme value distribution were fitted to the  $SP$  values. Beta probability distribution is a statistical distribution defined between 0 and 1 as,

$$f(SP; \alpha, \beta) = \begin{cases} \frac{SP^{\alpha-1}(1-SP)^{\beta-1}}{B(\alpha, \beta)} & 0 < SP < 1 \\ 0 & \text{otherwise} \end{cases} \quad (3)$$

where  $\alpha$  and  $\beta$  are shape parameters of the distribution and  $B(\alpha, \beta)$  is the beta function,

$$B(\alpha, \beta) = \int_0^1 t^{\alpha-1}(1-t)^{\beta-1} dt \quad (4)$$

As for the extreme value distribution, it is defined as,

$$f(SP; \mu, \sigma) = \sigma^{-1} \exp\left(\frac{SP - \mu}{\sigma}\right) \exp\left(-\exp\left(\frac{SP - \mu}{\sigma}\right)\right) \quad (5)$$

where  $\mu$  is the location parameter and  $\sigma > 0$  the scale parameter.

Third, to decide whether  $SP$  is distributed more accurately by a beta or an extreme value distribution, we have used probability plots of the data for both distributions using statistics toolbox<sup>TM</sup> available in MATLAB. The probability plot is a graphical technique for assessing whether or not a data set follows closely a given distribution. The plot includes a reference line useful for judging whether the data follows well or not the particular distribution. The closer the probability plot of data to this line, the better the data follows that particular distribution [11]. Finally, using the bivariate histogram, the weighted data was divided to six groups based on their global angle  $\alpha$ , starting from  $-90^\circ$  with  $30^\circ$  steps, and the probability density of the straightness parameter for each angle group was determined. Then, we fitted the beta distribution to all six groups of fibers and compared the distribution parameters. This step helped us to decide whether the distribution of the straightness parameter  $SP$  depends on the global angle or not.

## Local angle analysis

### Image analysis tool

To estimate the local orientation of the collagen fibers, we used OrientationJ, which is an ImageJ plug-in developed in-house based on structure tensors. Structure tensors are matrix representatives of partial derivatives and are commonly used in the field of image processing [3, 21]. OrientationJ evaluates the local orientation and isotropic properties (coherency and energy) of every pixel of the image. These values are derived from the structure tensor defined for each pixel as the 2x2 symmetric positive matrix  $J$ ,

$$J = \begin{bmatrix} \langle f_x, f_x \rangle_w & \langle f_x, f_y \rangle_w \\ \langle f_x, f_y \rangle_w & \langle f_y, f_y \rangle_w \end{bmatrix} \quad (6)$$

where  $f_x$  and  $f_y$  are the partial spatial derivatives of the image  $f(x, y)$ , along the principal directions  $x$  and  $y$  respectively. Furthermore, the weighted inner product between two arbitrary images  $g$  and  $h$  is defined as,

$$\langle g, h \rangle_w = \iint_{R^2} w(x, y) g(x, y) h(x, y) dx dy \quad (7)$$

$w(x,y)$  is the Gaussian weighting function that specifies the area of interest. Once the structure tensor is known, local orientation, energy and coherency for each pixel could be easily calculated [21]. The local predominant orientation  $\theta$  in the considered region corresponds to the direction of the largest eigenvector of the tensor and it is thus given by,

$$\theta = \frac{1}{2} \arctan \left( 2 \frac{\langle f_x, f_y \rangle_w}{\langle f_y, f_y \rangle_w - \langle f_x, f_x \rangle_w} \right) \quad (8)$$

The energy parameter  $E$  is the trace of the tensor matrix,

$$E = \text{Trace}(J) = \langle f_x, f_x \rangle_w + \langle f_y, f_y \rangle_w \quad (9)$$

Pixels with higher energy values correspond to less uniform and more clearly oriented structures.

The coherency parameter  $C$  is defined as the ratio between the difference and the sum of the tensor eigenvalues,

$$C = \frac{\lambda_{\max} - \lambda_{\min}}{\lambda_{\max} + \lambda_{\min}} = \frac{\sqrt{(\langle f_y, f_y \rangle_w - \langle f_x, f_x \rangle_w)^2 + 4 \langle f_x, f_y \rangle_w^2}}{\langle f_x, f_x \rangle_w + \langle f_y, f_y \rangle_w} \quad (10)$$

where  $\lambda_{\max}$  is the largest and the  $\lambda_{\min}$  the smallest eigenvalue, respectively. Coherency is bounded between 0 and 1, with 1 indicating highly oriented structures and 0 indicating isotropic areas.

In OrientationJ, the tensor  $J$  is evaluated for each pixel of an input image by computing the continuous spatial derivatives in  $x$  and  $y$  using a cubic B-spline interpolation [33]. The local orientation, coherency and energy are computed based on equations 8, 9 and 10. In our directional analysis we included only the angular values from parts (pixels) of the images which effectively correspond to fibers edges, as the orientation information from uniform areas is not significant. To do this, we used the energy of derivatives and the coherency values to discriminate between significantly and not-significantly oriented areas. Therefore, the histogram of the orientation is built with pixels which have at least 2% of normalized energy. Moreover, the orientation values in the histograms are weighted by the coherency values to give more importance to the orientations which correspond to elongated structures in the local neighborhood.

We made the OrientationJ plug-in and an ImageJ macro for angle analysis batching available online at <http://bigwww.epfl.ch/demo/orientation/>. OrientationJ allows computing the orientation, energy and coherency maps of an image and its weighted orientation histogram. It is possible to set thresholds on the energy and coherency maps to select the image orientation values to be included in the angles histogram. The plug-in also outputs a hue-saturation-brightness (HSB) color-coded map which shows the angles of the oriented structures in the image as shown in Figure 4.

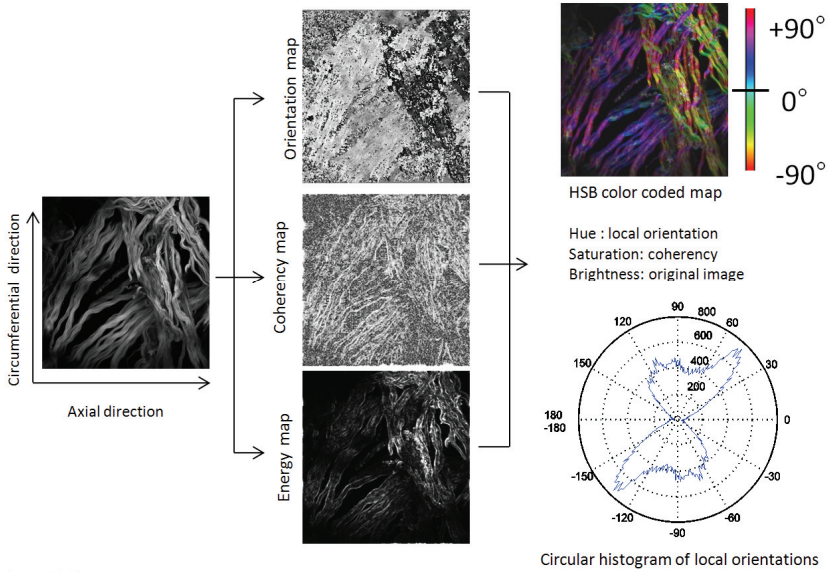


**Fig. 4 Results of the OrientationJ, the imageJ plug-in developed to get the histogram of local angles**

**Fitting local angles**

Using OrientationJ plug-in for ImageJ, we obtained the histogram of local angles for all individual images of collagen fibers. Next, we summed up the individual histograms from images in each group to calculate local orientation of both cut-open and intact groups. The probability density function (PDF) of the local angles for each group was then calculated by normalizing local angular histograms. We fitted an empirical PDF by a four modal directional PDF representing 4 families of fibers. The angular distribution of each family was modeled with a  $\pi$ -periodic von-Mises distribution [25] which is the  $\pi$ -periodic equivalent of a Gaussian distribution in directional statistics,

$$R(\theta; \phi, b) = \frac{1}{\pi I_0(b)} e^{b \cos(2(\theta - \phi))} \quad -\frac{\pi}{2} \leq \theta < \frac{\pi}{2} \quad (11)$$

$I_0$  denotes the modified Bessel function of the first kind and order 0, which is defined as,

$$I_0(b) = \frac{1}{2\pi} \int_0^{2\pi} e^{b \cos \theta} d\theta \quad (12)$$

The parameter  $\phi$  is the mean orientation and the parameter  $b$  is the concentration parameter.

The distribution is symmetric about  $\theta = \phi$  and the *circular standard deviation*  $\sigma$  of this distribution is [25],

$$\sigma = \left\{ -2 \log \left( \frac{I_1(b)}{I_0(\beta)} \right) \right\}^{1/2} \quad (13)$$

$I_1$  denotes the modified Bessel function of the first kind and order 1,

$$I_1(b) = \frac{1}{2\pi} \int_0^{2\pi} \cos \theta e^{b \cos \theta} d\theta \quad (14)$$

We assumed cylindrical symmetry around the  $z$  axis of arteries. Based on this assumption and the shape of the empirical PDF, families of fibers to fit the data were assumed having mean angles of  $\varphi_1$ ,  $-\varphi_1$ ,  $\pi/2$  and 0 with shape parameters  $b_1$ ,  $b_1$ ,  $b_3$  and  $b_4$  respectively. Therefore the fitted probability density distribution was defined as,

$$TR(\theta; \phi_1, b_1, b_3, b_4) = \frac{1}{4} R(\theta; \phi_1, b_1) + \frac{1}{4} R(\theta; -\phi_1, b_1) + \frac{1}{4} R(\theta; \frac{\pi}{2}, b_3) + \frac{1}{4} R(\theta; 0, b_4) \quad -\frac{\pi}{2} \leq \theta < \frac{\pi}{2}$$

### Transformation law

If the deformation of the arterial wall is assumed as an affine deformation and the collagen bundles are assumed to lie only in the circumferential-axial plane, one could obtain the density probability of local orientations in the deformed state (intact) based on the zero stress state (cut-open). As seen in figure 5, if  $\lambda_\theta$  and  $\lambda_z$  are the stretches in the circumferential and axial directions, respectively, and  $\theta_0$  and  $\theta_1$  are the local angle of fibers with respect to the axial direction in the initial state (cut-open) and the deformed state (intact), respectively, the angles are then related to each other by,

$$\tan \theta_1 = \frac{\lambda_\theta}{\lambda_z} \tan \theta_0 \quad (16)$$

$R_0$  and  $R_1$  are density distributions for local angles between  $-\pi/2$  and  $\pi/2$ . Therefore,

$$\int_{-\pi/2}^{\pi/2} R_0(\theta_0) d\theta_0 = \int_{-\pi/2}^{\pi/2} R_1(\theta_1) d\theta_1 = 1 \quad (17)$$

The function of  $\theta_1$  versus  $\theta_0$  is monotonic and the above equation results in,

$$R_0(\theta_0) d\theta_0 = R_1(\theta_1) d\theta_1 \quad (18)$$

$$R_1(\theta_1) = R_0(\theta_0) \frac{d\theta_0}{d\theta_1} = R_0(\theta_0) \frac{\cos^2 \theta_0}{\frac{\lambda_\theta}{\lambda_z} \cos^2 \left( \tan^{-1} \left( \frac{\lambda_\theta}{\lambda_z} \tan \theta_0 \right) \right)} \quad (19)$$

Therefore, if  $R_0$  is known,  $R_1$  could be calculated based on the ratio of  $\lambda_\theta/\lambda_z$  and the distribution  $R_0$ . The transformation law has been applied on the data to find out the corresponding ratio of  $\lambda_\theta/\lambda_z$ .

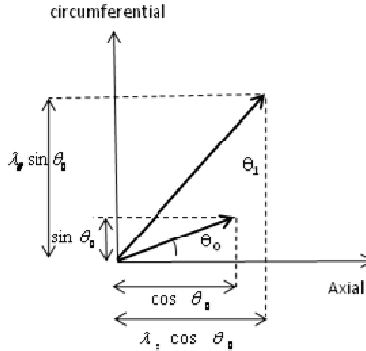


**Fig. 5 Mapping of local angles from the original state ( $\Theta_0$ ) to the deformed state ( $\Theta_1$ )**

## Results

In this study, we have used manual, semi-automatic and automatic techniques to quantify the statistical distribution of parameters related to the orientation and waviness of fibers in the adventitia of rabbit carotid arteries.

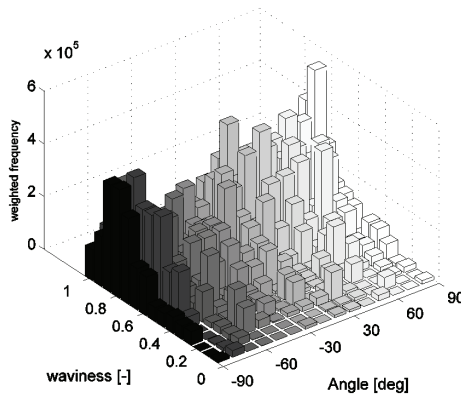
Figure 2 shows an example of 3D reconstruction of collagen fibers from the z-stacks. The latitude (radial) angles, manually measured from the 3D reconstruction of samples, are listed in Table 1. The mean value of absolute radial angle was measured as  $5.6^\circ$  and  $6.1^\circ$  in the cut group and  $4.8^\circ$  and  $1.7^\circ$  in the uncut group. Based on these small angle values, we conclude that fibers were practically lying in the z- $\Theta$  (axial-circumferential) plane in both groups. This trend was also observed visually in all z-stacks.

**Table 1 Latitude (radial) angle measurements of 4 representative samples**

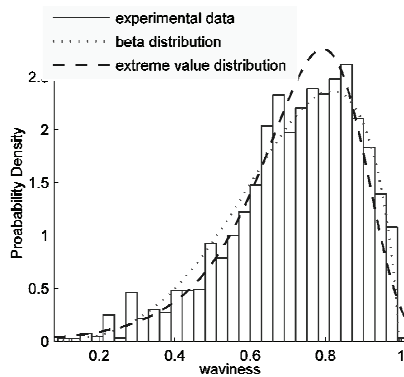
Group	cut		uncut	
Sample	S1	S2	S3	S4
$\varphi$ (deg)	13.8	3.0	5.4	-1.2
	9.2	3.0	4.6	-2.7
	3.3	7.0	3.8	0.3
	-9.0	14.9	-4.6	-0.8
	0.0	6.1	-2.8	2.0
	-0.6	9.6	-8.0	4.6
	-3.4	3.2	-3.3	1.5
	-5.9	2.3	-5.6	0.7
Mean( $ \varphi $ )	5.6	6.1	4.8	1.7
std( $ \varphi $ )	4.7	4.3	1.6	1.4



Figure 6 shows the weighted frequency of bi-variant data, i.e. the set of global orientations and straightness from the cut group. The same data set was used to create figures 7 and 9. Figure 7 shows the probability density of the *straightness parameter SP* regardless of the global angle of the data. This means simply that Figure 7 plots the density of all weighted *straightness parameters SP*. In addition, Figure 7 includes the best fits for beta and extreme value distributions on the experimental density distribution of the straightness. Parameter values from best fits are reported in Table 2. The best fit for beta distribution results in  $\alpha=4.47$  and  $\beta=1.76$  and the best fit for the extreme value distribution resulted in  $\mu=0.800$  and  $\sigma=0.133$ . To assess how well the data set followed each of these distributions, the probability plots of the data for both distributions were plotted in Figure 8. Based on Figure 8, the data is closer to the straight line for the beta distribution than the extreme value distribution. This indicates that the experimental data follows better the beta distribution than the extreme value distribution.



**Fig. 6** Bivariate histogram of waviness (SP) and global angles based on the entire weighted dataset.



**Fig. 7** uni-variate probability density of waviness (SP): empirical and corresponding fits from beta and extreme value distributions

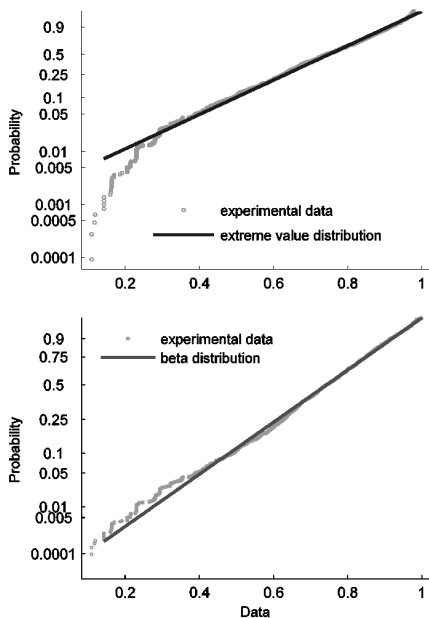


**Fig. 8** Probability plot of beta and extreme value distributions versus the experimental data

**Table 2** Parameters of the distribution fits on *straightness parameter, SP*

Distribution:	Extreme values	Distribution	Beta
Log Likelihood	2377	Log Likelihood	2480
Domain	$-\infty < y < \infty$	Domain	$0 < y < 1$
Mean	0.720	Mean	0.718
Variance	0.029	Variance	0.028
Parameter Estimate		Parameter Estimate	
$\mu$	0.800	$\alpha$	4.47
$\sigma$	0.133	$\beta$	1.76

Figure 9 shows probability densities of weighted straightness for groups of different global angle ranges and the corresponding fitted beta distribution. More precisely, Figure 9.a shows the probability density of the weighted *straightness parameter*  $SP$  for fibers with global angles between  $-89^\circ$  and  $60^\circ$ ,  $-59^\circ$  and  $-30^\circ$ ,  $-29^\circ$  and  $0^\circ$ ,  $1^\circ$  and  $30^\circ$ ,  $31^\circ$  and  $60^\circ$ , and  $61^\circ$  and  $90^\circ$ . To compare the distribution for the different angle ranges (Figure 9.a) and the one variable distribution (Figure 7), all the fits have been plotted in Figure 9.b. the thick line shows the best fit from Figure 7 (angle independent density distribution).

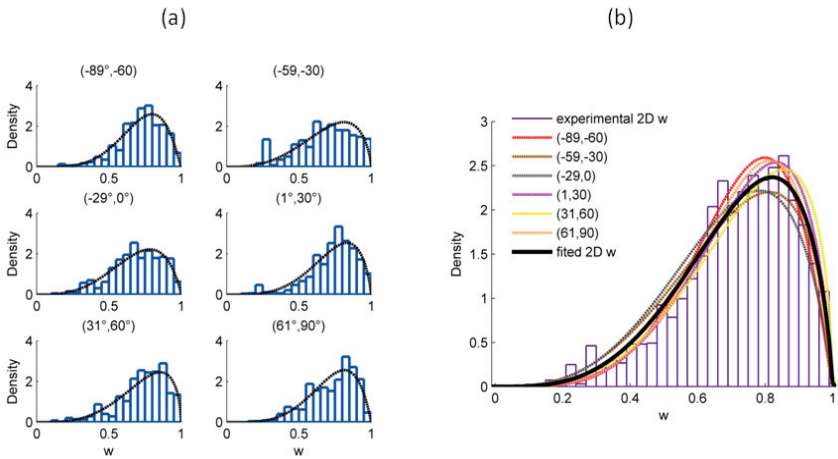


**Fig. 9** Distribution of *straightness parameter* in various ranges of global angles i.e. a) beta distribution fitted (dashed line) to experimental data (bars) and b) comparison of all fitted distributions for particular angle ranges (dashed lines) with the beta distribution fitted without considering angles

Table 3 shows the parameters of the beta distribution fits on straightness parameter distributions for all global angle dependant groups and the univariate set of the data (regardless of global angle). The shape parameters  $\alpha$  and  $\beta$ , related to the univariate  $SP$  distribution, were found to be  $\alpha=4.7$  and  $\beta=1.8$ . The distributions pertaining to different angle groups were similar in shape, the shape parameters differed only slightly in  $\alpha$  ( $\alpha=4.8\pm 0.5$ ) and were exactly the same for  $\beta$  ( $\beta=1.8\pm 0.2$ ).

**Table 3 Shape parameters of the fitted beta distributions**

Angle	Parameter		Mean	
	$\alpha$	$\beta$	Mean	Variance
(-89°, -60°)	5.5	2.1	0.721	0.023
(-59°, -30°)	4.4	1.7	0.701	0.031
(-29°, 0°)	4.2	1.9	0.691	0.030
( 1°, 30°)	4.9	1.8	0.734	0.025
( 31°, 60°)	4.4	1.6	0.736	0.028
( 61°, 90°)	5.2	2.0	0.727	0.024
<b>Univariate</b>	<b>4.7</b>	<b>1.8</b>	<b>0.718</b>	<b>0.028</b>

The orientational density of local angles as well as the fitted PDF has been plotted in polar coordinates in Figure 10 for both cut-open and intact groups. For simplicity, the densities are plotted over two periods between  $-\pi$  and  $\pi$  (the distribution is  $\pi$ -periodic). As it can be seen, the experimental data shows a four modal distribution. For this reason, we have used a PDF composed of four  $\pi$ -periodic von-Mises distributions, representing four families of fibers. Figure 10.a, shows the local angle densities related to the cut-open group. Based on the fitted distribution, the four modes occur at  $0^\circ$  (axial direction),  $90^\circ$  (circumferential direction),  $43^\circ$  and  $-43^\circ$  with the corresponding circular standard deviation (CSD) of  $40^\circ$ ,  $47^\circ$ ,  $37^\circ$  and  $37^\circ$ , respectively. Based on these derived CSDs, the distribution appears more concentrated around  $43^\circ$  and  $-43^\circ$  than around  $0^\circ$  and  $90^\circ$ .

Figure 10.b shows the local angle distributions for the uncut group. As it can be seen, compared to Figure 10.a (cut group), the distribution is shifted to the circumferential direction. The families of fibers with mean orientations of  $43^\circ$  and  $-43^\circ$  have been relocated to mean orientations of  $47^\circ$  and  $-47^\circ$ , respectively. Furthermore, the value of probability density function has decreased in the axial direction (at  $0^\circ$ ) by 32 % while it has increased in the circumferential direction (at  $90^\circ$ ) by 19% .

Figure 11, shows the measured density distribution of local angles for cut and uncut group. Figure 11 also shows the predicted density distribution for the intact group based on the distribution of the cut-open group and applying the deformation with  $\lambda_\theta/\lambda_z=1.24$ , which corresponds to the deformation needed to bring the cut-open group geometry to the intact (uncut) geometry. The results showed that a transformation of the probability density distribution for cut-open arteries using a deformation with equivalent circumferential to axial stretch ratios of  $\lambda_\theta/\lambda_z=1.24$ , results in the same distribution as the uncut arteries.

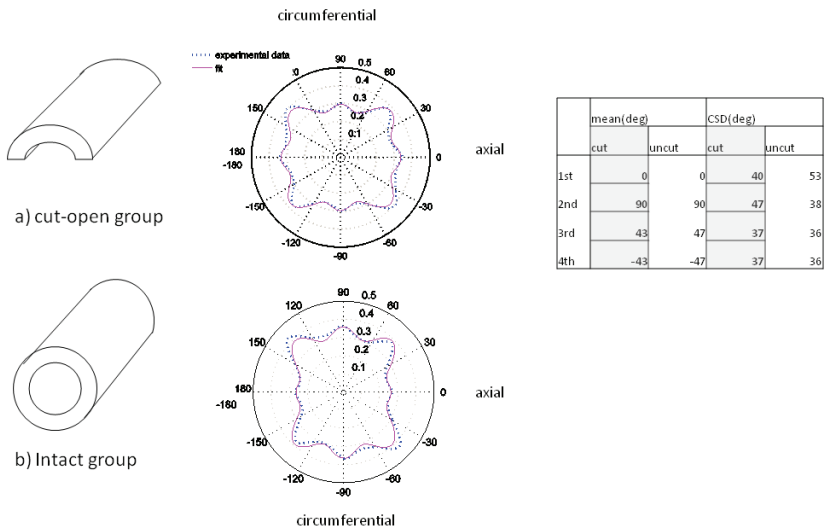


Fig. 10 local angles, cut and uncut arteries and corresponding circular distribution fits

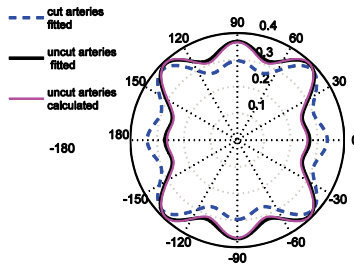


Fig. 11 mapping of local angles of arteries from cut-open (----) to intact (\_\_\_\_) state

## Discussion

We quantified waviness and angular distribution of collagen fibers in the adventitia of fresh rabbit common carotid arteries. Our results showed that the straightness of fibers at the zero stress state was best represented by a uni-modal beta distribution function with shape parameters  $\alpha$  and  $\beta$  equal to 4.5 and 1.8. In addition, the waviness distribution of fibers did not depend on global fiber angle. The beta distribution fitted the straightness densities for all different groups of global angles, though the values for shape parameters were slightly different in each group. Finally, the automatic analysis of local angle revealed the existence of four main families of fibers. The distribution of angles was fitted by a four modal orientational distribution composed of four  $\pi$ -periodic von-Mises distributions. The local angle distribution of the intact group (uncut arteries) was shifted to the circumferential direction compared to the corresponding distribution of the cut group (zero stress state). The mapping of the distributions from the ZSS (cut) to the intact group (uncut) could be explained by a simple geometrical transformation, the “folding and joining together”, of the cut-open artery (ZSS) to the intact zero-load state, which yields a circumferential to axial stretch ratio of around 1.24.

*Collagen visualization.* To visualize collagen fibers in the adventitia of unfixed arteries, we labeled adventitial collagen with CNA35-OG488 fluorescent marker recently developed by Kahn et al. [22] and imaged the adventitia layer using laser confocal microscopy. The CNA35 probe is specific for collagen and can reveal small collagen fibers as well as more mature structures in living tissues without altering the structure. Therefore, the probe can be potentially used to study collagen remodeling in living cells and tissues [22] for tissue engineering purposes. Moreover, the probe could be used to visualize collagen fibers of blood vessels under various mechanical loadings. The probe has a low binding affinity and does not affect mechanical properties of the tissue, is small, and can thus readily diffuse into the tissue. Collagen fibers and bundles can be also visualized in tissue without labeling agents or fixative as a result of its intrinsic properties such as birefringence under polarized light microscopy [17, 20], auto-fluorescence [34] and second harmonic generation (SHG) [8, 32]. Techniques for 3D visualization of collagen without specific probes include auto-fluorescence, confocal reflection microscopy [29], and second harmonic generation using femtosecond pulsed infrared excitation [32]. However, these techniques have some drawbacks. Auto fluorescence is not specific enough for collagen, as several tissue constituents possess intrinsic auto fluorescent properties. In addition, auto-fluorescence intensity is relatively low. Confocal reflection microscopy is subjected to the same drawbacks. As for the SHG, strong forward scattered SHG does enable the visualization of collagen in tissues, however, depending on tissue properties, forward SHG is not always feasible. In dense and thick tissues, such as large arteries, it is difficult to obtain images with the forward scattered SHG. These tissues require additional techniques to image collagen in backward geometry, which results in a much weaker signal. In a recent study, Boerboom et al. [5] compared the imaging of collagen with CNA35 probe and backward geometry SHG signal. They observed that the SHG in backward geometry was much weaker than the fluorescent signal of the probe. Similarly, this was observed in our preliminary studies on rabbit common carotids. On the other hand, the probe has some limitations mainly due to the diffusion depth into the tissue. Megens et al. [26] showed limited labeling of the probe in viable elastic and muscular arteries. In our preliminary study on rabbit common carotids, we also observed limited diffusion of the probe through the external and internal elastic lamellae after incubation overnight. In summary, labeling collagen with the CNA35-OG488 enabled us to visualize collagen fibers in fresh unfixed tissue. The fluorescent signal was collagen

specific and strong enough to image well and in good detail the adventitial fibers. However, diffusion depth of the probe is limited and probably could not be used in arteries with thick elastin lamellae to access collagen fibers in other layers of arterial wall.

*Analysis of collagen fiber waviness.* We quantified the collagen fiber *straightness parameter*, *SP*, in adventitia and calculated its empirical probability density function, which we fitted with a beta distribution. Straightness parameter, *SP*, defined as the ratio of the distance between endpoints and the arc length of the fibers, is the inverse of the straightening stretch of fibers. The straightening stretch is the stretch to be applied along the fiber to get it straightened. Therefore, *SP* distribution is of particular interest for developing structural models of arterial tissue, which take into account the waviness of fibers [7, 38]. These studies are mainly influenced by an earlier framework proposed by Lanier [23]. In this framework, to include waviness of fibers, it is assumed that fibers don't bear load at their wavy state and that there is a straightening stretch along the fiber,  $\lambda_s$ , at which the fiber engages and starts bearing load. *SP* is assumed to have a statistical distribution, which should be characterized at the zero stress state of the arteries. Despite the fact that a complete characterization of the statistical distribution of waviness or straightness parameter is needed to realistically model the tissue, the number of experimental studies which have addressed the issue are limited [14].

To the best of our knowledge, this is the first study which quantifies the waviness distribution of collagen fibers in adventitia under the zero stress state of arteries. Based on this work, the *SP* distribution could be fitted with a beta distribution with a mean value of 0.72 and a variance of 0.028. Both shape parameters are more than 1 ( $\alpha=4.7$ ,  $\beta=1.8$ ) and therefore the distribution is uni-modal. In this study, different distributions such as lognormal, log-logistic, extreme value, gamma and beta had been fit to the data (results not shown) and it was evident that the beta and extreme value distribution fit the empirical PDF the best. A more detailed study on probability plots of the data for the beta and extreme value distribution, showed that the data were best fitted by the beta distribution (Figure 8).

Our results have shown that the shape of the PDF for *SP* was similar for the fibers of groups with different global angles. This means that the same distribution for straightening stretch could be used for different families of fibers in different orientations, or, stated otherwise, the distribution for straightening stretch is not dependent on fiber angle. Shape parameters differed only slightly between groups. Mean and variance of these distributions are shown in Table 3. The difference between variances could be a result of sampling on the distribution as the number of measurements was fairly small (less than 500 for each group of angles). This information is indeed valuable for constructing structural models of arterial adventitia where both waviness and orientational distributions of collagen fibers are included in the model.

*Analysis of local angle distribution.* Based on our results, the distribution of local collagen fiber angles included four peaks (modes), suggesting four main orientations and therefore four families of fibers. This lead us to the choice of the distribution given by equation 15, which consists of four  $\pi$ -periodic von\_Mises distributions summed up and normalized between  $-\pi/2$  and  $\pi/2$ . The parameters  $b_i$   $i=1,2,3$  were free to fit the data. The  $b$  parameter of the von-Mises distribution determines its circular standard deviation (CSD), as defined in equation 13. However, the standard deviations derived from local angle data set should not be confused with the circular standard deviation of global angles of fibers. The standard deviation of local angle distribution does not only depend on the standard deviation of global angles, but also depends on local variations of angles due to fiber waviness. The separation between these two variations is not straightforward and requires segmentation of images into

areas with a common mean orientation. Elbischger et al. studied local extraction of crimp parameters of collagen fibers from a single image [15]. The images were taken using light microscopy from sliced fixed paraffin embedded human iliac arteries. The same image analysis method could be applied on the current data to get more detailed information of the standard deviation of global angle of fibers.

Few experimental studies are available on orientation of fibers in arterial adventitia. Smith et al. [31] studied the orientation of collagen in the adventitia of human cerebral arteries. The arteries were fixed under a transmural pressure of 100mm Hg. They reported an average circumferential direction with a surface component of longitudinal fibers [31]. Canham et al. [9] followed the same approach and reported a circumferential direction of fibers (CSD=22.3) for adventitia of human coronary arteries fixed at 120 mmHg. In a recent study, Finlay et al. [17] reported a mean helical angle of  $70^\circ$  (CSD=36),  $53^\circ$  (CSD=32) and  $14^\circ$  (CSD=23) with respect to the circumferential direction for human brain arteries fixed at 30, 120 and 200 mmHg. These studies have been mainly performed on sections from fixed and paraffin embedded arteries at a specific luminal pressure. The fixation, dehydration and paraffin embedding causes shrinkage and could change the morphology of the tissue [13]. Moreover, the measurements focus on pressurized blood vessels and do not quantify the organization of fibers at the zero stress state of arteries, as needed for modeling purposes. None of the studies reported the longitudinal stretch at which the arteries were fixed. In the current study, we have measured the structure-related parameters on fresh unfixed tissue and at zero stress state having in mind that such information is needed to develop structural models of the arterial wall.

In addition to the cut-open arteries, we also imaged the collagen on the adventitia of intact arteries at their zero load state (ZLS), i.e., at zero transmural pressure and no axial load. The local angle distribution in intact arteries showed a shift to the circumferential direction as seen from Figure 10. The PDF of the orientation angle in the axial direction ( $0^\circ$ ) was reduced by around 20%; in the circumferential direction it was increased by 23%. The transformation model predicts a value of 1.24 for  $\lambda_\theta/\lambda_z$ , when the arterial geometry goes from the zero stress state (cut-open) to zero load state (intact). The relative increase in circumferential stretch is a direct result of the “closing” of the artery from the ZSS to ZLS, which entrains a significant positive circumferential strain on outer (adventitial) layer of arteries. As adventitial fibers are strained more in the circumferential direction, their mean orientation would also shift to the circumferential direction, which is consistent with our results. This could also explain the results of Finlay et al., where, the higher the pressure at which arteries were fixed and imaged, the closer the circumferential direction was to the mean orientation of collagen fibers. This observation also emphasizes the fact that measurements of fiber angles at zero stress state could give different results from measurements done on intact or pressurized arteries.

*Limitations.* We have flattened the 3D data to 2D, which takes out some useful information such as tortuosity and out of plane structure of fibers. This was specifically done to facilitate the analysis and particularly the semi-manual calculation of the waviness. However, the data is not used in its full power and further image analysis tools should be developed to study appropriately the 3D set of data. Moreover, semi manual technique to calculate the SP parameter is time consuming and the size of fibers are approximated to weight the data. More elaborate image analysis techniques are needed to automatically segment the 3D images and calculate relevant values such as length and size of the fibers.



*Conclusions.* We have quantified the waviness and local distribution of collagen fibers in adventitia of fresh unfixed rabbit common carotids. The results from 50 arterial locations, ~100  $\mu\text{m}$  depth each, show the existence of four families of fibers in the zero load stress state of the arteries. The waviness of fibers does not depend on fiber orientation. The significant shift of local angular distributions to the circumferential direction from cut open arteries to intact (no load) arteries shows that angular data from arteries at no load conditions as well as loaded and axially stretched arteries could not be used to define the angular orientation of fibers in ZSS. Despite its limitations, the results of this study could be particularly useful for developing structural models of arterial tissue.

## Acknowledgements

The authors would like to thank Aristotelis Agianniotis for the assistance with image analysis, Dr. Dimitrios Kontaxakis for helpful discussions on statistical distributions and Dr. Tyler Thacher for proofreading the article.

## Grants

This work was supported by the Swiss National Science Foundation (Grant No. 325230\_125445).

## References

1. **Axer H, Keyserlingk DGV, and Prescher A.** Collagen fibers in linea alba and rectus sheaths: II. Variability and biomechanical aspects. *J Surg Res* 96: 239-245, 2001.
2. **Bayan C, Levitt JM, Miller E, Kaplan D, and Georgakoudi I.** Fully automated, quantitative, noninvasive assessment of collagen fiber content and organization in thick collagen gels. *J Appl Phys* 105: 2009.
3. **Bigun J, Bigun T, and Nilsson K.** Recognition by symmetry derivatives and the generalized structure tensor. *IEEE Transactions on Pattern Analysis and Machine Intelligence* 26: 1590-1605, 2004.
4. **Billiar KL, and Sacks MS.** A method to quantify the fiber kinematics of planar tissues under biaxial stretch. *J Biomech* 30: 753-756, 1997.
5. **Boerboom RA, Krahn KN, Megens RT, van Zandvoort MA, Merckx M, and Bouten CV.** High resolution imaging of collagen organisation and synthesis using a versatile collagen specific probe. *J Struct Biol* 2007.
6. **Braga-Vilela AS, Pimentel ER, Marangoni S, Toyama MH, and De Campos Vidal B.** Extracellular matrix of porcine pericardium: Biochemistry and collagen architecture. *J Membr Biol* 221: 15-25, 2008.
7. **Cacho F, Elbischger PJ, Rodriguez JF, Doblare M, and Holzapfel GA.** A constitutive model for fibrous tissues considering collagen fiber crimp. *International Journal of Non-Linear Mechanics* 42: 391-402, 2007.
8. **Campagnola PJ, and Loew LM.** Second-harmonic imaging microscopy for visualizing biomolecular arrays in cells, tissues and organisms. *Nature biotechnology* 21: 1356-1360, 2003.
9. **Canham PB, Finlay HM, Dixon JG, Boughner DR, and Chen A.** Measurements from light and polarised light microscopy of human coronary arteries fixed at distending pressure. *Cardiovasc Res* 23: 973-982, 1989.

10. **Canham PB, Talman EA, Finlay HM, and Dixon JG.** Medial collagen organization in human arteries of the heart and brain by polarized light microscopy. *Connect Tissue Res* 26: 121-134, 1991.
11. **Chambers JM, Cleveland WS, Kleiner B, and Tukey PA.** *Graphical methods for data analysis*. Pacific grove, California: Wadsworth & Brooks/Cole Publishing company, 1983.
12. **Dingemans KP, Teeling P, Lagendijk JH, and Becker AE.** Extracellular matrix of the human aortic media: an ultrastructural histochemical and immunohistochemical study of the adult aortic media. *Anat Rec* 258: 1-14, 2000.
13. **Dobrin PB.** Effect of histologic preparation on the cross-sectional area of arterial rings. *J Surg Res* 61: 413-415, 1996.
14. **Elbischger PJ, Bischof H, Holzapfel GA, and Regitnig P.** Computer vision analysis of collagen fiber bundles in the adventitia of human blood vessels. *Stud Health Technol Inform* 113: 97-129, 2005.
15. **Elbischger PJ, Bischof H, Regitnig P, and Holzapfel GA.** Automatic analysis of collagen fiber orientation in the outermost layer of human arteries. *Pattern Analysis and Applications* 7: 269-284, 2004.
16. **Ferdman AG, and Yannas IV.** Scattering of light from histologic sections: A new method for the analysis of connective tissue. *J Invest Dermatol* 100: 710-716, 1993.
17. **Finlay HM, McCylyough L, and Canham PB.** Three-dimensional collagen organization of human brain arteries at different transmural pressures. *J Vasc Res* 32: 301-312, 1995.
18. **Franchi M, Fini M, Quaranta M, De Pasquale V, Raspanti M, Giavaresi G, Ottani V, and Ruggeri A.** Crimp morphology in relaxed and stretched rat Achilles tendon. *J Anat* 210: 1-7, 2007.
19. **Hansen KA, Weiss JA, and Barton JK.** Recruitment of tendon crimp with applied tensile strain. *J Biomech Eng* 124: 72-77, 2002.
20. **Hilbert SL, Sword LC, Batchelder KF, Barrick MK, and Ferrans VJ.** Simultaneous assessment of bioprosthetic heart valve biomechanical properties and collagen crimp length. *J Biomed Mater Res* 31: 503-509, 1996.
21. **Jahne B.** *Spatio-temporal Image Processing: Theory and Scientific Applications*. Berlin: Springer-Verlag, 1993.
22. **Krahn KN, Bouten CV, van Tuijl S, van Zandvoort MA, and Merckx M.** Fluorescently labeled collagen binding proteins allow specific visualization of collagen in tissues and live cell culture. *Anal Biochem* 350: 177-185, 2006.
23. **Lanir Y.** Constitutive equations for fibrous connective tissues. *J Biomech* 16: 1-12, 1983.
24. **Magnusson SP, Qvortrup K, Larsen JO, Rosager S, Hanson P, Aagaard P, Krosgaard M, and Kjaer M.** Collagen fibril size and crimp morphology in ruptured and intact Achilles tendons. *Matrix Biol* 21: 369-377, 2002.
25. **Mardia KV, and Jupp PE.** *Directional statistics*. John Wiley 2000.
26. **Megens RTA, Reitsma S, Schiffers PHM, Hilgers RHP, De Mey JGR, Slaaf DW, Oude Egbrink MGA, and Van Zandvoort MAMJ.** Two-photon microscopy of vital murine elastic and muscular arteries: Combined structural and functional imaging with subcellular resolution. *J Vasc Res* 44: 87-98, 2007.
27. **Meijering E, Jacob M, Sarria JC, Steiner P, Hirling H, and Unser M.** Design and validation of a tool for neurite tracing and analysis in fluorescence microscopy images. *Cytometry A* 58: 167-176, 2004.

28. **Rieppo J, Hallikainen J, Jurvelin JS, Kiviranta I, Helminen HJ, and Hyttinen MM.** Practical considerations in the use of polarized light microscopy in the analysis of the collagen network in articular cartilage. *Microsc Res Tech* 71: 279-287, 2008.
29. **Roeder BA, Kokini K, Sturgis JE, Robinson JP, and Voytik-Harbin SL.** Tensile mechanical properties of three-dimensional type I collagen extracellular matrices with varied microstructure. *J Biomech Eng* 124: 214-222, 2002.
30. **Sacks MS, Smith DB, and Hiester ED.** A small angle light scattering device for planar connective tissue microstructural analysis. *Ann Biomed Eng* 25: 678-689, 1997.
31. **Smith JFH, Canham PB, and Starkey J.** Orientation of collagen in the tunica adventitia of the human cerebral artery measured with polarized light and the universal stage. *J Ultrastruct Res* 77: 133-145, 1981.
32. **T. Boulesteix AMPNPGMPSEBMCS-K.** Micrometer scale Ex Vivo multiphoton imaging of unstained arterial wall structure. *Cytometry Part A* 69A: 20-26, 2006.
33. **Unser M, Aldroubi A, and Eden M.** B-spline signal processing. Part I. Theory. *IEEE Transactions on Signal Processing* 41: 821-833, 1993.
34. **Voytik-Harbin SL, Rajwa B, and Robinson JP.** Three-dimensional imaging of extracellular matrix and extracellular matrix-cell interactions. *Methods Cell Biol* 63: 583-597, 2001.
35. **Wicker BK, Hutchens HP, Wu Q, Yeh AT, and Humphrey JD.** Normal basilar artery structure and biaxial mechanical behaviour. *Computer Methods in Biomechanics and Biomedical Engineering* 11: 539-551, 2008.
36. **Xia Y, and Elder K.** Quantification of the graphical details of collagen fibrils in transmission electron micrographs. *J Microsc* 204: 3-16, 2001.
37. **Young AA, Legrice IJ, Young MA, and Smail BH.** Extended confocal microscopy of myocardial laminae and collagen network. *J Microsc* 192: 139-150, 1998.
38. **Zulliger MA, Fridez P, Stergiopoulos N, and Hayashi K.** A strain energy function for arteries accounting for wall composition and structure. *J Biomech* 37: 989-1000, 2004.



# Summary, Conclusions and Perspectives

---



## Summary, Conclusions and Perspectives

Vascular tissue shows a non-linear anisotropic behavior, as a result of material properties, structural arrangements and interconnections of its main constituents, elastin, collagen and vascular muscle cells. Constitutive modeling of vascular tissue has been a challenging area for several decades. Structural constitutive models, in particular, attempt to integrate information on composition and structural arrangements of tissue to avoid ambiguities in material characterization and offer an insight into the function, structure and mechanics of the vascular wall.

This thesis aimed to contribute to the field of biomechanics of vascular tissue, with particular focus on the modeling of vascular wall based on the organization and structural characteristics of its passive constituents, namely elastin and collagen. Most of the previously published structural strain energy functions have considered that collagen is the only wall element which contributes to the anisotropic behavior of vascular wall. However, these strain energy functions fail to describe both pressure-radius and pressure-longitudinal force curves, as those are measured in a typical inflation-extension experiment. Here, we proposed that both elastin and collagen contribute to anisotropic properties of vascular wall and introduced, for the first time, an anisotropic strain energy function for elastin with one family of fibers in the longitudinal direction for rabbit facial veins and in the circumferential direction for rabbit common carotids. Based on our results, including an isotropic term for elastin significantly improved the quality of the simultaneous fit of pressure-radius and pressure-longitudinal force curves in both veins and arteries. Assessment of arterial tissue ultra-structure, based on scanning microscopy techniques, revealed interlamellar elastin fibers running in the circumferential direction between the elastin lamellar sheets, thereby providing substantial evidence for this anisotropy. Our results also indicated that, in the absence of a structurally functional elastin, collagen engages more abruptly and the angle of collagen fibers is altered, suggesting an interaction between elastin and collagen constituents. This is an important feature often neglected in the definition of arterial SEFs. In this way, elastin plays an indirect role on anisotropic properties of vascular tissue in the collagen-dominant region.

We also studied the contribution of collagen to multi-axial mechanical behavior of vascular wall. Two main features of collagen fiber organization are waviness and angular dispersion. Earlier structural models of the vascular wall have included individually one but never both of these features. We developed a model for the vascular wall to include both waviness and orientational distribution of collagen fibers. To our knowledge, this is the first model for vascular wall that accounts for both features. We studied the effect of orientational distribution parameters on the mechanical behavior of the wall in typical inflation-extension tests. Finally, we applied the model to experimental data of rabbit facial veins to assess the usefulness and necessity of including fiber angle dispersion. Our results showed that including the dispersion of collagen fibers into the model, particularly in the absence of adventitia, did not improve significantly the fit of pressure-radius and pressure-longitudinal force curves from inflation-extension tests. However, the model predicted a less abrupt and shifted to higher strain collagen engagement pattern than the model including only the waviness. This becomes important when the model is fitted to experimental data and model parameters are used to study structural modifications of collagen fiber network in physiology and disease.

Finally, we quantified waviness and angular distribution of collagen fibers in the adventitia of common carotids of rabbits at their zero stress state. The quantification of structural features of collagen fibers at their zero stress state is necessary for a constituent-based modeling

approach of the vascular tissue. We related the waviness of collagen fibers to a straightness parameter bounded between 0 and 1, which was defined as the ratio of the length of the straight line between endpoints of a fiber to the fiber's length. This parameter could be measured directly from the images of adventitial collagen. To obtain these images collagen was marked with a recently developed collagen marker CNA38-OG488. The marker enables the imaging of the tissue without fixatives and thus allows the structure to remain intact. A uni-modal beta distribution function was fitted to the straightness parameter distribution. The waviness distribution of fibers did not depend on principal orientation of fibers. In addition, a plug-in for the open source software ImageJ was developed and made available online to calculate local orientation of fibers. Analysis of local orientations showed four main families of fibers in the adventitia with an angle of approximately 45 degrees to each other.

Our model and testing methods are subject to a few limitations. We have neglected the contribution of vascular smooth muscle in the passive state of vascular wall, the state at which smooth muscle cells are maximally dilated. Maximally dilated smooth muscle is assumed to have a negligible effect on mechanical properties of blood vessels, because its effective elastic modulus is an order of magnitude lower than that of elastin. The models suggested in this study are one-layer models with structural properties homogeneously distributed throughout the arterial wall thickness. We have also considered a planar distribution for collagen fibers while the distribution is three-dimensional, specifically in adventitia. Finally, the image analysis techniques have not been used to their maximum power and further development of specific analysis tools is needed, for instance for the automatic measurement of parameters related to fiber waviness.

In conclusion, our work has led to a number of improvements over previous theoretical and experimental studies, which have dealt with the role of elastin and collagen in vascular biomechanics. Our studies on the contribution of elastin in vascular mechanics revealed that elastin directly and indirectly contributes to the anisotropic behavior of both veins and arteries. The direct role of elastin was justified by its intermural organization. The anisotropic structure was integrated into a new model based on the previous model of Zulliger et al. The indirect contribution of elastin to anisotropy was explained by its inter-links with collagen structure and collagen engagement pattern. As for the collagen, we improved the Zulliger et al. model and developed a model with both main structural features of collagen, i.e. waviness and orientational dispersion. Collagen fibers in adventitia were imaged and waviness and orientational dispersion of collagen fibers were quantified to provide for detailed structural information of collagen. The model developed for healthy arteries may then be extended in a continuum-mechanics or a finite-element context to study and analyze more complicated geometries under different types of pathophysiological processes or cardiovascular diseases, such as aging, aneurysm and atherosclerosis.

There are several improvements which could follow this work. First, a future model should consider the contribution of vascular smooth muscle even at their dilated state. Second, the model could be extended to include the contribution of the active stress produced by the vascular smooth muscle. Third, the model could be extended to a heterogeneous multi layer model. Fourth, the microscopy techniques should be used to elucidate the alterations due to pathophysiological processes and diseases. Fifth, more powerful image analysis tools should be developed a) to segment elastin, collagen and smooth muscle cells b) to obtain 3D orientational distributions c) to automate calculation of the waviness and main orientations. Sixth, the pattern of collagen engagement should be measured at different stages of inflation-extension tests. Seventh, the model could be used to study remodeling processes. Finally, the strain energy function may be introduced in a finite element context to allow for structure-based analysis of geometrically complicated cases in health and disease.



# Curriculum Vitae

---



# Rana Saitta-Rezakhaniha

Avenue Dapples 19  
1006 Lausanne  
Switzerland  
Born April 10<sup>th</sup> 1981

Nationality: Iranian  
Marital status: married  
Tel: +41 76 428 40 51  
[rana.saitta@gmail.com](mailto:rana.saitta@gmail.com)



## EDUCATION

**Ph.D. Student in Biotechnology and Biomedical Engineering**, Ecole Polytechnique Fédérale de Lausanne (EPFL), Switzerland (2004-2010)

I am near completion of my Ph.D. in the laboratory of Hemodynamics and Cardiovascular Technology at EPFL. My work focuses on biomechanics of soft tissue with particular attention on structural constitutive modeling of vascular wall.

**B.Sc. in Mechanical Engineering**, Sharif University of Technology, Tehran, Iran (1999-2004)

As my diploma project, I developed a model for a passive walking robot.

**High School Diploma**, Farzanegan School, under the supervision of **NODET** (National Organization for Developing Exceptional Talents), Tehran, Iran (1999-2004)

## ADDITIONAL EDUCATIONS

**Courses offered by the Executive MBA in management of Technology (MOT) program**, EPFL, Switzerland (2007-2009):

Advances in Economics of Innovation and Decision Making Under Risk, Uncertainty and Crisis situation; Entrepreneurial Opportunity Identification and Exploitation; Special modules on Management of Biotech/medtech/pharma ventures: Marketing of Biotech, Medtech, Pharma, Clinical Trial Management and Regulatory Affairs, Management of Technical Innovations

**Courses offered by Life Science and Engineering Faculties**, EPFL, Switzerland (2004-2010):

Vascular Biology, Basic principles of drug action at the cardiovascular system, Bioengineering Ethics, Orthopedic Engineering, Hemodynamics, Advanced Biomicroscopy

**Laboratory animal science course**, Module I, **practical and theoretical aspects** (2006), CHUV/EPFL, Lausanne, Switzerland

## TEACHING

**M.Sc. and B.Sc. student supervisor** (2006-2010):

One master student from TUE (Technical University of Eindhoven, the Netherlands) for the Master project, and one bachelor student from MIT (Massachusetts Institute of Technology, USA) for an internship

**Teacher Assistant** in Practical Physiology course and Fluid mechanics, School of Life Sciences, EPFL, 2006-2009

**High School Teacher** in Mathematics, Teamwork and Creativity courses, Tehran, Iran (1999-2001)

## WORKING BACKGROUND

**Research assistant** in the laboratory of **Hemodynamics and Cardiovascular Technology** (LHCT) at EPFL, Switzerland (2004-2010)

I have developed a theoretical-experimental project on modeling of vascular tissue, initiated and managed collaborations with different institutes such as university of Eindhoven (Netherlands) and participated in European and international conferences to present my work.

**Internship Program** in Mega Motors car manufacturing company, Tehran, Iran (2001-2002)

Following my experience in assembly line to engineering departments, I took the opportunity to suggest ideas to improve the product line.

## HONORS

**Max Anliker Memorial Poster Award** by Swiss society of biomedical engineering (SSBE), 2007

**Fellowship awarded by EPFL**, doctoral school of life sciences, 2004-2005

**Ranked 43<sup>th</sup> in the nationwide university entrance exam** among ~300 000 participants, Iran, 1999

## PUBLICATIONS

**Rezakhaniha, R.** and Stergiopoulos, N., 2008, *A Structural Model of the Venous Wall Considering Elastin Anisotropy*, Journal of Biomechanical Engineering, 130(3).

**Rezakhaniha, R.**, Fonck, E., Genoud, C., Stergiopoulos, N., 2009, *Role of elastin anisotropy in structural strain energy functions of arterial tissue*, submitted to Biomechanics and Modeling in Mechanobiology

**Rezakhaniha, R.** and Stergiopoulos, N., 2010, *A Structural Constitutive Model for Vascular Wall Considering Angular Dispersion and Waviness of Collagen Fibers*, submitted to Annals of Biomedical Engineering

**Rezakhaniha, R.**, Schrauwen, J.T.C., Griffa, A., Sage, D., van De Vosse, F.N., Bouten, C.V. C. , , Unser, M., Stergiopoulos, N., 2010, *Experimental investigation of collagen waviness and orientation in the adventitia*, to be submitted to AJP Heart and circulatory physiology

Bagnost Teddy, Ma Linga, da Silva Rafaela F., **Rezakhaniha, Rana**, Nappey Maude, Houdayer Christophe, Stergiopoulos Nikos, André Claire, Guillaume Yves, Berthelot Alain, Demougeot Céline, 2010, *Long-term treatment of spontaneously hypertensive rats with arginase inhibitor lowers blood pressure, improves vascular function and reduces vascular and cardiac fibrosis*, accepted in Cardiovascular Research

## ORAL/PODIUM PRESENTATIONS

**Rezakhaniha, R.**, Fonck, E.E., Stergiopoulos, N., *Role of Elastin in Anisotropic Behavior of Arterial Wall*, 3<sup>rd</sup> Switzerland japan workshop on biomechanics, Engelberg, Switzerland, 2009

**Rezakhaniha, R.**, Fonck, E.E., Stergiopoulos, N., *Role of Elastin Anisotropy to Identify Structural Strain Energy Functions in Intact and Elastin-Degraded Arteries*, Bioengineering09, Oxford, UK, Oral presentation, 2009

**Rezakhaniha, R.**, Stergiopoulos, N., *The effect of collagen fiber directional distribution on the mechanical response of the vascular wall* , the ASME 2009 Summer Bioengineering Conference, Lake Tahoe, CA, USA, Oral presentation, 2009

**Rezakhaniha, R.**, Fonck, E.E., Stergiopoulos, N., *Role Of Elastin Degredation In Identification Of Vascular Strain Energy Functions* , the ASME 2009 Summer Bioengineering Conference, Lake Tahoe, CA, USA, Oral presentation, 2009

**Rezakhaniha R.** and Stergiopoulos N., *Biomechanics of Vascular Tissue: Role of 3D Organization of Matrix*, Bioengineering Institute (IBI) Seminar series, EPFL, Switzerland, 2009

**Rezakhaniha, R.**, Fonck, E.E., Stergiopoulos, N., *Role Of Elastin Degredation In Identification Of Vascular Strain Energy Functions* , 16th congress of European society of Biomechanics, Luzern, Switzerland, 2008, Oral presentation

**Rezakhaniha, R.**, Fonck, E., Stergiopoulos, N, *Role of Elastin Anisotropy in Identification of Strain Energy Functions Describing Vascular Tissue*, Swiss Society of Biomedical Engineering (SSBE) annual meeting, Neuchatel, Switzerland, 2007

- This work received the **SSBE Max Anliker Memorial Poster Award**.

**Rezakhaniha R.** and Stergiopoulos N., *A structural strain energy function considering elastin anisotropy applied on vascular tissue*, 2007 Summer Bioengineering Conference, Keystone, Colorado, USA, 2007

**Rezakhaniha R.** and Stergiopoulos N., *A 3-D Model for the biomechanical properties of venous wall*, 5th World Congress of Biomechanics, Munich, Germany, 2006, CDROM.

**Rezakhaniha R.** and Stergiopoulos N., *A structural model of the venous wall considering elastin anisotropy*, 17th congress of the Cardiovascular System Dynamics Society, Vaals, Netherlands, 2006, poster presentation

#### LANGUAGES

French	fluent	Italian	beginner
English	fluent	German	beginner
Persian	mother tongue	Arabic	beginner

#### LEISURE TIME ACTIVITIES

##### Social activities:

**Vice president of the BMES** section at EPFL, 2007, Switzerland,

**Representative of Mechanical Eng. students** in the faculty council, Sharif University of Technology, 2002-2003, Tehran, Iran

##### Hobbies:

**Cooking:** my blog on the topic: <http://cuisine-de-lila.blogspot.com/>

**Painting:** watercolor and figure drawing

**Sports:** water-polo (university of Lausanne's club) and yoga